10-14-2020

Aeroelastic Testing to Evaluate Wind Effects on Transmission Systems

Ziad Azzi
zazzi001@fiu.edu

FLORIDA INTERNATIONAL UNIVERSITY

Miami, Florida

AEROELASTIC TESTING TO EVALUATE WIND EFFECTS ON TRANSMISSION SYSTEMS

A dissertation submitted in partial fulfillment of

the requirements for the degree of

DOCTOR OF PHILOSOPHY

in

CIVIL ENGINEERING

by

Ziad Azzi

2020

To: Dean John L. Volakis
College of Engineering and Computing

This dissertation, written by Ziad Azzi, and entitled Aeroelastic Testing to Evaluate Wind Effects on Transmission Systems, having been approved in respect to style and intellectual content, is referred to you for judgment.

We have read this dissertation and recommend that it be approved.

Ioannis Zisis

Seung Jae Lee

Peter Irwin

Nipesh Pradhananga

Caesar Abi Shdid

Amal Elawady, Co-Major Professor

Arindam Gan Chowdhury, Co-Major Professor

Date of Defense: October 14, 2020

The dissertation of Ziad Azzi is approved.

Dean John L. Volakis
College of Engineering and Computing

Andrés G. Gil
Vice President for Research and Economic Development
and Dean of the University Graduate School

Florida International University, 2020

DEDICATION

I dedicate this dissertation manuscript to my entire family and most importantly, to my parents. Without their support, patience, constant motivation, understanding and most of all, unconditional love, the completion of this work would not have been possible.

ACKNOWLEDGMENTS

I would like to express my deepest gratitude to my major professor Dr. Arindam Gan Chowdhury for his unwavering patience, guidance, strong encouragement and most importantly, endless support. I wish to thank him for accepting me into a very welcoming and encouraging atmosphere at the Wall of Wind (WOW), in addition to participating in research works outside my dissertation scope in order to advance my knowledge and broaden my skills. Special thanks go to my co-major professor Dr. Amal Elawady for her constant support, advice, and guidance throughout the entirety of the work on my dissertation topic. I truly appreciate her humbleness, patience, and quick responses whenever situations arise. I would also like to thank Dr. Peter Irwin for his invaluable support and encouragement along every step of this dissertation work. Working with such a highly reputable person in the wind and structural engineering community was extremely inspirational. This manuscript would not have been possible without his expertise. Last but not least, I would like to thank my committee members Dr. Ioannis Zisis, Dr. Seung Jae Lee, Dr. Nipesh Pradhananga and Dr. Caesar Abi Shdid for their cooperation and support in this dissertation work. Special praise goes to Dr. Abi Shdid for recommending Florida International University (FIU) to pursue my PhD and for his constant assistance and guidance in my dissertation work.

I gratefully acknowledge the scholarship support provided by the Dissertation Year Fellowship (FIU, University Graduate School). The WOW experiments were conducted with financial support from the National Science Foundation (NSF Award No. 1520853, NSF Award No. 1635569). The help from the WOW team including Walter

Conklin, Roy-Liu Marques, Mohammataghi Moravej, Krishna Vutukuru, Manuel Matus and all undergraduate as well as graduate students is highly appreciated.

Finally, yet very importantly, I would like to thank my parents Charbel and Marie-Rose, my siblings, Bachir and Nadine, my entire family and friends for their love, support and understanding throughout my PhD journey.

ABSTRACT OF THE DISSERTATION

AEROELASTIC TESTING TO EVALUATE WIND EFFECTS ON TRANSMISSION SYSTEMS

by

Ziad Azzi

Florida International University, 2020

Miami, Florida

Professor Arindam Gan Chowdhury, Co-Major Professor

Assistant Professor Amal Elawady, Co-Major Professor

The transmission infrastructure in the U.S. faces substantial risk from hurricanes. Wind-induced damage poses an immense threat to the electric power grid; such hazards have significantly impacted the supply, generation, and delivery of power to large portions of the U.S. in the past. When exposed to strong winds, critical demands in several elements in transmission tower-line systems may exceed corresponding capacities and trigger various modes of failure. Enhancing the resilience of the transmission grid against increasing threats from hurricanes and strong winds is therefore of critical importance. The results of 1:50 aeroelastic scaled models of a self-supported steel lattice tower and a multi-span transmission lines system under simulated hurricane wind speeds are presented. The aeroelastic tests are conducted at the NSF Wall of Wind Experimental Facility (WOW EF) at the Florida International University (FIU). The models are tested at various wind speeds ranging from 35 m/s to 77 m/s (full-scale) for wind directions varying between normal and parallel to the alignment of the transmission line. Two system identification (SID) techniques are utilized to validate the analytical along-wind aerodynamic damping

of the model and provide insights on its crosswind counterpart. A buffeting analysis is conducted to estimate the response of the tower, the conductors and the entire system and compare it to measured values at the WOW. Similarly, drag and moment coefficients are calculated from the measured response, and dynamic amplification factors (DAF) are computed. Results show that the coupling effects between the transmission tower and the conductors are significant. In some instances, such effects are favorable and in others, unfavorable. Other findings also show that there is a need to include the change in turbulence intensity along the height of the tower in the established analytical modeling approach. The drag coefficients are shown to be in agreement with values proposed in the standards. However, there is a need to consider moment in lattice tower design to account for bending in the members that might be introduced by any rigid connection. The resonance contribution is shown to reach a maximum of 18% and 30% of the peak response for the single tower and multi-span transmission lines systems, respectively.

TABLE OF CONTENTS

CHAPTER PAGE

LIST OF TABLES

LIST OF FIGURES

FIGURE PAGE

CHAPTER I. INTRODUCTION

1.1 Background Information and Project Motivation

Nowadays, electricity has become one of the most essential needs for our economy and in our daily lives. Its continuous supply forms the lifeline for factories, businesses, infrastructure, and homes. Electrical current is transported from the source of production to the distribution system and ultimately, to customers using transmission lines.

However, the transmission infrastructure in the United States, especially in coastal areas, faces substantial risk from hurricanes. Wind-induced damage poses an immense threat to the electric power grid; such hazards have significantly impacted the supply, generation, and delivery of power to large portions of the U.S. in the past. In fact, statistical analysis of power outages has shown that severe weather is the leading cause of power outages in the U.S. Between 2003 and 2012, 87% of all power outages were triggered by severe weather, making it the leading cause of blackouts in the United States (Executive Office of the President, 2013). Major storm-related power outages are often caused by damage to electrical transmission lines that carry power over long distances (Campbell, 2012). In 2004 and 2005, seven hurricanes struck the coast of Florida causing severe damage to electrical infrastructure (Rollins, 2007). A record 3.2 million customers were left without electricity as Hurricane Wilma's (2005) winds damaged transmission lines, transformers, and substations [(Rollins, 2007); (Hines et al., 2009); (Chatterjee and Mozumder, 2015)]. Hurricane Rita (2005) caused progressive collapse of steel-lattice transmission towers in the Gulf region that led to replacing 26 towers in eastern Texas (Rollins, 2007). More recently, Hurricane Irene (2011) caused 6.69 million customer outages across 14 states while Hurricane Sandy (2012) left 8.66 million customers without elec-

tricity in 20 states (Hoffman and Bryan, 2013). Significant damage to power infrastructure occurred and over 480 transmission lines, combined, failed during these hurricanes (Hoffman and Bryan, 2013). In 2017, due to the destruction of power grids and transmission towers, Hurricanes Irma and Maria (both Category 5 Hurricanes on a Saffir-Simpson scale) left an approximate 5 million and 3.4 million residents without power in Florida and Puerto Rico, respectively [(Pasch et al., 2017); (Cangialosi et al., 2018); (Kwasinski et al., 2019)]. Hurricane Michael (2018) caused widespread power outages in Florida and Georgia (Beven II et al., 2019). The issue becomes even more serious due to the interconnected nature of the grid. Even a few failures in the transmission system may result in cascading power loss across large geographic areas leaving millions in the dark. Owing to the interdependencies among various engineering and socio-economic systems, weather-related power outages inflicted average annual losses of $20 to $55 billion to the U.S. economy (Campbell, 2012). Outages lasted from several days to more than three weeks thus negatively impacting society and impeding business continuity [(Balducci et al., 2002), (Kunz et al., 2013)].

The power line system in the U.S. is composed of more than 725,000 kilometers of high and extra-high voltage lines and hundreds of thousands of transmission support structures (ASCE, 2011). In 2011, the cost of upgrading the national electricity infrastructure to meet needs by 2020 was estimated at $673 billion, out of which $107 billion are dedicated to transmission infrastructure (ASCE, 2011). Therefore, enhancing the resilience of the transmission grid against increasing threats from hurricanes and strong winds is of critical importance. More specifically, the identification and upgrade of vulnerable transmission line systems using retrofitting technologies to achieve acceptable

performance levels is hence, a matter of strategic importance for the security and economic prosperity of the nation.

1.2 Previous Studies, Limitations, and Knowledge Gaps

Support towers, conductors, ground wires and insulators are the main components of overhead transmission lines systems. Electricity is transported through conductors that span for kilometers. Conductors are attached to the towers using porcelain insulators. Ground wires play an important role in the transmission line system as they help to protect it from possible lightning strikes. Fig. 1.1 shows a typical span of a transmission line system with two supporting towers. Fig. 1.2 shows a typical view of an electrical insulator for high voltage transmission lines.

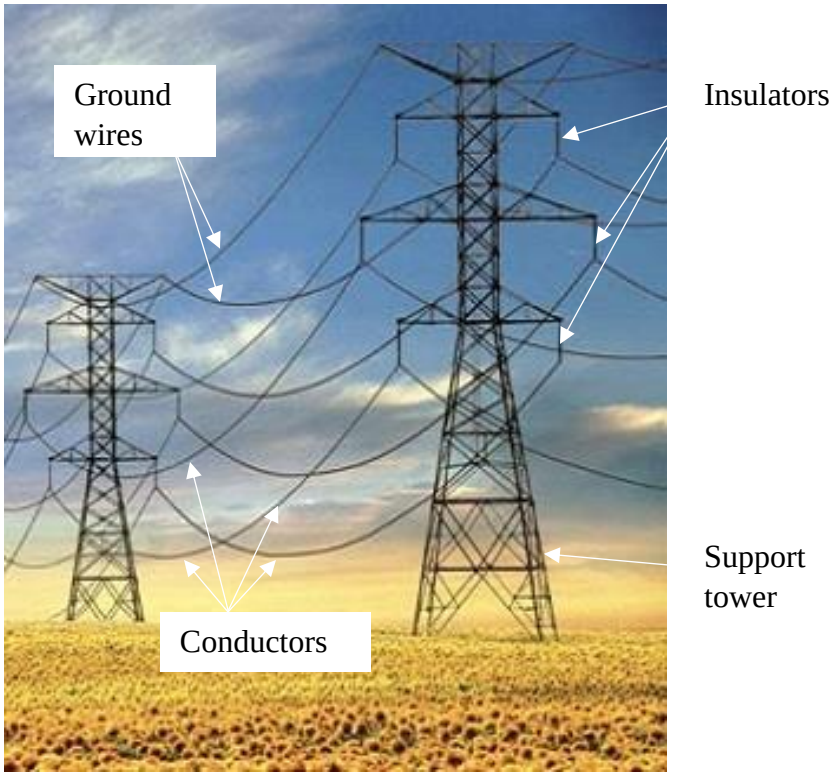

Fig. 1.1: One span of a typical transmission lines system

Although lattice towers come in various shapes and designs, such structures are classified by their type. According to ASCE 74 (2010) and ANSI/TIA-222 (2005), three types of towers are well established for electrical transmission, telecommunication, and antenna use. The three types are presented as follows: (i) poles and guyed masts, (ii) H-frames, and (iii) self-supported latticed towers. The main difference between all three types is their fundamental frequency. Generally, poles have the smallest natural frequency with a range of 0.5 to 1 Hz, followed by H-frames with a range of 1 to 2 Hz, and latticed towers with a range of 2 to 4 Hz.

Fig. 1.2: Typical view of an electrical insulator

Most transmission towers are constructed using steel lattice structures. Such a configuration is light and relatively less expensive to build, and lattice towers can be easily designed for different strengths and heights depending on demand and situations. Another advantage in using lattice towers is that they can be assembled at the final location, which makes it easy to get such structures to difficult-to-reach and remote locations like mountains, valleys, and deserts (Cockfield, 2019). However, lattice towers come with their own drawbacks. Such structures aren't the strongest available in some situations and

they have a relatively wide footprint which could be troublesome in urban environments. On another note, steel can be a very poor material choice when used in swampy areas with high humidity levels or coastal areas where saltwater spray from the ocean can easily cause corrosion. As such, transmission lines using steel lattice structures are best used for rural and inland communities [(Cockfield; 2019); (Texas Co-op Power, 2019)].

Therefore, to compensate for the weaknesses of lattice towers in coastal areas, other structures are used such as concrete poles. Such a configuration has superior performance in hurricane-prone areas, have less of a footprint than a lattice tower of similar height, and is much easier to construct. The downside is that they are typically more expensive, they must be built with specialized equipment and then transported by truck to the site (Cockfield, 2019).

Generally, a large number of structures are not designed to withstand hurricane or tornado loads because such events have very low probabilities of occurrence and the chance that such structures are exposed to them is minimal. However, that is not the case of transmission lines due to the fact that they are long span structures and extend for kilometers (Hamada, 2014). Therefore, in the event of occurrence of high intensity winds coming from a hurricane or tornado, the probability that such event hits one of the towers becomes significantly larger. Subsequently, the failure of one tower can lead to cascading failures of adjacent towers due to the unbalanced forces triggered by the snapping of one or more conductors [(Aboshosha and El Damatty, 2014); (Hamada, 2014); (Yang and Zhang, 2016); (Shehata, 2020)].

During extreme wind events, the system of transmission lines and supporting towers is exposed to a complex set of loadings such as drag forces and spatially and tem-

porally stochastic gust forces. The simultaneous impact of a combination of these loadings along with gravity loads induces a set of complex nonlinear dynamic behaviors in towers, conductors, and other components. Concerning the responses of transmission lines to wind-induced dynamic loading, they can be grouped into three phenomena: galloping, vortex shedding, and buffeting from incoming turbulence [(Matsumiya and Nishihara, 2012); (Aboshosha et al., 2016); (Haddadin et al., 2016)].

The dynamic properties of the different components of a transmission line system are significantly diverse. On the one hand, the tower's natural frequency is typically higher than 1 Hz, leading to insignificant resonant tower responses. On the other hand, the tower's conductors have natural frequencies ranging between 0.2 and 0.3 Hz, which make them susceptible to turbulent winds that have significant energy corresponding to those frequencies. This might lead to excessive excitation and possible resonance.

In general, wind tunnel experiments on transmission structures can be grouped into aeroelastic model tests and rigid tests. By carefully estimating aerodynamic coefficients from rigid tests and combining them with analytical approaches, one can estimate the dynamic responses of a certain system [(Mara et al., 2010); (Chen and Pan, 2014)]. However, such tests do not consider the aeroelastic forces induced by motions of the structure and its various components and the wind structural interaction effects. In addition, the response of transmission line systems was barely examined by previous wind tunnel studies due to the complexity of satisfying basic scaling laws concerning geometric, dynamic, and kinematic similitudes [(Loredo-Souza and Davenport, 2001); (Cluni et al., 2008)]. A few experimental studies on tower-conductor systems only considered a single span system and did not properly model the boundary effects caused by the pres-

ence of adjacent spans when a multi-span system is subjected to turbulent winds [(Lin et al., 2011); (Liang et al., 2015)]. Therefore, the coupled interactions among transmission spans due to torsional, in plane, and out-of-plane dynamic responses of towers and lines were not evaluated.

Moreover, the effects of failure of a conductor (e.g., broken wire) or a point of attachment at insulators, as well as the post-elastic behavior of a tower, on the wind performance of adjacent systems in multi-span models of transmission systems have not been investigated. Furthermore, when exposed to strong winds, critical demands in several elements in transmission tower-line systems may exceed corresponding capacities and trigger various modes of failure including, among others, failure of a support structure element, rupture of a conductor, failure of a suspension insulator and foundation failure. Additionally, the failure of a conductor or an element in the tower can lead to the progressive collapse within the tower and even cascading failures of a larger number of towers in transmission lines. A variety of wind-induced failure modes of lattice towers and transmission line systems are shown in Fig. 1.3 [(Aboshosha et al., 2016); (Shehata, 2020)].

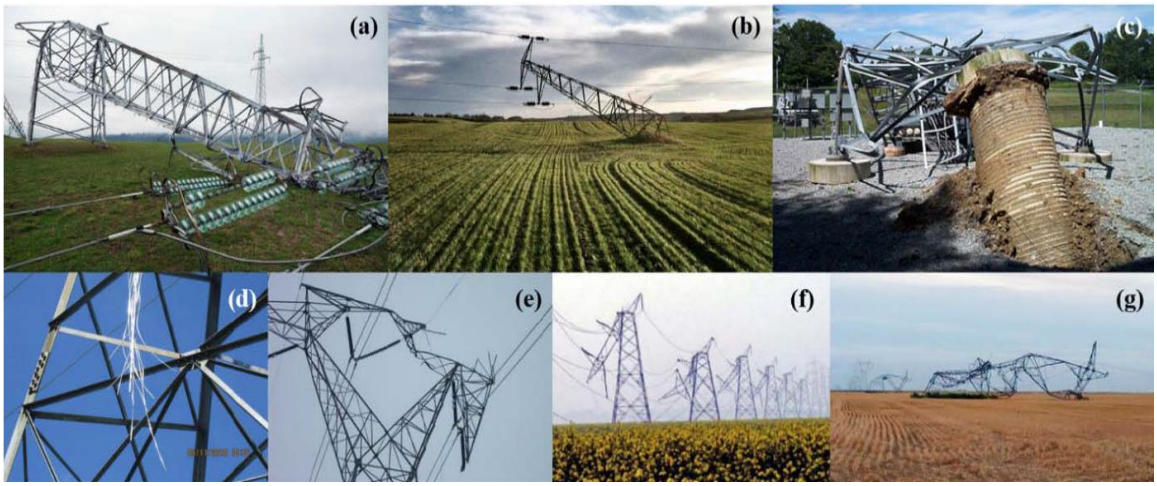

Fig. 1.3: Wind-induced failure modes of lattice towers and transmission lines systems: (a) failure of tower body, (b) failure of tower legs, (c) pullout of foundation in a lattice telecommunication tower, (d) rupture of conductor, (e) damage to cross-arm, (f) cascading failure of cage and cross-arm, and (g) cascading collapse of tower

1.3 Research Objectives and Tasks

The main aim of this research is to fill the current knowledge gaps by performing an analytical study coupled with an extensive experimental program to study the aeroelastic response of a multi-spanned transmission line system subjected to hurricane winds. This study will provide deeper insights into the highly complex coupled dynamic behavior at system and component levels and validate critical aerodynamic and aeroelastic responses produced by a Finite Element Model (FEM). The FEM will be generated by Ohio State University (OSU), the collaborating research team on this project. Note that this manuscript will only address the experimental and analytical parts of the project, i.e., the design, construction, validation, and subsequent analysis of the aeroelastic model results. To fulfill this aim, five objectives are strategically planned as follows:

- Design and conduct aeroelastic tests on a single self-supported lattice tower. This will provide an insight into the drag coefficients for lattice sections. In

addition, this test will allow the investigation of the dynamic response of a single lattice tower subjected to hurricane winds.

- Design and conduct aeroelastic tests on a multi-span transmission-insulator-conductor system to investigate coupling effects among system components and boundary effects. Buffeting and possible instability of the conductors will also be studied.
- Perform aeroelastic tests to investigate the consequences of insulator failure or rupture of conductors on the system global behavior.
- Analytically validate measured responses at the component level at the WOW. Analyses include, but are not limited to, system identification (SID), buffeting theory, signal decomposition, quantification of background and resonant components, etc…

Achieving the previously mentioned objectives is expected to significantly improve the state-of-the-art knowledge on transmission systems and subsequently, the reliability of power grids in the U.S., potentially saving billions of dollars on the economy.

1.4 Organization of Dissertation

The remainder of this dissertation is organized into the following chapters:

Chapter 2 tackles the design theory, validation, construction, and behavior of a 1:50 aeroelastic model of a self-supported steel lattice tower subjected to hurricane winds. Test results show that the design of transmission towers should take into account their along-wind and crosswind behavior. The measured response demonstrates good agreement with the theoretical predictions derived by previous researchers. Incorporating

the change in the turbulence intensity along the height of the tower significantly improves the convergence between theoretical and measured responses.

Chapter 3 provides an insight into a novel design approach of a multi-span transmission-insulator-conductor system. The system is subsequently validated, constructed, and tested under extreme wind loading. Findings have shown that it is necessary to take into account the coupling of the tower and conductor in the design of transmission lines. Comparisons with analytical solutions for predicting the response of transmission towers have shown that the presence of the conductors reduces the forces and moments on the tower. It was also shown that, at higher wind speeds, the dynamic response of the system does not contribute much to the total response due to the high aerodynamic damping of the conductors.

Chapter 4 summarizes the major findings and contributions of this study towards the performance of transmission systems under wind loading.

Chapter 5 proposes potential future work in the transmission systems field.

1.5 Chapter I References

Aboshosha, H. and El Damatty, A. (2014). "Effective Technique to Analyze Transmission Line Conductors under High Intensity Winds." Wind and Structures, Vol. 18, No. 3.

Aboshosha, H., Elawady, A., El Ansary, A. and El Damatty, A. (2016). "Review on dynamic and quasi-static buffeting response of transmission lines under synoptic and non-synoptic loads." Engineering Structures, 112, 23-46.

American National Standards Institute (ANSI) / Telecommunications Industry Association (TIA), ANSI/TIA-222-G (2005). "Structural Standard for Antenna Supporting Structures and Antennas". Standards and Technology Department, Arlington, VA, U.S.A.

American Society of Civil Engineers (ASCE) 74 (2010). "Guidelines for electrical transmission line structural loading". ASCE manuals and reports on engineering practice, No. 74, New York, NY, USA.

American Society of Civil Engineers (2011). "Failure to Act: The Economic Impact of Current Investment Trends in Electricity Infrastructure." American Society of Civil Engineers (ASCE), World Headquarters, 1801 Alexander Bell Drive, Reston, Virginia, USA.

Balducci, P. J., Roop, J. M., Schienbein, L. A., DeSteese, J. G. and Weimar, M. R. (2002). "Electric Power Interruption Cost Estimates for Individual Industries, Sectors, and the US Economy." Pacific Northwest National Laboratory, U.S. Department of Energy.

Beven II, J. L., Berg, R., and Hagen, A. (2019). "Hurricane Michael (AL142018)." National Hurricane Center, Tropical Cyclone Report, National Oceanic and Atmospheric Administration (NOAA).

Campbell, R. J. (2012). "Weather-related power outages and electric system resiliency." Congressional Research Service, Library of Congress, R42696.

Cangialosi, J. P., Latto, A. S., and Berg, R. (2018). "Hurricane Irma (AL112017)." National Hurricane Center, Tropical Cyclone Report, National Oceanic and Atmospheric Administration (NOAA).

Chatterjee, C. and Mozumder, P. (2015). "Hurricane Wilma, utility disruption, and household wellbeing." International Journal of Disaster Risk Reduction, Vol. 14, pp. 395-402.

Chen, Y. and Pan, L. (2014). "Dynamical response of transmission line towers subjected to thunderstorm downbursts based on experimental study." 2014 World Congress on Advances in Civil, Environmental and Materials Research (ACEM14), Busan, Korea, August 24-28.

Cluni, F., Gusella, V. and Bartoli, G. (2008). "Wind tunnel scale model testing of suspended cables and numerical comparison." Journal of Wind Engineering and Industrial Aerodynamics, Vol. 96, Issues 6-7, pp. 1134-1140.

Cockfield, B. (2019). "A Field Guide to Transmission Lines." June 11, 2019. Available: https://hackaday.com/2019/06/11/a-field-guide-to-transmission-lines/. [Accessed: 07/29/2020].

Executive Office of the President (2013). "Economic Benefits of Increasing Electric Resilience to Weather Outages-August 2013." IEEE USA Books & eBooks, p.29.

Hamada, A. (2014). "Numerical and Experimental Studies of Transmission Lines Subjected to Tornadoes." University of Western Ontario, Electronic Thesis and Dissertation Repository, Paper 2479.

Haddadin, S., Aboshosha, H. and El Ansary, A. M. (2016). "Sensitivity of Wind Induced Dynamic Response of a Transmission Line to Variations in Wind Speed." Resilient Infrastructure, London, June 1-4.

Hines, P., Apt, J. and Talukdar, S. (2009). "Large blackouts in North America: Historical trends and policy implications." Energy Polocy, Vol. 37, No. 12, pp. 5249-5259.

Hoffman, P. and Bryan, W. (2013). "Comparing the impacts of Northeast hurricanes on energy infrastructure." Office of Electricity Delivery and Energy Reliability, U.S. Department of Energy.

Kunz, M., Mühr, B., Kunz-Plapp, T., Daniell, J. E., Khazai, B., Wenzel, F., and others (2013). "Investigation of Superstorm Sandy 2012 in a multi-disciplinary approach." Natural Hazards and Earth System Sciences, Vol. 13, No. 10, p. 2579.

Kwasinski, A., Andrade, F., Castro-Sitiriche, M. J., and O'Neill-Carrillo, E. (2019). "Hurricane Maria Effects on Puerto Rico Electric Power Infrastructure." IEEE Power and Energy Technology Systems Journal, Volume 6, No. 1.

Liang, S., Zou, L., Wang, D. and Cao, H. (2015). "Investigation on wind tunnel tests of a full aeroelastic model of electrical transmission tower-line systems." Engineering Structures, Vol. 85, pp. 63-72.

Lin, W. E., Savory, E., McIntyre, R. P., Vanderlaarb, C. S. and King, J. P. C. (2011). "A single-span aeroelastic model of an overhead electrical power transmission line with guyed lattice towers." 13th International Conference on Wind Engineering, Amsterdam.

Loredo-Souza, A. M. and Davenport, A. G. (2001). "A Novel Approach for Wind Tunnel Modelling of Transmission Lines." Journal of Wind Engineering and Industrial Aerodynamics, Vol.89, Issues 11-12, pp. 1017-1029.

Mara, T. G., Galsworthy, J. K. and Savory, E. (2010). "Assessment of vertical wind loads on lattice frame-work with application to thunderstorm winds." Wind and Structures, Vol. 13, No. 5, pp. 413-431.

Matsumiya, H. and Nishihara, T. (2012). "Wind tunnel tests for simulating large-amplitude, low-frequency galloping on overhead transmission lines." The Seventh International Colloquium on Bluff Body Aerodynamics and Applications (BBAA7), Shanghai, China, September 2-6.

Pasch, R. J., Penny, A. B., and Berg, R. (2017). "Hurricane Maria (AL152017)." National Hurricane Center, Tropical Cyclone Report, National Oceanic and Atmospheric Administration (NOAA).

Rollins, M. (2007). "The Hardening of Utility Lines – Implications for Utility Pole Design and Use." Presented at the Utility Pole Conference & Trade Show, Vancouver, WA.

Shehata, A. (2020). "Cascade Failure of Transmission Lines under Downbursts." Electronic Thesis and Dissertation Repository, Paper 6924.

Texas Co-op Power (2019). “Field Guide to Power Lines.” July 2019. Available: https://www.texascooppower.com/local/medina/field-guide-to-power-lines. [Accessed: 07/29/2020].

Yang, F. and Zhang, H. (2016). “Two case studies on structural analysis of transmission towers under downburst.” Wind and Structures, Vol. 22, No.6, 685-701.

CHAPTER II. AEROELASTIC MODELING TO STUDY THE WIND-INDUCED RESPONSE OF A SELF-SUPPORTED LATTICE TOWER

2.1 Introduction

2.1.1 Extreme Wind Effects on Lattice Towers

High-intensity wind (HIW) events such as thunderstorms or hurricanes are frequent natural hazards that impact the built environment around the world. The frequency of occurrence of extreme wind events varies greatly from continent to continent. At any time over the Earth's surface, there are nearly 2,000 thunderstorms in progress (Choi and Hidayat, 2002).

As highlighted by Letchford et al. (2002), thunderstorms produce the highest recorded wind speeds for most of the continental United States, Australia, South Africa, Mexico, and Argentina. In addition, these events dominate the high return period end for several US weather stations. Recorded wind speeds may reach values as high as 80 m/s, which is equivalent to Category 5 on a Saffir-Simpson hurricane scale (Kalaga and Yenumula, 2017).

Like any other structure, electrical transmission lines and their supporting towers are affected by severe windstorms and their safe and economic design for wind loading is of concern to the power utilities all over the planet (Holmes, 2015). Generally, transmission towers are made of steel lattice sections. Such structures are normally designed to be as lightweight as possible to minimize the cost of carrying lines over distances of hundreds of kilometers (Lin et al., 2011). Therefore, transmission towers are a typical class of high-rise, slender, flexible structures sensitive to wind effects, with very small structural damping. Wind loads normally control the design of these towers, and so, it is ex-

tremely important to study the wind-induced dynamic responses of this kind of structure, in the form of buffeting or vortex shedding [(Badruddin Ahmad et al., 1984); (Hiramatsu and Akagi, 1988); (Lou et al., 2000); (Lou et al., 2009); (Lin et al., 2011)]. On another hand, wind direction plays an important role in lattice sections design due to the aerodynamic properties of the latter such as shielding and projected frontal area (solidity ratio). Such parameters can greatly vary over small angles of wind direction (Mara et al., 2010). Lattice steel towers are also used to support TV and cellular antennas as well as microwave communication dishes. As part of today's expanding communication systems, these types of towers cover almost the entirety of the United States continent [(Bayar, 1986); (Lou et al., 2000); (Carril Jr. et al., 2003)].

Traditional wind design codes for such structures still assume that an atmospheric boundary layer profile provides the basis of wind loading in their design process [(Savory et al., 2001); (Yang and Zhang, 2016)]. There is a need to evaluate wind-induced resonant dynamic response due to the fact that the tower's natural frequency might be low enough to be excited by the turbulence in the natural wind (Holmes, 1994). Typically, transmission structures have natural frequencies varying between 0.5 and 4 Hz, depending on classification and shape (ASCE 74, 2010). Furthermore, the HIW events might be so localized that only the tower, not conductors, is significantly affected by them. In such off-design conditions, tower failure may occur [(Savory et al., 2001); (Letchford et al., 2002); (Mara et al., 2010)].

The failure of a transmission tower carrying electrical lines can be crucial since it might lead to a disruption of electrical services. Such disruption will likely create negative economic and social consequences (Shehata and El Damatty, 2008). Boudreaux

(1962) first reported damages caused by Hurricane Carla in 1961 to the Houston Lighting & Power Company, which approximated about $1.5 million at that time. In Japan, Shichiri (1971) stated numerous damages observed in hundreds of transmission towers due to typhoons. A small group of line engineers conducted failure investigations in Argentina, Australia, South Africa, the United States and Canada in the 1980s. They reported the devastating impact of HIWs, in the form of downbursts and tornadoes, on lattice transmission lines (Dempsey and White, 1996). Other investigation results in America, South Africa and Australia revealed that around 80% of all-weather related failures of transmission towers are due to HIW events [(Chen et al., 2014); (Yang and Zhang, 2016)]. In 1996, electrical power companies in Manitoba, Canada reported the failure of nineteen transmission towers during HIW events. The costs of such a catastrophe amounted to around $10 million in material and blackouts lasted around five days [(Shehata and El Damatty, 2008); (Mara et al., 2010)]. According to Savory et al. (2001), since the flow field for different HIW events varies, the actual failure modes of transmission towers would also be largely different. Observed failure modes of lattice transmission towers in the literature reported the following: (i) buckling of the compression members, (ii) uplift failure of a tension footing, (iii) buckling of a face member, and (iv) horizontal shear failure of the tower [(Dempsey and White, 1996); (Shehata and El Damatty, 2008)].

Currently, several numerical, experimental, and field studies have been conducted to assess the behavior of transmission towers and lines. However, numerical models have been very difficult to verify for many reasons while both wind tunnel testing and full-scale measurements are particularly challenging [(Loredo-Souza and Davenport, 2001); (Loredo-Souza, 2014)]. Concerning wind tunnel testing, two different types are being uti-

lized: static and dynamic testing. In static testing, mean aerodynamic forces are collected from force balances and force (drag and lift) coefficients are obtained whereas, in dynamic testing, a two-dimensional section modeling method is used. A more meticulous wind tunnel testing approach is to design the entire specimen aeroelastically. Such modeling technique comes with many advantages. However, it also presents serious difficulties that will be discussed in the next subsection [(Irwin, 1992); (Loredo-Souza and Davenport, 2001); (Loredo-Souza, 2014)].

2.1.2 Challenges of an Aeroelastic Modeling

Historically, the collapse of the Tacoma Narrows bridge in 1940 was a significant milestone in the wind engineering field. The failure of the bridge encouraged researchers to undertake significant efforts to understand the reasons behind the collapse. This phenomenon caused the conception of building full aeroelastic models (Irwin, 1992). The resulting 1:100 scale model was vital in many ways: (i) in terms of forensics, the failure mechanism was clearly pinpointed; (ii) in terms of design, the aerodynamic instability that led to the failure of the predecessor was eliminated from the characteristics of the replacement bridge; (iii) in terms of education, it provided substantial understanding to wind engineering researchers of the different parameters that might cause instability, and subsequently, failure (Irwin, 1992).

Constructing full aeroelastic models present many advantages over sectional or other partial models. These advantages are summarized hereafter (Irwin, 1992):

- Full aeroelastic models allow for better simulation of turbulence effects without the need for mathematical extrapolation.

- Nearby topographical features, which can affect local wind flows, can be included.
- Wind effects during construction can be examined.
- Influence of mode shapes and the interaction between them can be incorporated.

However, some disadvantages still arise when using full aeroelastic models. Such drawbacks include a longer build time, a much greater cost and smaller model scales (1:50 and smaller) [(Irwin, 1992); (Loredo-Souza and Davenport, 2001); (Loredo-Souza, 2014)].

On another note, the previously mentioned advantages of utilizing full aeroelastic models require that designers respect strict scaling parameters. This will ensure that the behaviors of both prototype and model are identical, or in other words, there is a complete dynamic similarity. In order to adhere to these laws of dynamic similarity, the following parameters have to be correctly simulated in the models: the drag forces, the mass, the reduced frequency, the aerodynamic damping along with the exact properties of the natural wind among others [(Badruddin Ahmad et al. 1984); (Irwin, 1992); (Loredo-Souza and Davenport, 2001); (Loredo-Souza, 2014)]. The similarity equations provided in this section clearly present the conditions that should be met for a successful and accurate aeroelastic design. Note that subscripts *p* and *m* refer to quantities on the prototype and model, respectively [(Loredo-Souza and Davenport, 2001); (Loredo-Souza, 2014)]. Generally, for any quantity Q_p measured on the prototype, Equation 2.1 can be used to calculate its model counterpart Q_m, where λ_Q is the scaling factor (Azzi, 2016):

$$Q_m = Q_p \times \lambda_Q \tag{2.1}$$

Geometric Similarity: The ratio of geometric dimensions between the prototype and the model should be maintained. Equation 2.2 presents the length scale λ_L:

$$\lambda_L = \frac{L_m}{L_p} \tag{2.2}$$

Velocity: Since the resistance of transmission lines (i.e., conductors) to deformation is largely influenced by gravity, Froude number *Fr* similarity is critical. Equation 2.3, where λ_U is the velocity scale, denotes the requirement to maintain that similarity (assuming the gravitational acceleration *g* is the same for both specimens):

$$\lambda_U = \sqrt{\lambda_L} \tag{2.3}$$

Mass Modeling: To model the exact total mass *M*, the inertia forces of the structure and the flow must be scaled consistently. If equivalent small-scale models are built with materials similar to the prototype ones, then the mass scale λ_M is a function of the length scale λ_L only. Equation 2.4 illustrates the previous sentence:

$$\lambda_M = \lambda_L^3 \tag{2.4}$$

Time: Since the length scale λ_L and velocity scale λ_U are already defined in Equations 2.2 and 2.3 respectively, the time scale λ_T can be automatically obtained using Equation 2.5:

$$\lambda_T = \frac{\lambda_L}{\lambda_U} = \sqrt{\lambda_L} \tag{2.5}$$

Elastic Stiffness: The elastic stiffness *EI* is probably the most important parameter in any aeroelastic modeling exercise. It governs the basis for the design and selection of any structural component on the model by scaling down the elastic stiffness of its full-scale counterpart. Equation 2.6 represents the elastic stiffness scale λ_{EI}, which is a function of both the length and velocity scales, λ_L and λ_U, respectively:

$$\lambda_{EI} = \lambda_U^2 . \lambda_L^4 \tag{2.6}$$

Acceleration: Since both the velocity and length scales λ_U and λ_L have already been previously defined, then the acceleration scale λ_a is simply given by Equation 2.7:

$$\lambda_a = \frac{\lambda_U}{\lambda_T} = \frac{\sqrt{\lambda_L}}{\sqrt{\lambda_L}} = 1 \tag{2.7}$$

Aerodynamic Damping: In strong winds, the entire damping of a flexible structure is a function of both its structural damping ζ_s and the aerodynamic damping ζ_a. The latter is a retarding force, obtained from the relative motion between the structure and the air, and proportional to the wind speed *U*. If the model is constructed with the same material as the prototype, then the aerodynamic damping ζ_a should remain the same.

Frequency: For a particular mode of vibration of a given structure, the connection between velocity, time, and length is strongly dependent on the equality of reduced frequency in small- and full-scale. To maintain that equality, Equation 2.8 presents the frequency scale λ_f that should be preserved in the design:

$$\lambda_f = \frac{f_m}{f_p} = \frac{1}{\sqrt{\lambda_L}} \tag{2.8}$$

Provided that the previous equations are maintained throughout the design of the aeroelastic model, dynamic similarity will be achieved [(Irwin, 1992); (Lou et al., 2000); (Loredo-Souza, 2014); (Elawady et al., 2016); (Azzi, 2016)]. However, in aeroelastic modeling, it is almost impossible to satisfy all the previously mentioned requirements, which means that some compromise has to be made. In the case of the Reynolds number *Re*, it is impossible to match its full-scale counterpart as the drag on a lattice structure constructed from cylindrical/square members will be affected by the distortion in *Re* similitude [(Lou et al., 1995); (Lou et al., 2000); (Loredo-Souza, 2014)]. On another note,

transmission towers are made of very thin and small steel latticed sections and most of the design is governed by the elastic stiffness *EI* parameter, which means that finding small-scale sections in the market that fit the frequency, mass and stiffness parameters can prove to be quite challenging. As an example of the challenges faced during aeroelastic modeling, selecting a relatively large length scale λ_L of 1:50 yields an elastic stiffness scale λ_{EI} of $1:3.2x10^{-9}$ (Equation 2.6). Consequently, this makes the model components very small and hard to find on the market or even to manufacture. However, it is common practice to substitute sections made of steel with aluminum in the design of the model in order to have slightly bigger sections since the modulus of elasticity of steel is almost three times that of aluminum. This procedure will maintain the frequency scaling requirement, but it will violate the mass by a certain small percentage. As noted by Irwin (1992), the exact matching of the parameters is impossible. It may be violated in small instances without severely compromising the validity of the results.

2.1.3 Limitations of Previous Work and Knowledge Gap

Previous studies on individual lattice towers focused on field observations, numerical analyses, and finite element computer models to investigate the wind-induced response on such structures [(Badruddin Ahmad et al., 1984); (Holmes, 1996a); (Holmes, 1996b); (Savory et al., 2001); (Choi and Hidayat, 2002); (Lou et al., 2009); (Chen et al., 2014); (Yang and Zhang, 2016)]. The majority of previous aeroelastic testing of transmission towers investigated the behavior and the buffeting response of the whole transmission tower-conductor system [(Lin et al., 2011); (Loredo Souza, 2014); (Liang et al., 2015); (Aboshosha et al., 2016); (Elawady et al., 2016)]. To date, very few research focused on the wind-induced behavior of tall lattice steel towers or sections using aeroelas-

tic models [(Lou et al., 2000); (Mara el al., 2010)]. Lou et al. (2000) were the first to test an aeroelastic model of a tall steel lattice tower at a length scale of 1:100. They reported that a substantial part of the tower response is a buffeting at the fundamental natural frequency of the model. In addition, they also observed that the response of a lattice tower in two sway directions is approximately the same, emphasizing on the need to include across-wind vibrations in the design standards which currently deal with along-wind response only. Mara et al. (2010) investigated the aerodynamic forces on two 1:10 models of vertical steel lattice towers as well as guyed ones. The models were rotated about two axes and the behavior was recorded for different pitch and yaw angles. The study concluded that the most severe forces occur when the most frontal area of the structure is subjected to wind. It was also emphasized that current standards do not consider the wind-induced forces coming from simultaneous vertical and horizontal directions.

This study aims to fill the existing gap in the literature and advance the knowledge in lattice structure design. This would be achieved by conducting full aeroelastic tests on a complete lattice tower steel section constructed in a relatively large length scale of 1:50. The following sections describe the design, modeling, and construction of the lattice tower , along with their validation as a first effort. The along-wind and cross-wind aerodynamic damping coefficients are then obtained from acceleration time histories using an iterative approach and subsequently, compared with analytical values. The crosswind response, neglected in all design standards around the world, could prove to be crucial in the resiliency of such structures, if properly included. Then, the wind-induced buffeting response of the model is investigated. This includes possible resonance between the model natural frequency and that of the incoming wind. Finally, force and moment

coefficients along with dynamic amplification factors are calculated using the data collected from the sensors installed on the model and are compared with similar parameters specified in different design standards utilized around the world.

2.2 Experimental Setup, Design, and Validation of the Lattice Tower Model

2.2.1 Wall of Wind Experimental Facility (WOW EF)

The experiments of this project were carried out at the National Science Foundation (NSF) Natural Hazards Engineering Research Infrastructure (NHERI) Wall of Wind Experimental Facility (WOW EF). The WOW EF utilizes a powerful 12-fan system with the latter organized in two curved rows of six fans each, capable of wind speeds reaching up to 70 m/s. Moreover, turbulence characteristics of terrain exposures are achieved using a set of adjustable triangular spires and roughness elements located inside a flow management box. The test section, designated as open jet, is 4.3 m high by 6 m wide (Feng et al., 2020). The turntable, on which specimens are erected and rotated to allow testing at different wind directions, has a diameter of about 4.9 m. Such characteristics of the WOW EF allow for full- and large-scale aerodynamic testing of building components and appurtenances as well as low-rise buildings (Azzi et al., 2020a). Fig. 2.1a and 2.1b show the intake side of the WOW EF and the flow management box, respectively. More details on the design and validation of the WOW EF is presented in Chowdhury et al. (2017) along with several case studies at different scales.

a) b)

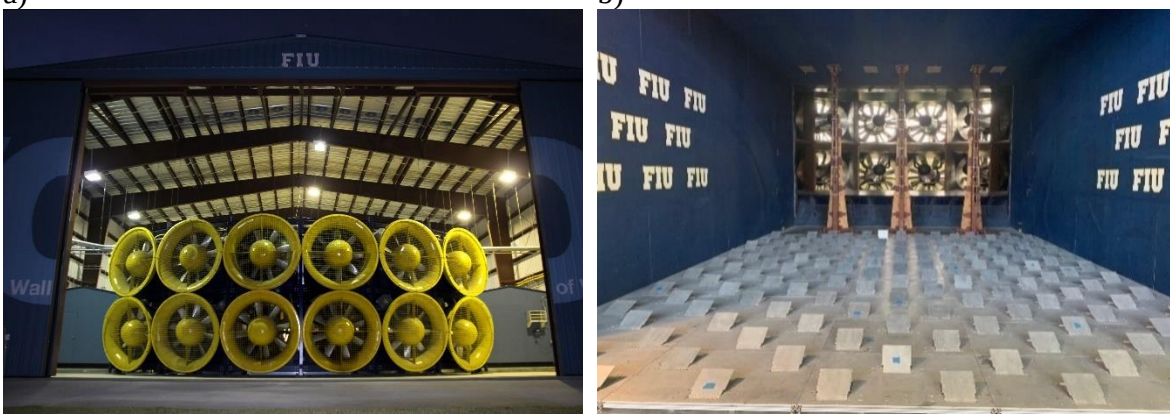

Fig. 2.1: Some pictures of the WOW EF: a) 12-fan system captured from the intake side (south side of the facility), and b) flow management box

2.2.2 Aeroelastic Modeling for Wind Testing

2.2.2.1 Scaling, Design, and Construction

Although lattice towers come in various shapes and designs, such structures are classified by their type. According to ASCE 74 (2010) and ANSI/TIA-222 (2005), three types of towers are well established for electrical transmission, telecommunication, and antenna use. The three types are: (i) poles and guyed masts, (ii) H-frames, and (iii) self-supported latticed towers (shown in Fig. 2.2). The main difference between all three types is their fundamental frequency. Generally, poles have the smallest natural frequency with a range of 0.5 to 1 Hz, followed by H-frames with a range of 1 to 2 Hz and latticed towers with a range of 2 to 4 Hz.

The lattice tower selected for this study is classified as a steel double circuit vertical self-supported lattice tower typically used in transmission line industry. This particular tower design is located in coastal areas in the state of Texas, along the Gulf of Mexico. The prototype lattice tower has the following full-scale dimensions: a height h of 27.5 m, a rectangular base with length L of 7.6 m, and width B of 2.7 m. The cross-section of

the tower uniformly decreases along its height until it reaches a constant section at about two-thirds of its height. Additionally, the tower has three different levels of identical cross-arms at the top. This allows the attachment of six bundles of conductors, with two at each vertical level. Fig. 2.2a and 2.2b illustrate the isometric and frontal views of the tower, respectively.

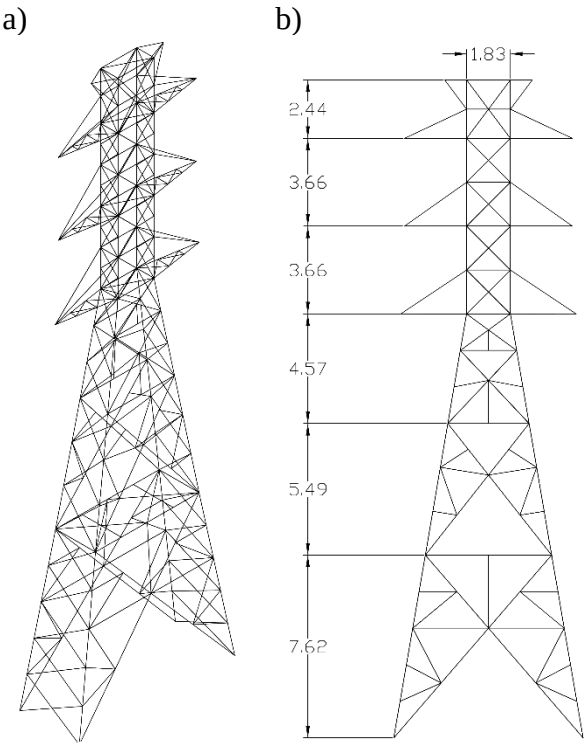

Fig. 2.2: Steel lattice tower: a) isometric view, and b) frontal view (all dimensions are in m and at full-scale)

Whenever the geometry and physical properties of a prototype have to be reproduced as a model at a smaller scale, great care needs to be taken in order to mimic the same dynamic behavior (previously discussed in section 2.1.2). Normally, it is preferred to use prototype material in the construction of the aeroelastic model to maintain the structural damping which is crucial in the dynamic responses of the system (Isyumov, 1972). However, since lattice towers are lightweight structures, it is challenging to satisfy

the mass scaling using prototype steel material. Therefore, a different metal such as aluminum is usually selected to satisfy the mass scaling requirement. Although the structural damping of aluminum is less than that of steel (Mevada and Patel, 2016), the aerodynamic damping for flexible structures such as the lattice tower in this project, tends to be much more dominant than its structural counterpart. Therefore, the discrepancy does not severely impact the results.

For this project, a relatively large length scale λ_L of 1:50 is selected. Note that this lattice tower will be later used in a multi-span transmission tower-insulator-conductor system. Therefore, a length scale of 1:50 was the highest that could be used to satisfy both wind tunnel tests: (i) a single lattice tower, and (ii) a complete transmission lines system with four full spans of conductors (all four spans are designed to fit on the WOW turntable). Moreover, Froude number *Fr* scaling is maintained in the model as that in the prototype. This means that the ratio between the inertial and gravitational forces is preserved. This is achieved by linking the velocity scale λ_U to the square root of the length scale λ_L, i.e., setting the velocity scale to 1:7.07 for a length scale of 1:50 (Equation 2.3). Some of the other essential parameters required to correctly design the aeroelastic model along with their scaling ratios are presented in Table 2.1.

Table 2.1: Scaling parameters used in the design of the aeroelastic model

Quantity Q	Scaling factor λ_Q	Quantity Q	Scaling factor λ_Q
Length L	1:50	Damping ζ	1
Velocity U	$1:50^{1/2}$	Elastic stiffness EI	$1:50^5$
Mass m	$1:50^3$	Elastic stiffness EA	$1:50^3$
Mass moment of inertia I	$1:50^5$	Force F	$1:50^3$
Time t	$1:50^{1/2}$	Bending moment M	$1:50^4$
Acceleration a	1	Torsional moment T	$1:50^4$

In building the aeroelastic model, an aluminum spine with a uniform rectangular cross-section of 5.6 mm width by 13.7 mm length was selected. The spine had a height of 0.55 m (small-scale) and its role was to mimic the structural properties of the tower, most importantly, the elastic stiffness *EI*. The spine was embedded inside an aluminum bearing plate and then glued together using epoxy in order to create a fixity connection. The cross-arms were also designed based on the elastic stiffness *EI* of their prototype counterparts. Aluminum sheets of 4.6 mm height and 0.51 mm thickness were utilized in the construction and glued to the spine using epoxy. To accurately recreate the tower shape and the wind flow around it, non-structural cladding elements were 3D printed using a plastic like material and were carefully attached to the spine using thin polystyrene rods. Polystyrene is a lightweight and hard material. Such a connection between the rods and the cladding elements was carefully selected so as not to add too much mass to the model. Fig. 2.3a and 2.3b show isometric and frontal views of the actual constructed aeroelastic model, respectively.

a) b)

Fig. 2.3: Aeroelastic model after construction: a) isometric view, and b) frontal view

2.2.2.2 Validation of Dynamic Parameters

In order to validate the design of the aeroelastic model and the different sectional dimensions, properties and materials selected, a replica model was generated on the Finite Element Methods (FEM) software SAP2000 (2020). The spine and the cross-arms were modeled as rigid frame elements with the former having a fixed restraint at its bottom. The loads introduced by the weight of the non-structural cladding elements were added as gravity point loads at each joint between the elements and the spine. A modal analysis was performed, and the modal shapes were recorded along with their respective frequencies. The obtained frequency values were compared with prototype frequencies, acquired from a modal analysis of the full-scale tower. The results of the modal analysis and the percent difference between the obtained and target model frequencies are summa-

rized in Table 2.2. Fig. 2.4a and 2.4b illustrate the first two modes of vibrations generated by the FEM model. Note that, in Table 2.2, the target frequency f_t is equal to the prototype frequency times the relevant scaling factor (λ_f = 7.07 from Table 2.1).

Table 2.2: Summary of modal analysis results of the lattice tower

Mode of vibration	Prototype frequency f_p (Hz)	Target frequency f_t (Hz)	FEM-Model frequency f_m (Hz) (design)	Percent difference (%)
Longitudinal	2.25	15.88	15.56	2.02
Transversal	5.10	36.08	35.82	0.72

As can be seen in Table 2.2, the model frequencies f_m obtained from the modal analysis for both mode shapes closely match the target frequencies f_t. The highest percent difference between the two is around 2%, obtained for mode shape 1. This demonstrates that the choice of materials along with the section dimensions used to generate the aeroelastic model on the FEM software were adequate. The construction and instrumentation of the model, as well as the subsequent wind tunnel testing could proceed.

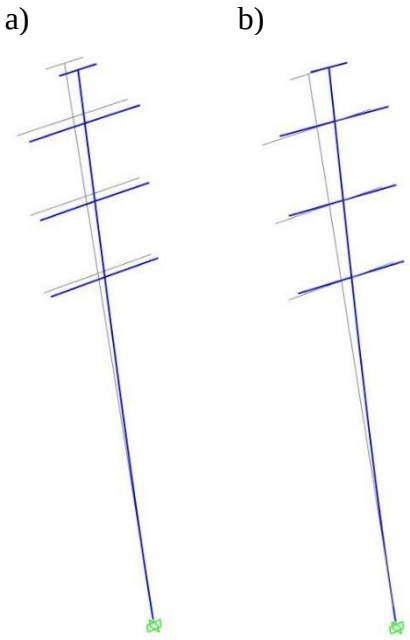

Fig. 2.4: Mode shapes 1 and 2, respectively: a) longitudinal vibration (along weak axis), and b) transverse vibration (along strong axis)

2.2.3 Instrumentation and Testing Protocol

The tower was instrumented with the following sensors: (i) three 3-axis accelerometers, (ii) one 6-Degrees-Of-Freedom (6-DOF) load cell, and (iii) six strain gauges. Two accelerometers were installed at the top of the tower on the cross-arms, and another was glued at mid-height of the spine. The load cell was fixed at the bottom of the tower in order to capture base shears, base moments, and torsional reactions. Four strain gauges were installed at one third height of the spine, one on each face. The remaining two strain gauges were installed on the bottom cross-arm. The strain gauges were calibrated to allow the measurement of moments in the principal directions at the respective point of attachment. Data for the previously described sensors were sampled at 100 Hz. Fig. 2.5a, 2.5b and 2.5c show the location of some of the sensors installed. Finally, two cobra probes were installed at a distance of 4 m behind the model to capture time histories of wind velocities. One probe was installed at mid-height (27.5 cm) and the other probe was installed at tower height (55 cm). Data from the probes were sampled at 2,500 Hz.

Concerning the testing protocol, it was decided to expose the model to four different wind speeds: 7, 9, 11 and 13 m/s at model tower height (0.55 m, small-scale), representing 49.5, 63.6, 77.8 and 91.9 m/s at prototype tower height (27.5 m, full-scale). The tower was rotated between 0^o and 90^o at 15^o increments and each angle duration exposure lasted 2 min (about 14 min, full-scale). Note that a wind direction of 0^o represents wind along the strong-axis (parallel to the cross-arms) and a wind direction of 90^o pertains to wind along the weak-axis of the tower (normal to the cross-arms). The spires and roughness elements depicted in Fig. 2.1b were adjusted so that the turbulence profile matched that of an equivalent open terrain exposure.

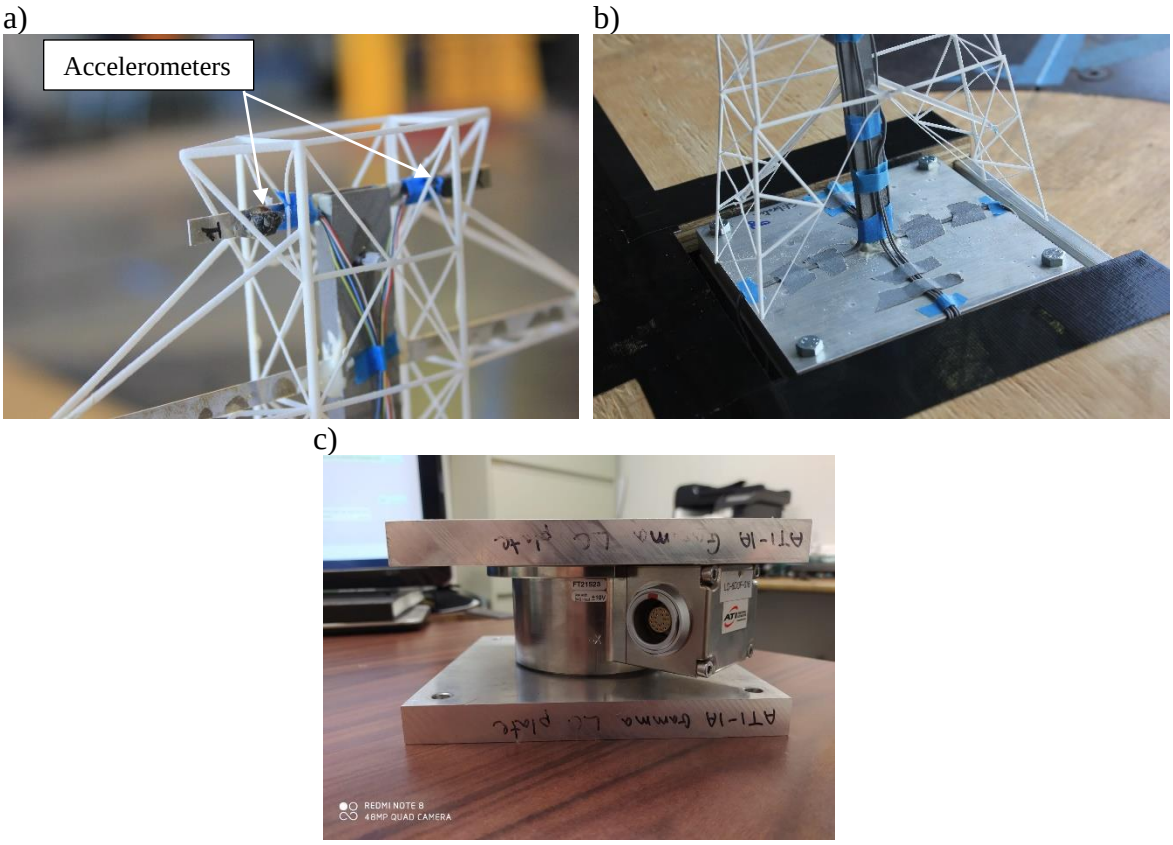

Fig. 2.5: Location of some of the sensors: a) two 3-axis accelerometers on top cross-arm, b) base of tower (load cell is below bearing plate), and c) 6-DOF load cell used

2.3 Results and Discussion

This section presents the analysis and discussion of the results obtained from the wind tunnel testing of the aeroelastic lattice tower model. First, free vibration tests in both directions are conducted on the model in order to verify the appearance of the mode shapes and their respective frequencies. Second, two system identification (SID) techniques are introduced and applied to the model acceleration data to obtain an estimate of the structural and aerodynamic damping coefficients. Then, experimental damping values are compared with analytical ones in the along-wind direction. Third, the buffeting theory is briefly explained and theoretical RMS of accelerations, base shears and base moments are compared with experimentally obtained ones. Finally, drag and moment coefficients

for the aeroelastic lattice tower are calculated experimentally from the sensors and compared with code suggested values. Similarly, dynamic amplification factors (DAF) are computed for all recorded parameters and suggestions as well as recommendations are formulated.

2.3.1 System Identification (SID) Method based on Free Vibration

Before the actual wind tunnel testing of the tower specimen, a free vibrations test was conducted for the purpose of comparing the frequencies of the constructed model with those obtained numerically in the design stage. The tower was excited twice: (i) along its strong axis, and (ii) along its weak axis. This ensured the replication of both mode shapes obtained by the modal analysis of the FEM model (Table 2.2, section 2.2.2.2). The excitation consisted of manually pushing the top of the tower in one direction and allowing it to freely oscillate until it goes back to its initial position while recording its instantaneous acceleration in that same direction. From the captured acceleration time histories, the fluctuating response as well as the corresponding frequencies can be obtained using a Fast Fourier Transform (FFT) application. Fig. 2.6a and 2.6b illustrate the power spectral densities (PSD) of the acceleration time histories along the weak and strong axes, respectively.

By inspecting Fig. 2.6a and 2.6b, it can be noted that the frequency of both modes of vibration along weak and strong axes is 16.02 Hz and 35.06 Hz, respectively (seen in the data boxes). By comparing the previously obtained values with the entries in Table 2.2 concerning the target frequencies, the percent difference is about 0.88% for mode shape 1 and about 2.83% for mode shape 2. Such small percent differences obtained be-

tween both frequencies indicate that the construction of the model was adequate, and its behavior should mimic that of its full-scale counterpart during the wind tunnel testing.

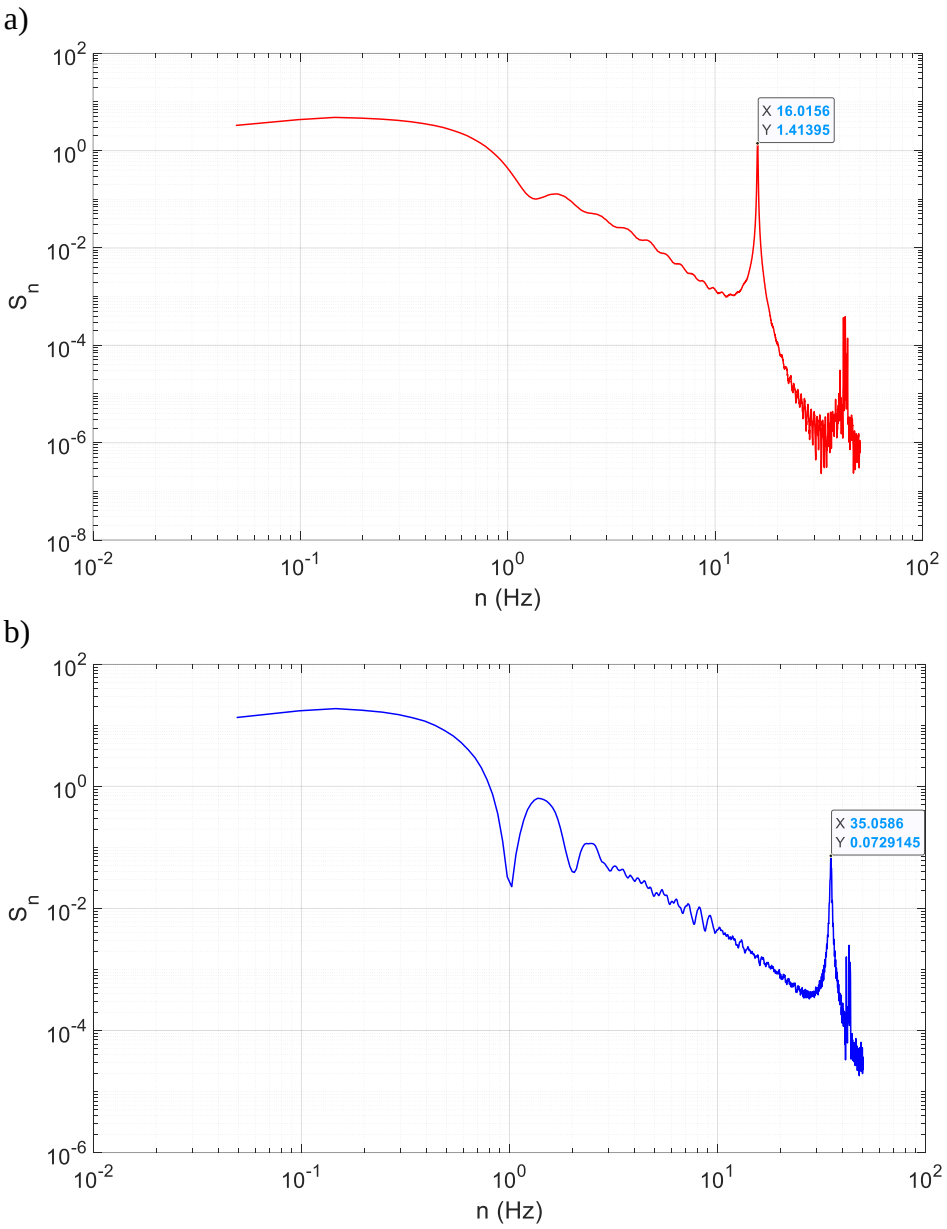

Fig. 2.6: PSD of acceleration time histories: a) along weak axis, and b) along strong axis

2.3.2 Damping Estimation

The self-supported lattice tower can be compared to a single-degree-of-freedom (SDOF) system. For approximation purposes, the system consists of a particle of mass *M*

concentrated at the top of the tower. The tower has a linear elastic behavior and negligible mass with the particle being subjected to an aeroelastic force $F_{ae}(t)$. The displacement at the top of the tower $x(t)$ is opposed by: (i) a restoring force $-kx$ where k is the stiffness of the tower, and (ii) a damping force $-c\dot{x}$ where c is the damping coefficient (Simiu and Yeo, 2019). Equation 2.9 shows Newton's second law of motion of the system, which states that the product of the particle's mass M by its acceleration $\ddot{x}$ is equal to the total aeroelastic force applied to the particle above:

$$M.\ddot{x} + c.\dot{x} + k.x = F_{ae}(t) \tag{2.9}$$

Assigning n (= $\sqrt{(k/M)}/(2\pi)$) and ζ_{eff} (= $c/(2\sqrt{(k.M)})$) as the frequency of vibration and the effective damping ratio in the direction of the motion, respectively, Equation 2.9 can then be rewritten as Equation 2.10 [(Simiu and Yeo, 2019); (Azzi et al., 2020b)]:

$$\ddot{x} + 2\zeta_{eff}.(2\pi.n).\dot{x} + (2\pi.n)^2.x = \frac{F_{ae}(t)}{M} \tag{2.10}$$

In case of free vibrations of a SDOF system in one direction, the damping ratio ζ_{eff} becomes the structural damping of the system ζ_s and the term on the right side of Equation 2.10 becomes zero since no loading is applied on the structure. Chowdhury and Sarkar (2003, 2004) developed a new system identification technique, called the Iterative Least Squares (ILS) approach, that allows all eighteen flutter derivatives for a streamlined bridge deck to be obtained from free vibrations displacement time histories. By definition, flutter derivatives are dimensionless aerodynamic damping terms for vibration of a specimen in a certain degree-of-freedom (DOF) [(Scanlan and Tomko, 1971); (Zasso, 1996); (Wang and Dragomirescu, 2016)]. In order to obtain the flutter derivatives using the ILS approach, it is necessary to first find the aeroelastically modified effective damping C^{eff}

and stiffness K^{eff} matrices, respectively. Both of the previously mentioned parameters include the aeroelastic vector component [(Sarkar, 1992); (Sarkar et al., 1994)]. In this case, the latter component is the aeroelastic drag force D_{ae}. Subsequently, if the free vibrations tests are done twice, once with and once without the WOW fans turned on (i.e., with and without wind loading), then one can obtain the structural and effective damping ratios ζ_s and ζ_{eff}, correspondingly. Hence, the aeroelastic damping ratio ζ_a can be calculated by subtracting ζ_s from ζ_{eff}. For that purpose, Equation 2.10 needs to be represented as the state-space model shown in Equation 2.11 [(Chowdhury and Sarkar, 2003); (Chowdhury and Sarkar, 2004)]:

$$\dot{\underline{X}} = \underline{A}.\underline{X} \text{ with, } \underline{X} = \begin{Bmatrix} \underline{y} \\ \dot{\underline{y}} \end{Bmatrix}, \text{ and } \underline{A} = \begin{bmatrix} \underline{0} & \underline{I} \\ -\underline{K^{eff}} & -\underline{C^{eff}} \end{bmatrix} \tag{2.11}$$

The $\underline{A}$ matrix is a $2n$ x $2n$ square matrix, where n is the number of degrees of freedom for the dynamic system and $\underline{I}$ is the identity matrix of size n x n. As a result, the $\underline{A}$ matrix in Equation 2.11 can be determined if the acceleration $\ddot{\underline{y}}$, the velocity $\dot{\underline{y}}$ and the displacement $\underline{y}$ can be recorded for all n degrees of freedom (n = 1 in the case of the lattice tower) for at least $2n$ different instants of time [(Ibrahim and Mikulcik, 1976); (Chowdhury and Sarkar, 2003); (Chowdhury and Sarkar, 2004); (Azzi et al., 2020b)].

A mechanism was constructed at the WOW using steel supports and electromagnets in order to free vibrate the transmission tower by giving it an initial displacement in both strong and weak axes (0^o and 90^o). A fine string with a negligible mass was attached to the top of the tower in order to displace it by the required amount without altering any of its properties. The two 3-axis accelerometers previously described in the methodology were also utilized in this set of experiments in order to record the acceleration time histo-

ries of the transmission tower at its topmost point. Fig. 2.7a and 2.7b show the mechanism that was constructed at the WOW to conduct the free vibration tests.

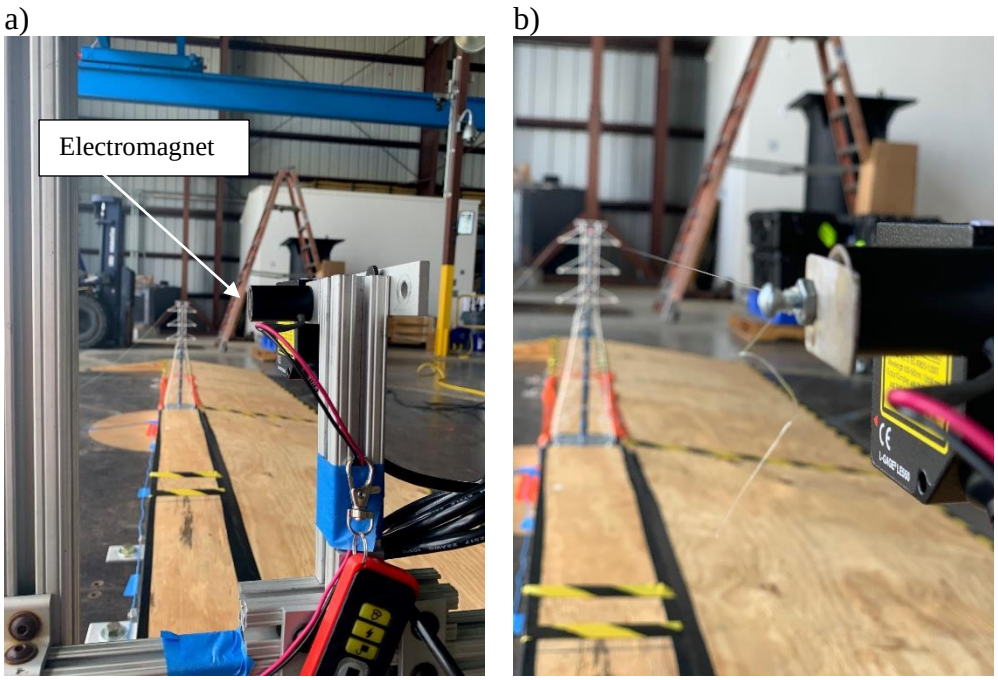

Fig. 2.7: Mechanism to conduct free vibration tests: a) electromagnet, and b) electromagnet turned on and tower displaced

Subsequently, a MATLAB (2020) code was developed in order to integrate the acceleration data and obtain the subsequent velocity and displacement time histories using the Newmark (1959) integration method. Last but not least, the ILS method was adopted along with the obtained time histories until the convergence of $\underline{A}$ matrix was determined to be sufficient. Hence, C^{eff} and K^{eff} are determined and the damping ratios, both structural and effective, could be estimated.

Consequently, the transmission tower was given an initial displacement of: (i) 0.8 cm along the strong axis, and (ii) 1.5 cm along the weak axis. The initial displacement was measured using a laser displacement transducer and the electromagnet was turned on whenever the required value was reached. Then, the latter was turned off and the struc-

ture could freely oscillate until reaching its rest position. For the case of no wind loading, the procedure was conducted twice in order to measure the structural damping ζ_s of the lattice structure for mode shapes 1 and 2. For the case of wind loading, the exercise was repeated five times (at five different wind speeds) for two separate directions (0^o and 90^o) and mode shapes 1 and 2, for a total of twenty times. Accelerations in the x- and y-directions were recorded for each test. This allowed the capture of the total damping ζ_{tot} (structural + aerodynamic) for along-wind and crosswind directions at 0^o and 90^o.

In addition to the use of the ILS method, the authors decided to use another well-established approach for damping estimation called the random decrement (RD) technique [(Jeary, 1986); (Jeary, 1992); (Tamura and Suganuma, 1996); (Takeuchi et al., 2010)]. In brief, the RD technique uses a time-domain approach in which the structural responses to operational loads of a certain structure are transformed into random decrement functions. The latter are proportional to the correlation functions of the system operational responses and hence, could be considered as free vibration responses. As such, values obtained using the two previously mentioned methods (ILS and RD) are compared to the analytical method of obtaining along-wind aerodynamic damping coefficients for lattice towers [(Davenport, 1988); (Loredo-Souza, 1996); (Loredo-Souza and Davenport, 2003)].

Recall that, for the case of no wind loading, the obtained effective damping is no other than the structural ζ_s of the tower. As a check, for both mode shapes 1 and 2, the damping values obtained from the ILS and RD methods were compared with the traditional structural damping formula established for any typical decay of motion phenomenon [(Strelkov, 1964); (Chopra, 2017)]. The latter is presented in Equation 2.12:

$$\zeta_s = \left(\frac{1}{2\pi . j}\right) . ln\left(\frac{\ddot{x}_1}{\ddot{x}_{j+1}}\right) \tag{2.12}$$

In Equation 2.12, j is the number of cycles selected, $\ddot{x}_1$ and $\ddot{x}_{j+1}$ are the acceleration at time steps *1* and *j+1* in m/s^2, respectively. Fig. 2.8a and 2.8b show two acceleration time histories of free vibration tests conducted to excite two separate mode shapes, 1 and 2.

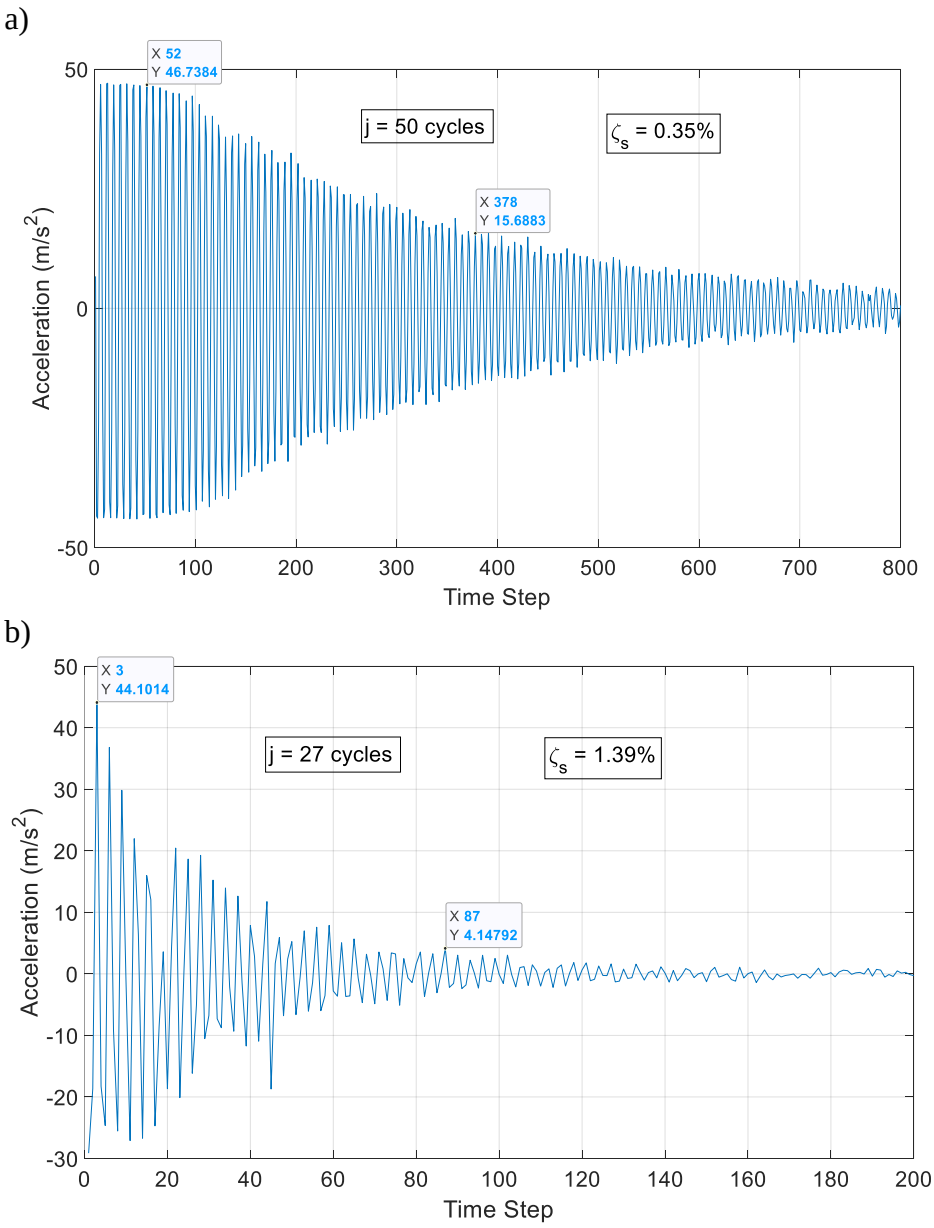

Fig. 2.8: Acceleration time histories of free vibration tests along: a) weak axis (mode shape 1), and b) strong axis (mode shape 2)

As can be seen in Fig. 2.8a and 2.8b, the structural damping values for mode shapes 1 and 2, calculated using Equation 2.12, are 0.35% and 1.39%, respectively. Using the ILS and RD techniques, the damping values are estimated at 0.37% and 0.39% for mode shape 1 and 1.37% and 1.36% for mode shape 2. Both experimental techniques are well in agreement for no wind loading case. With the WOW fans turned on, Fig. 2.9a and 2.9b show the comparison between the same experimental methods and their analytical counterpart. Note that the values presented in the following figures are at the reduced velocity $U/(n.B)$ with U being the wind speed at the top height of the tower in m/s, n being the natural frequency of the tower in the representative mode shape in Hz (15.9 Hz in weak axis direction and 35.9 Hz in the strong axis direction) and B being the width of the face of the tower at its mid-height in m (the value of B is 10 cm for the wide face of the tower and 4 cm for the narrow face, at small-scale). The analytical method to calculate the aerodynamic damping is based on the formula proposed by Loredo-Souza and Davenport (2003), given in Equation 2.13:

$$\zeta_a = \left(\frac{\rho_a}{4\pi . f_T}\right) . \left(\frac{\int_0^h \bar{U}(z) . C_D(z) . w(z) . \mu_j^2(z) . dz}{\int_0^h m(z) . \mu_j^2(z) . dz}\right) \tag{2.13}$$

Also note that the tower of height h is divided into a number of zones z in order to apply Equation 2.13 where ζ_a is the accumulative aerodynamic damping for all tower zones, ρ_a is the density of air in kg/m^3, f_T is the frequency of the mode shape in which the structure is excited, $\bar{U}$, C_D, w, μ_j and m are the mean wind speed (in m/s), drag coefficient, width (in m), mode shape and mass (in kg) of zone z, respectively.

As observed in Fig. 2.9a and 2.9b, the damping values estimated using the ILS and RD techniques agree very well with the analytical values computed using the equa-

tion proposed by Loredo-Souza and Davenport (2003), especially for the 90º wind direction. At 0º wind direction, there is a small discrepancy at lower wind speeds, but the results converge at higher ones.

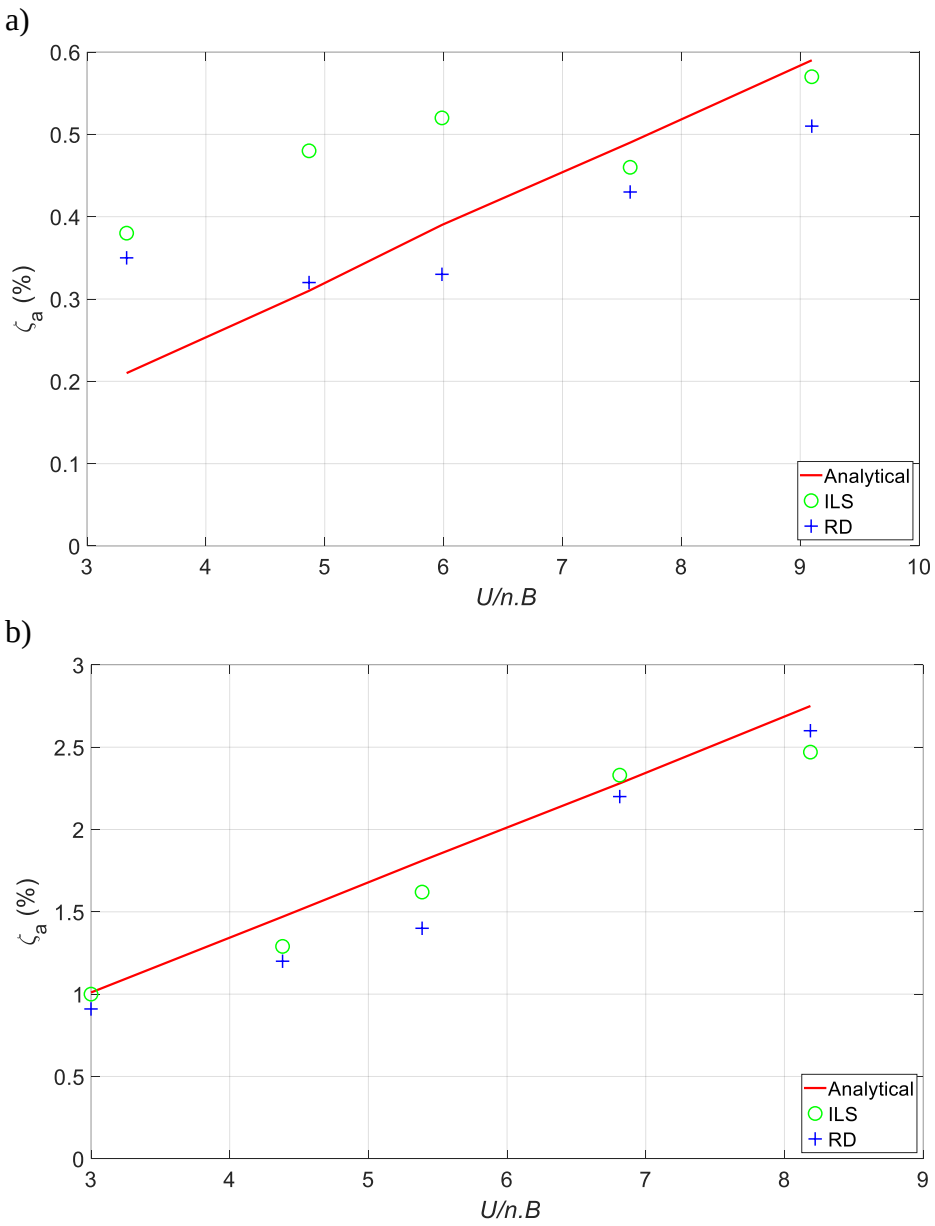

Fig. 2.9: Along-wind aerodynamic damping values at: a) 0º wind direction, and b) 90º wind direction

Through the analysis conducted to estimate the along-wind aerodynamic damping at several wind speeds, the authors noted that the spike observed in the PSD of accelera-

tion time histories at the natural frequency of the structure is reducing in magnitude with increasing wind speeds. This means that the increase in aerodynamic damping values, seen in Fig. 2.9a and 2.9b, is reducing the inherent energy of the power spectrum of the acceleration response. Such an observation was previously reported by Loredo-Souza and Davenport (2001) in their work on the aerodynamic damping of cable structures. They noted that, with increasing wind speeds, the peaks in the spectra of the drag forces on cable structures decreased and became less noticeable. They attributed this phenomenon to the increase in aerodynamic damping. Fig. 2.10 shows the PSD of the acceleration time histories of the lattice tower at different wind speeds for 90^{o} wind direction. It is worthwhile mentioning that the variance of the damping ratio estimated from the measured response data can reach up to 70%. This is due to the number of estimation methods and the accuracy depends on the selected method [(Haviland, 1976); (Davenport, 1983); (Takeuchi et al., 2010)].

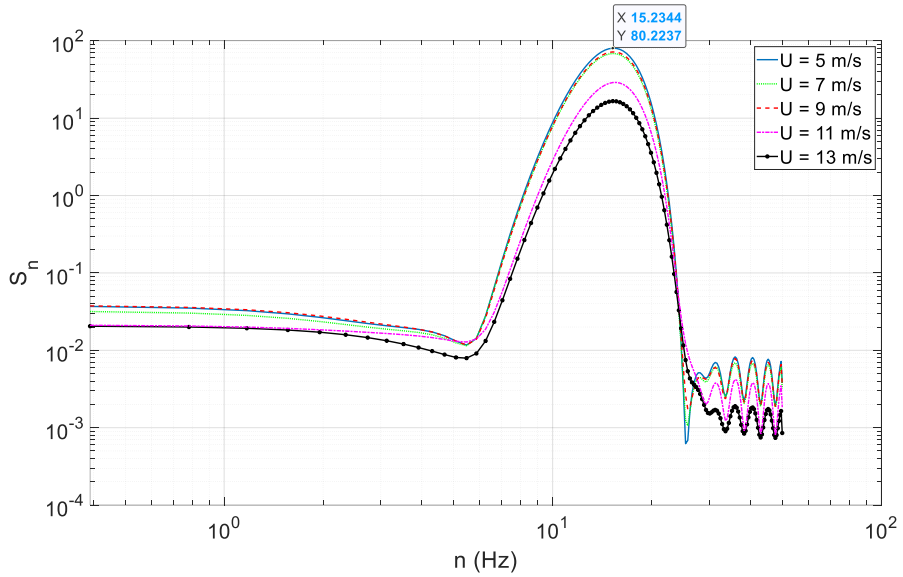

Fig. 2.10: PSD of acceleration time histories at different wind speeds (90^{o} wind direction)

The crosswind aerodynamic damping of the lattice tower for 0° and 90° wind directions is shown in Fig. 2.11. Generally, there is no recommendation on the crosswind aerodynamic damping of lattice structures and standards mostly design for the along-wind direction only. Consequently, the cross wind ζ_a is commonly assumed to be zero and no analytical method has been developed in order to check the adequacy of such a statement. Furthermore, the Australian standard for design of steel lattice towers AS 3995 (1994) specifically states that the crosswind response of lattice structures could be neglected if the solidity ratio ϕ is less than 0.5 in that direction. When ϕ is greater than 0.5, usually the case near the top of lattice towers where diagonal members are very close to each other, structural effects due to a combination of along-wind and crosswind responses must be considered, in accordance with AS/NZS 1170.2 (2011).

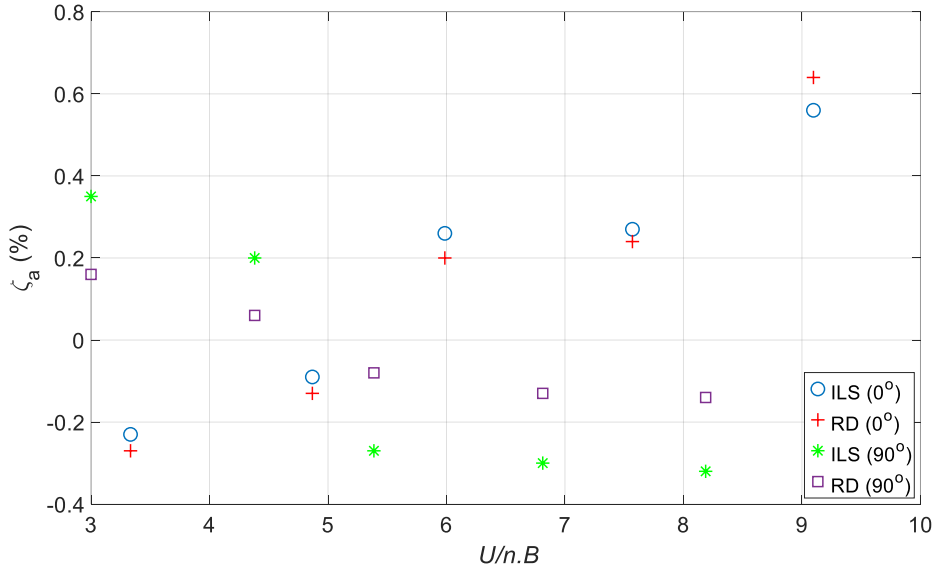

Fig. 2.11: Crosswind aerodynamic damping for two wind directions (0° and 90°)

However, as can be seen in Fig. 2.11, ζ_a tends to change sign with increasing wind speeds. For 0° wind direction, the crosswind aerodynamic damping starts off as negative then rises with increasing wind speeds. For 90° wind direction, ζ_a is positive at low wind

speeds and gradually decreases with increasing wind speeds. Note that the solidity ratio ϕ of the lattice tower in this study is about 0.35 for wind along the weak axis and 0.47 for wind along the strong axis. Surprisingly, the values of ζ_a tend to switch signs at a $U/(n.B)$ of about 4.8 for both wind directions. This behavior was previously observed and documented in the literature by Marukawa et al. (1996) and Huang et al. (2013) in their experimental assessment of the aerodynamic damping of typical tall buildings. This observation was reported for tall buildings having a length to width ratio of 2.5, almost identical to the ratio of the spine rectangular dimensions in this study. However, because the solidity ratio along the strong axis was relatively large (around 0.5), the crosswind aerodynamic damping results might have been more representative of the behavior of the spine rather than the lattice tower. Therefore, more research is required in order to develop an analytical procedure to quantify the crosswind aerodynamic damping on lattice structures. Such procedure could then be adopted in guidelines that address lattice structures by themselves as well as those used as part of larger electrical transmission systems.

2.3.3 Buffeting Theory and Comparison between Analytical and Experimental Results

This section discusses the theoretical buffeting of a flexible tower line-like structure. By conducting a buffeting analysis on the response of the tower in both longitudinal and transverse directions, one can estimate the theoretical root-mean-square (RMS) values of acceleration, base shear, and base moment fluctuations. Consequently, values could be compared with experimentally recorded ones by the 3-axis accelerometers and the 6-DOF load cell. However, in order to perform the buffeting analysis on the lattice tower, some assumptions need to be made first:

- The different elements and angles of the lattice tower are significantly small in cross-section that they do not greatly disturb the flow.
- Using a quasi-steady approach, the fluctuating wind loads can be determined from the aerodynamic force coefficients measured in a steady flow.
- The motions involved in the natural modes of vibration are purely in the along-wind direction. The analysis will be done for two along-wind directions: 0^o and 90^o, i.e., along both strong and weak axes, respectively.
- In calculating the RMS of accelerations, the lattice tower is treated as a 1-DOF rectangular cylindrical spine with a fixity at the bottom. The tower assumes all the physical and geometric properties of the spine.
- In calculating the RMS of base shears and base moments, equations specifically developed by Loredo-Souza (1996) are adopted and comparisons are made with measured values. Modifications to the equations developed by Loredo-Souza (1996) are then proposed in this study.

In its most simplified form, the power spectrum of deflection S_q at the top of the tower is given by Equation 2.14 [(Davenport, 1962a); (Davenport, 1962b); (Irwin, 1977); (Irwin, 1979); (Irwin, 1996)]:

$$S_q(n) = \frac{(\rho . U . C_{x0} . A)^2}{M_G^2 \omega_0^4} . \left| H\left(\frac{n}{n_0}, \zeta_{tot}\right) \right|^2 . \left|\chi_y(n)\right|^2 . |\chi_{2D}(n)|^2 . S_u(n) \qquad (2.14)$$

In Equation 2.14, the density of air ρ is in kg/m^3, the wind speed U at tower height h is in m/s, C_{xo} is the drag coefficient of the spine, the frontal area of the spine A is in m^2, the total mass of the system M_G is in kg and the angular frequency of the system ω_o is in rad/s. Furthermore, n *and* n_o are the forcing and natural frequencies in Hz, ζ_{tot} is the total

damping of the structure (i.e., the structural plus the aerodynamic) (estimated in section 3.2), $H\ (n/n_o\ ,\ \zeta_{tot})$ is the mechanical admittance function, $\chi_y(n)$ and $\chi_{2D}(n)$ are the lateral and two-dimensional aerodynamic admittance functions, respectively. Additionally, $S_u(n)$ is the power spectrum of the longitudinal velocity time history. If Equation 2.14 is integrated over all frequencies, one can obtain the variance of the deflection fluctuations σ_q^2 from the power spectrum and the RMS of the deflection σ_q can then be expressed in terms of background and resonant terms using Equation 2.15.

$$\sigma_q = \frac{\rho.U^2.C_{x0}.A.I_u}{M_G.\omega_0^2}.\sqrt{B+R} \tag{2.15}$$

where I_u is the longitudinal turbulence intensity. B and R are the background and resonant terms. Subsequently, using structural dynamics principles, the RMS of acceleration σ_{acc} may be obtained by multiplying Equation 2.15 by the square of the angular frequency ω_o, as shown in Equation 2.16.

$$\sigma_{acc} = \frac{\rho.U^2.C_{x0}.A.I_u}{M_G}.\sqrt{B+R} \tag{2.16}$$

The background and resonant responses (B and R) are defined in Equations 2.17 and 2.18, respectively.

$$B = \int_0^{+\infty} \left|\chi_y(n)\right|^2.|\chi_{2D}(n)|^2.\frac{S_u(n)}{\sigma_u^2}.dn \tag{2.17}$$

$$R = \left|\chi_y(n_o)\right|^2.|\chi_{2D}(n_o)|^2.\frac{n_0.S_u(n_0)}{\sigma_u^2}.\frac{\pi}{4.\zeta_{tot}} \tag{2.18}$$

with σ_u^2 being the variance of the velocity time history. Note that n_o is the natural frequency of the structure in the relevant mode shape. The rest of the parameters of Equations 2.17 and 2.18 are defined in Equations 2.19 and 2.20.

$$\left|\chi_y(n)\right|^2.|\chi_{2D}(n)|^2 = \frac{8}{\eta_b^2.\eta_d^2.\eta_L^2}.(\eta_b - 1 + e^{-\eta_b}).(\eta_d - 1 + e^{-\eta_d}).(\eta_L - 1 + e^{-\eta_l}) \quad (2.19)$$

$$\frac{n_0.S_u(n_0)}{\sigma_u^2} = \frac{4.\frac{n_0.\ {}^xL_u}{U}}{(1 + 70.78(\frac{n_0.\ {}^xL_u}{U})^2)^{5/6}} \quad (2.20)$$

In the previous equations, η_b, η_d and η_L are parameters linked to the width, depth and length of the structure and defined in Equations 2.21, 2.22 and 2.23. ${}^xL_u$, ${}^yL_u$ and ${}^zL_u$ are the integral length scales of longitudinal, lateral, and vertical components of turbulence in m, respectively, whereas d is the depth of the spine (in m). Likewise, θ can be taken as 0.75 and b as well as L are the width and length of the rectangular spine in m [(Irwin, 1977); (Irwin, 1979); (Irwin, 1996)]:

$$\eta_b = 0.95\theta.\frac{b}{{}^xL_u}.(1 + 70.78(\frac{n.\ {}^xL_u}{U})^2)^{1/2} \quad (2.21)$$

$$\eta_d = 0.475\theta.\frac{d}{{}^zL_u}.(1 + 70.78(\frac{2n.\ {}^zL_u}{U})^2)^{1/2} \quad (2.22)$$

$$\eta_L = 0.475\theta.\frac{L}{{}^yL_u}.(1 + 70.78(\frac{2n.\ {}^yL_u}{U})^2)^{1/2} \quad (2.23)$$

Estimation of Tower Acceleration: By using Equation 2.16, the RMS of acceleration time histories σ_{acc} are calculated for different wind speeds and values are compared with their experimental counterparts. Fig. 2.12 showcases the results of the buffeting analysis along with the experimental values of the RMS of accelerations, recorded by the sensors for two wind directions: 0^o and 90^o.

It can be observed in Fig. 2.12, at 0^o wind direction, the analytical and measured responses show almost complete agreement for all reduced velocity values. There is a slight discrepancy that starts to appear at $U/(n.B)$ values above 9. This is explained by the

fact that, at higher wind speeds, the frequency of the structure tends to become slightly lower, thereby increasing the measured RMS of accelerations. This was observed while using the ILS method, as the outputs of the latter are the stiffness and damping matrices. With increasing wind speeds, the stiffness matrix K^{eff} was observed to slightly reduce, thereby decreasing the natural frequency of the tower. In the analytical solution, the natural frequency of the structure was assumed to remain constant for all wind speeds, which could lead to slightly lower calculated values. Another justification to this minor discrepancy could be due to the extra self-generated turbulence of the model itself, which the buffeting theory does not account for. At 90^o wind direction, there is a very good agreement between the measured data and the analytical model at lower speeds. However, some divergences start to appear with increasing wind speeds. This is explained by the observed crosswind vibrations of the model during the wind tunnel testing. As such, this phenomenon would reduce the deflection of the model in the along-wind direction (90^o), thereby reducing the recorded values of σ_{acc}. Since the buffeting theory only addresses along-wind responses, this phenomenon is not accounted for. Nonetheless, the measured and calculated values are very satisfactory for both analyzed wind directions.

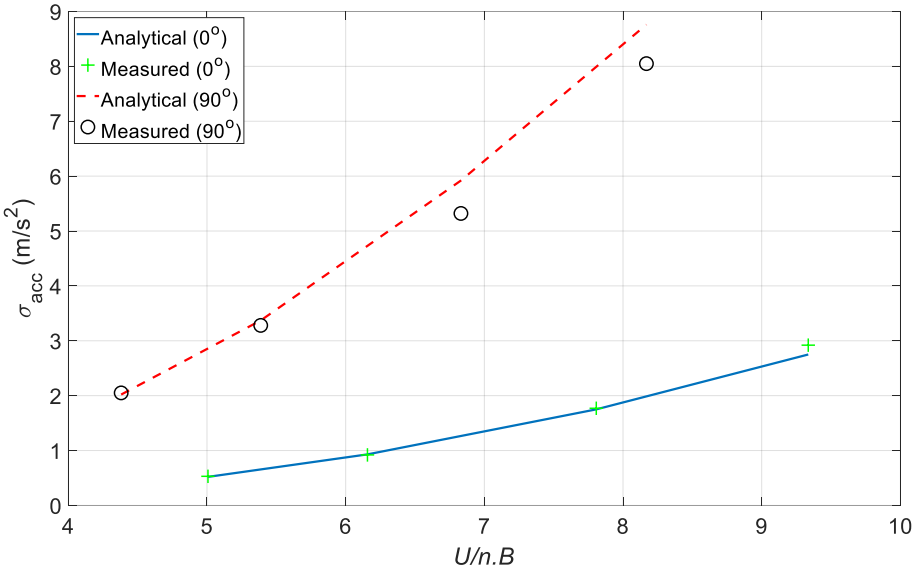

Fig. 2.12: Comparison of analytical and measured RMS of accelerations for 0º and 90º

Estimation of Tower Base Shear and Tower Base Moment: Similarly, a buffeting analysis is conducted in order to estimate the RMS of base shears and base moments at different wind speeds, acting on the lattice structure. According to Loredo-Souza (1996) and Loredo-Souza and Davenport (2003), the total fluctuating response (RMS) of forces on a self-supported lattice tower is equal to the square root of the sum of the squares of the background and resonant responses, as shown in Equation 2.24. The expressions for the background and resonant responses are given in Equations 2.25 and 2.26:

$$\sigma_{for} = \sqrt{\sigma_{B,for}^2 + \sigma_{R,for}^2} \tag{2.24}$$

$$\sigma_{B,for}^2 = (\rho . U_h^2 . I_u)^2 . I_1 \tag{2.25}$$

$$\sigma_{R,for} = \sqrt{\frac{\pi}{4} . \frac{n . S_F(n)}{\zeta_{tot}}} . \frac{\int_0^h m(z) . \mu_j(z) . i(z) . dz}{\int_0^h m(z) . \mu_j^2(z) . dz} \tag{2.26}$$

In Equation 2.25, U_H is the mean wind speed at tower height h in m/s and I_1 is the value of the first double integral, defined in Equation 2.27. Similarly, in Equation 2.26, $n.S_F(n)$

is the spectra of the generalized force, given in Equation 2.28 and $m(z)$, $\mu_j(z)$, and $i(z)$ are the respective mass, mode shape and influence line per zone z along the height of the tower.

$$I_1 = \int_0^h \int_0^h C_D(z)C_D(z')\phi(z)\phi(z')\left(\frac{z}{h}\right)^{\alpha}\left(\frac{z'}{h}\right)^{\alpha} e^{-\left(\frac{\Delta z}{z_{L_u}}\right)} i(z)i(z')w(z)w(z')dzdz' \quad (2.27)$$

$$n.S_F(n) = (\rho.\overline{U}_h^2.I_u)^2.\frac{n_0.S_u(n_0)}{\sigma_u^2}.|\chi_{2D}(n_o)|^2.I_2 \quad (2.28)$$

In Equations 2.27 and 2.28, $C_D(z)$, $\phi(z)$, and $w(z)$ are the drag coefficient, solidity ratio and average width of zone z, α is the wind shear exponent for open-terrain exposure and Δz is the difference in heights between two zones z and z' along the vertical axis of the tower. Note that, for influence lines pertaining to base shear calculation, $i(z)$ of each zone is equal to 1 (Loredo-Souza, 1996). I_2 is the value of the second double integral, given in Equation 2.29.

$$I_2 = \int_0^h \int_0^h C_D(z)C_D(z')\phi(z)\phi(z')\left(\frac{z}{h}\right)^{\alpha}\left(\frac{z'}{h}\right)^{\alpha} e^{\frac{-c|\Delta z|n_o}{U_{0.5h}}} \mu_j(z)\mu_j(z')w(z)w(z')dzdz' \quad (2.29)$$

In Equation 2.29, c is the exponential decay factor for "narrow band" correlation (usually taken as 7) and $U_{0.5h}$ is the mean wind speed at mid-height of the tower ($0.5h$) in m/s. As such, the RMS of the base shear force fluctuations σ_{for} are calculated using Equation 2.24 and the theoretical and measured results are plotted in Fig. 2.13 for comparison. The values of σ_{for} have been converted to full-scale using the appropriate factor from Table 2.1 ($\lambda_F = 50^3$). Note that "Analytical" in the legend of Fig. 2.13 corresponds to the values calculated from Equations 2.24 through 2.29, developed by Loredo-Souza (1996) and Loredo-Souza and Davenport (2003).

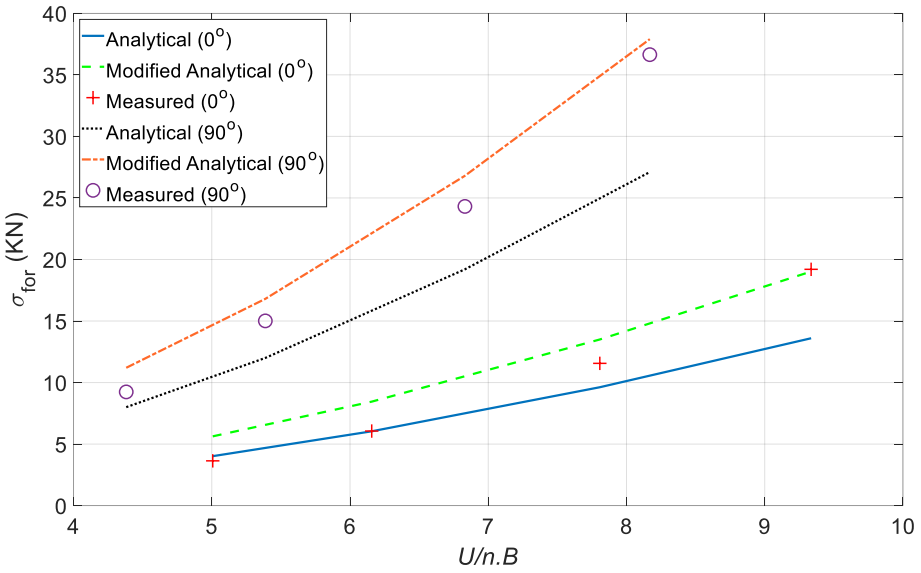

Fig. 2.13: Comparison of analytical and measured RMS of forces for 0° and 90°

As shown in Fig. 2.13, the "Analytical" values of σ_{for} estimated using Equations 2.24 through 2.29 tend to underestimate the measured response of the aeroelastic model at almost all tested wind speeds. This observation is evident, especially at 90° wind direction, where the divergence becomes wider with increasing wind speeds. At 0° wind direction, the analytical results show good agreement at low values of $U/(n.B)$.

The discrepancies between the measured and calculated σ_{for} can be attributed to the turbulence intensity I_u factor at tower height h, shown in Equations 2.25 and 2.28. Typically, the turbulence intensity is much higher near ground surface and reduces exponentially with increasing height. As such, this change in intensity should be accounted for in the equations, in order to get a more realistic estimate of the response of the lattice tower. This would translate into higher calculated values, especially in the lower zones of the tower, potentially resulting in better agreement with the measured response using the 6-DOF load cell. Based on the two cobra probe measurements collected in the experiments of the current study and with the help of some estimation from ESDU item 85020

(2001) full-scale turbulence intensity approximation, the authors suggest the use of Equation 2.30 for the estimation of I_u at any height z:

$$I_u(z) = I_u(h).(\frac{z}{h})^{\gamma} \tag{2.30}$$

Similarly, to the power law used in the wind speed estimation at any height z, Equation 2.30 could be used for the estimation of I_u. In the present tests, the exponent γ was found to be approximately equal to -0.15. Consequently, the terms $(z/h)^{-0.15}$ and $(z'/h)^{-0.15}$ were added to the double integral values I_1 and I_2 in Equations 2.27 and 2.29 and the buffeting analysis was conducted again. Calculated responses are also plotted in Fig. 2.13. Note that "Modified Analytical" refers to the initial equations proposed by Loredo-Souza (1996) and modified by the WOW team.

As can be observed in Fig. 2.13, although the values obtained using the modified analytical equations show slightly larger numbers at low wind speeds, the agreement is far better than the initial equations developed by Loredo-Souza (1996). At high wind speeds, the convergence between measured and calculated responses is almost perfect. Additionally, from a structural design point of view, the modified analytical equations are more conservative and hence, the authors strongly recommend the inclusion of the change in turbulence intensity along the height of the structure. Therefore, considering the previous suggestions, Equations 2.27 and 2.29 should be rewritten as follows:

$$I_1 = \int_0^h \int_0^h C_D(z)C_D(z')\phi(z)\phi(z')\left(\frac{z}{h}\right)^{\alpha+\gamma}\left(\frac{z'}{h}\right)^{\alpha+\gamma} e^{-\left(\frac{\Delta z}{\frac{z}{L_u}}\right)} i(z)i(z')w(z)w(z')dzdz' \tag{2.31}$$

$$I_2 = \int_0^h \int_0^h C_D(z)C_D(z')\phi(z)\phi(z')\left(\frac{z}{h}\right)^{\alpha+\gamma}\left(\frac{z'}{h}\right)^{\alpha+\gamma} e^{\frac{-c|\Delta z|n_o}{U_{0.5h}}} \mu_j(z)\mu_j(z')w(z)w(z')dzdz' \tag{2.32}$$

Lastly, from the previous equations, one can obtain the theoretical RMS of base moments from that of the base shear by incorporating the height of the tower and using the appropriate values for the influence lines *i(z)*. In Equations 2.25 and 2.28, the term $(\rho.U_h.I_u)^2$ becomes $(\rho.U_h.I_u.h)^2$. This multiplication of the force by the distance to the base of the tower will yield the overturning moment. Note that, for influence lines pertaining to base moment calculation, *i(z)* is equal to the height of the zone *z* divided by the total height of the tower *h* (or *z/h*) (Loredo-Souza, 1996). Fig. 2.14 shows a comparison between measured and calculated base moments. Once again, the full-scale values were utilized by multiplying with the appropriate factors from Table 2.1 ($\lambda_M = 50^4$).

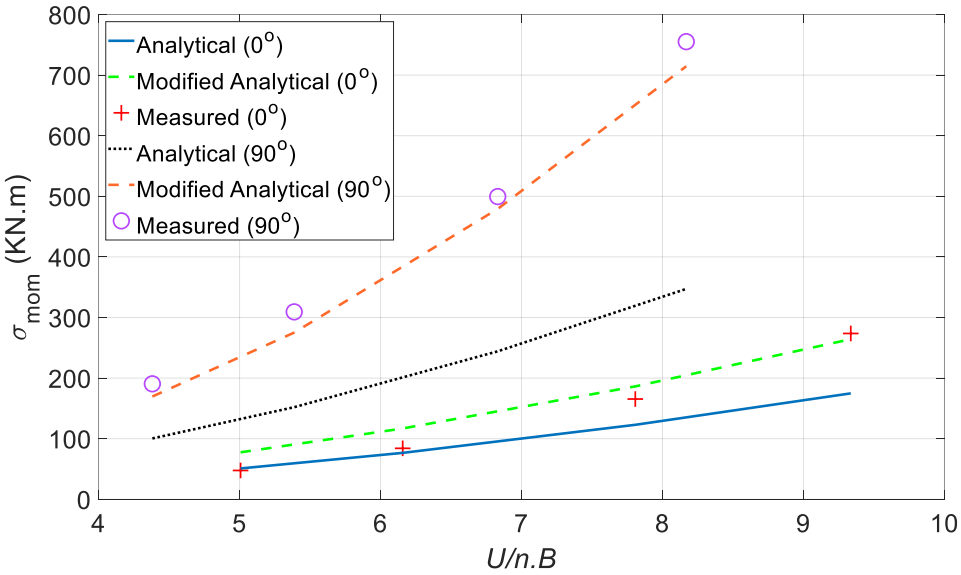

Fig. 2.14: Comparison of analytical and measured RMS of moments for 0° and 90°

As shown in Fig. 2.14, there is very good agreement at 0° wind direction. Values are almost equal for all tested wind speeds. For 90° wind direction, the analytical model slightly underestimates the measured response. As previously mentioned, this could be due to the self-generated wake turbulence of the tower, which is not accounted for in the equations used for the analytical estimation. Nonetheless, the agreement is very satisfac-

tory for the RMS of accelerations, base shears, and base moments at all wind speeds and for both wind directions adopted.

2.3.4 Drag and Moment Coefficients

This subsection discusses the calculation of the drag and moment coefficients from the measured strain data in the wind tunnel testing and subsequent comparison with values proposed by standards from different institutions around the world. Theoretically, according to ASCE 7 (2016), the drag coefficient C_D and the moment coefficient C_M are given in Equations 2.33 and 2.34, respectively:

$$C_D = \frac{F_D}{\frac{1}{2}\rho.U^2.A} \tag{2.33}$$

$$C_M = \frac{M_o}{\frac{1}{2}\rho.U^2.A.h} \tag{2.34}$$

In Equations 2.33 and 2.34, F_D is the mean drag force in N, M_o is the mean overturning moment in N.m (at the base), A is the net area in m^2, and h is the height of the structure in m. The rest of the parameters were defined earlier.

Experimentally, the drag coefficients can be estimated based on the data collected from the strain gauges installed on different parts of the spine. By definition, the maximum bending stress at any point in a structure can be expressed using Equation 2.35.

$$\sigma = \frac{M.c}{I} \tag{2.35}$$

In Equation 2.35, M is the measured bending moment at the point of location in N.m, c is the distance from the extreme most fiber to the centroid of the section in m, and I is the moment of inertia of the section about the axis of bending in m^4. Using Hook's law and

assuming that the spine section of the tower remains elastic, Equation 2.36 (Azzi et al., 2020b) can be used to obtain the strain at any point:

$$\varepsilon = \frac{M.b}{2E.I} \tag{2.36}$$

In Equation 2.36, ε is the strain in the direction of the loading, E is the modulus of elasticity of the spine in N/m^2 and b is the distance to the centroid in m. Additionally, the moment coefficients C_M can be experimentally obtained from the base moments recorded by the load cell at the base of the lattice tower.

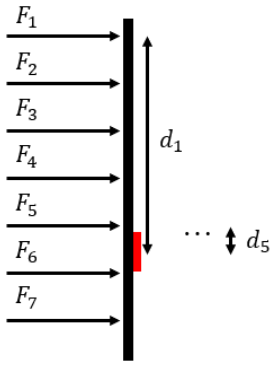

Fig. 2.15: Forces applied on the spine (strain gauge shown in red)

Fig. 2.15 shows a sketch of the forces acting on the spine. Recall that during the design stage of the model and more specifically the cladding elements, the tower geometry was divided into seven zones. Each zone had its own drag coefficient, based on its solidity ratio. For the sake of this study, the drag coefficients of the entire tower are assessed with respect to both wind speeds and directions.

From Fig. 2.15, the measured bending moment M at the location of the strain gauge mounted on the spine can be expressed using Equation 2.37 (Azzi et al., 2020b):

$$M = \sum_{i=1}^{5} F_{Di}.d_i = \sum_{i=1}^{5} \frac{1}{2}\rho.A_i.C_D.U_i^2.d_i = \frac{1}{2}\rho.C_D.\sum_{i=1}^{5} A_i.U_i^2.d_i \tag{2.37}$$

In Equation 2.37, i represents the zone number above the strain gauge, U_i is the wind speed at the height of the zones in m/s, A_i is the area of the elements in the plane perpendicular to the wind direction in zone i in m^2 and d_i is the distance from the strain gauge to the point of application of the force on zone i, in m. Note that a total of five zones are above the strain gauge portrayed in red in Fig. 2.15. Combining Equations 2.36 and 2.37, the drag coefficient can be obtained experimentally using Equation 2.38:

$$C_D = \frac{4.\epsilon.E.I}{b.\rho.\sum_{i=1}^{5} A_i.U_i^2.d_i} \tag{2.38}$$

Similarly, and for squared trussed towers as in the case of lattice towers, ASCE 7 (2016), ASCE 74 (2010), and ANSI/TIA-222 (2005) suggest Equation 2.39 for the calculation of the force coefficients (or drag coefficients per zone). Equation 2.39 presents C_D as a function of the solidity ratio ϕ, which is defined as the ratio of the solid or net area to the gross area of the tower zone, in the direction of the loading. Additionally, the BS EN (2006) suggests Equation 2.40 for the calculation of the drag forces on the tower. Note that the previous standards suggest such equations for any tower zone, regardless of its shape. Also note that the solidity ratio for each wind direction tested was calculated as an average for the entire tower.

$$C_D = 4\phi^2 - 5.9\phi + 4 \tag{2.39}$$

$$C_D = 3.96\phi^2 - 5.94\phi + 3.96 \tag{2.40}$$

Fig. 2.16a shows a comparison between the drag coefficients obtained using the experimental strain gauge data and the ones specified by the standards. Examining Fig. 2.16a, it can be seen that the experimental values of C_D obtained are well in agreement with values obtained using Equations 2.39 and 2.40. This trend is seen for all experi-

mental values except for a solidity ratio ϕ of 0.47, i.e., at a wind direction of 0^o, where the drag coefficient C_D obtained from the experiment was almost half the value suggested by the standards. Nevertheless, for the rest of the wind directions, the C_D values were well in range of the theoretically suggested ones.

Since lattice towers are truss structures, design standards treat them as perfect trusses with frictionless hinged connections in between angles and members. Therefore, to the authors' best knowledge, no previous studies addressed the moment coefficients in the design of lattice structures.

However, the actual type of connection between such truss members might differ. Previous researchers have shown that typical truss connections could be single bolted, multiple bolted or welded using a gusset plate, or any combination of welds and bolts. Such connection types often have a degree of rigidity, therefore introducing potential bending moments and possible twist. [(da Silva et al., 2005); (Zhangqi et al., 2014); (Axisa et al., 2017)]. After plotting the moment coefficients obtained, it was decided to use a fitting toolbox in order to obtain the best trendline.

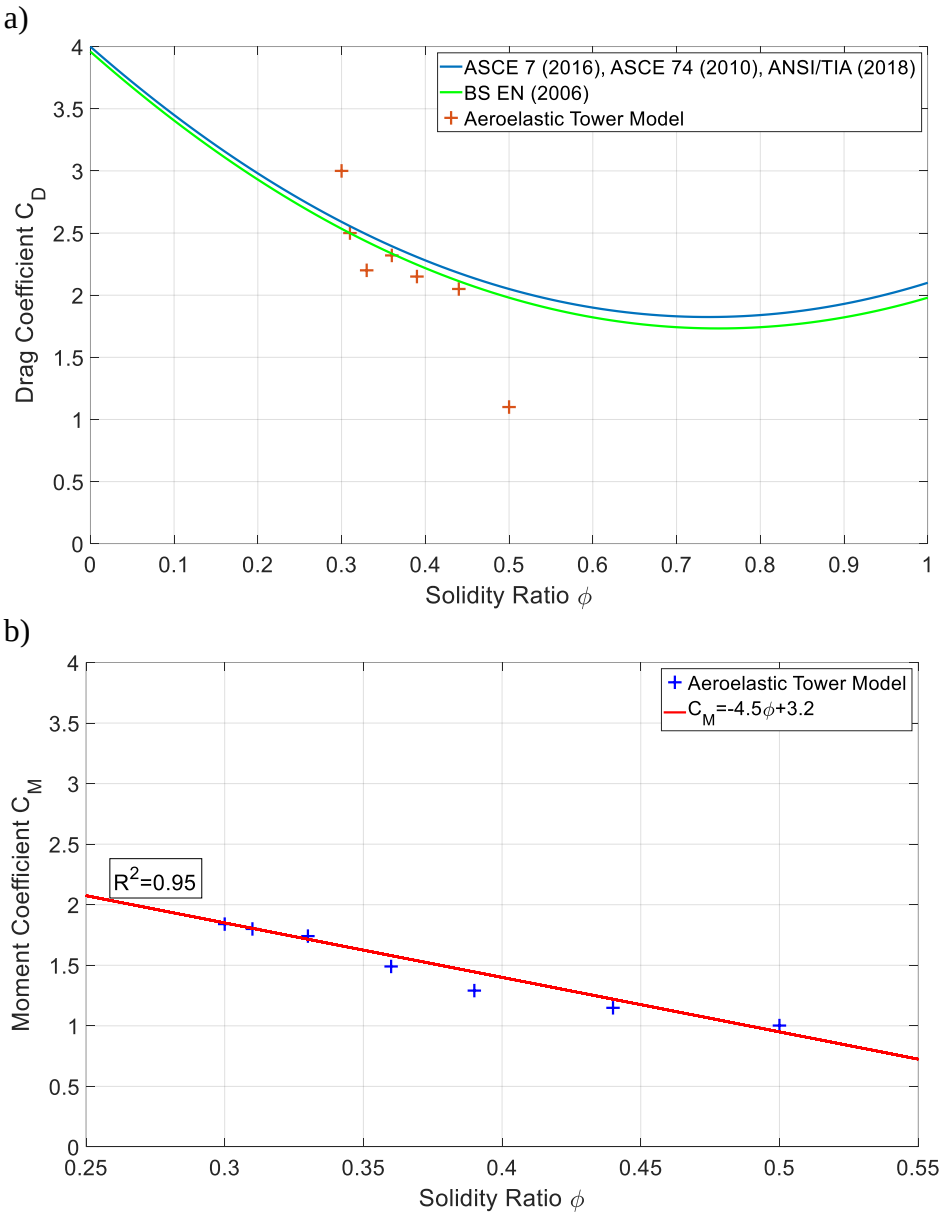

Fig. 2.16: Values of: a) drag coefficient C_D, and b) moment coefficient C_M

Consequently, it was observed that values of C_M tend to linearly decrease with the increase of the solidity ratio. Therefore, a first-degree polynomial equation is proposed with a R-squared value of 0.95, linking the moment coefficient to the solidity ratio. The latter is presented in Equation 2.41 and plotted in Fig. 2.16b:

$$C_M = -4.5\phi + 3.2 \tag{2.41}$$

It is worthwhile noting that, typically, the solidity ratio of lattice towers ranges between 0.2 and 0.6. For the tower tested at the WOW, the solidity ratio ranged between 0.3 and 0.5. Therefore, Equation 2.41 might be only valid for the range of solidity ratios tested in this project. Thus, more research and testing are required in order to better understand the behavior of truss joints and to provide a better moment coefficient equation for design purposes. This would potentially reduce the failure of connection members in lattice structures, which are commonly used not just in civil engineering as transmission towers, but also in telecommunication as radio towers and mechanical engineering as wind turbine supports amongst others.

2.3.5 Dynamic Amplification Factors

This last subsection discusses the dynamic amplification factors (DAF) relative to lattice structures. This factor defines the ratio between the maximum peak and the quasi-static responses. According to Elawady et al. (2017) and Azzi et al. (2020c), the DAF is given in Equation 2.42:

$$DAF = \frac{Maximum\ Peak\ Response}{Maximum\ Quasi\text{-}static\ Response} \tag{2.42}$$

In Equation 2.42, the quasi-static response is the summation of the mean and the background responses. Note that on the one hand the resonant response is associated with resonant amplification due to components (forces or moments) with frequencies close or equal to the fundamental natural frequency of the structure in the desired mode. On the other hand, the background response involves no resonant amplification [(Simiu and Yeo, 2019); (Azzi et al., 2020c)].

However, it should be noted that the entire procedure revolves around the concept that the fluctuating response is excited by the fluctuating wind field. In brief, the following steps were adopted in the calculation of the DAF [(Elawady et al., 2017); (Azzi et al., 2020c)]:

1. In order to distinguish between the background and resonant components, the PSD of the fluctuating response (peak response minus mean response) and the corresponding frequencies are calculated and plotted with the application of a Fast Fourier Transform (FFT).
2. At each identified frequency, the cumulative PSD is computed and subsequently normalized by the variance of the PSD of the fluctuating response. At the highest frequency of the response itself, the cumulative PSD takes a maximum value of 1.0.
3. The average slope s_{cum} of the common logarithmic values of two successive data points in the cumulative PSD is calculated. The same is applied to the logarithmic values of two successive data points of the PSD of the fluctuating response (s_{flu}).
4. The ratio between s_{flu} and s_{cum} is evaluated, and the resonance frequencies are distinguished when this ratio exceeds a chosen threshold value R. A trial and error basis is utilized in the determination of R and a value is selected when the resonance contribution remains the same. This suggests that when $s_{flu}/s_{cum} > R$, the developed approach marks this frequency as a resonance frequency.
5. Once all the resonance frequencies have been identified, a Bandstop filter is adopted to separate the resonance frequencies from the fluctuating response. The result of that process is the background response.

The previously described procedure is applied for all tested wind angles and wind speeds. Values of DAF are generated for the forces and moments acting on the lattice tower as well as for axial forces in the cross-arms. Fig. 2.17a shows a sample of the signal decomposition process that was applied. This figure shows the decomposition of the base moment M_y. Fig. 2.17b shows a zoomed in plot of the resonance detected in Fig. 2.17a. More information and detailed description on the DAF method is available in Elawady et al. (2017).

Some response measurements have shown a high contribution of the resonant component while others did not. As can be seen in Fig. 2.17a, the slope of the cumulative PSD of the base moment about the weak axis (drawn in green) shows a sudden steep behavior when the resonance is detected (blue circles) around the natural frequency of the structure (mode shape 1, around 16 Hz, Table 2.2). This means that the resonant component significantly contributes to the structural response at that particular frequency. This can be seen in Fig. 2.17b where the resonance is detected between about 13 and 16.5 Hz (blue circles). Similarly, the DAF for the rest of the responses (F_x, F_y, M_x, M_y, P_{arm}) are plotted in Fig. 2.18.

The DAF seems to range between 1.01 and 1.18. It can be seen that the DAF of the base shears F_x and F_y are decreasing with increasing wind speeds. This is due to the increase in the aerodynamic damping which was reported in the previous sections. This phenomenon could be slightly suppressing the resonant component, thereby reducing its contribution to the total response of the entire structure. On another note, the DAF of the base moments M_x and M_y are shown to increase with increasing wind speeds. The previously mentioned excessive vibrations observed at particularly higher wind speeds, espe-

cially in the crosswind direction, might have played a role in altering the behavior of the DAF of the moments, thereby overshadowing the effect of the increase in the aerodynamic damping.

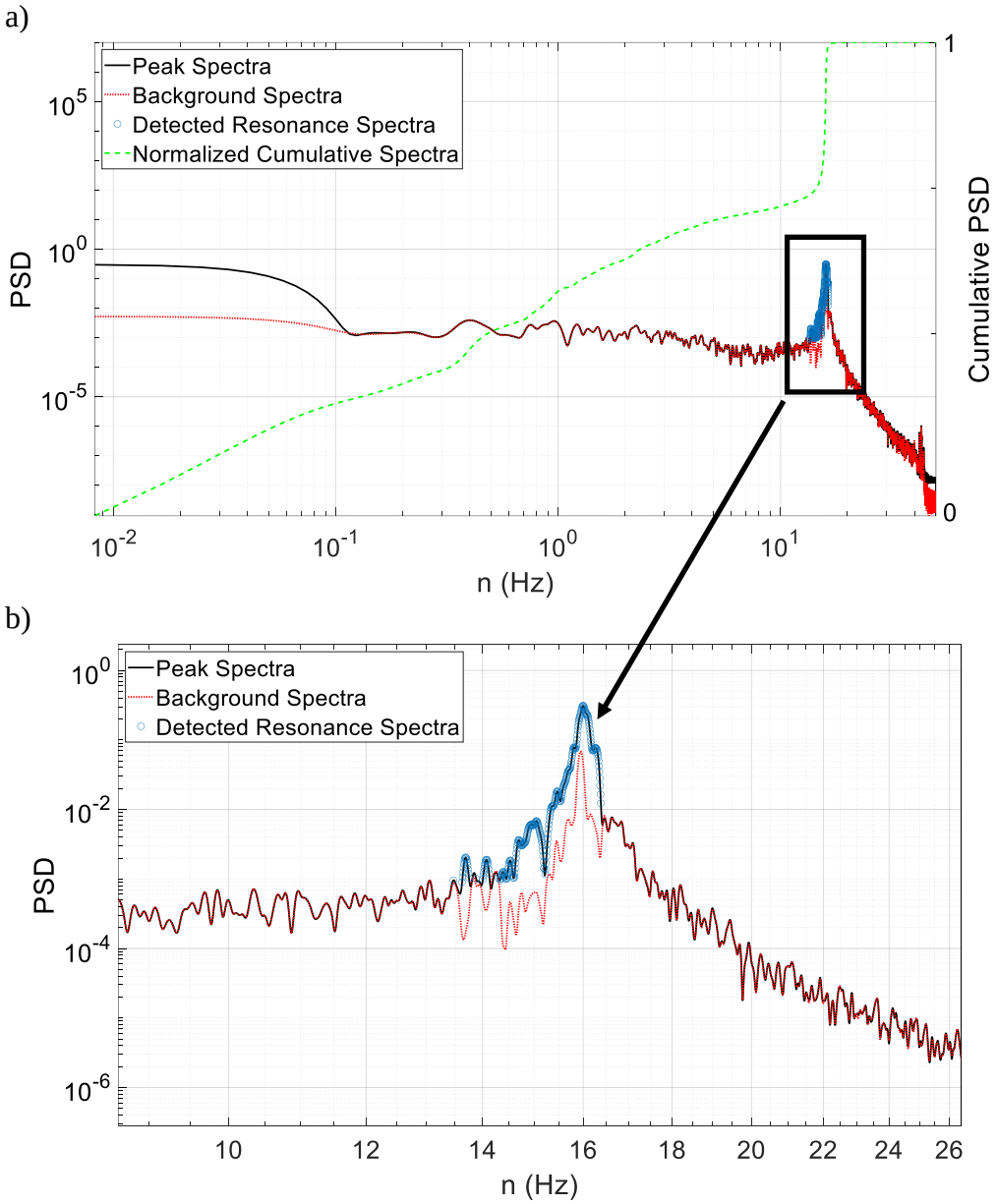

Fig. 2.17: Decomposition of the base moment M_y time history (about weak axis): a) initial plot, and b) resonance detection (zoomed in plot of Fig. 2.17a)

Finally, the values of the DAF of the cross-arm force P_{arm} are also shown to increase with increasing wind speeds. This was also observed by Elawady et al. (2017) for

the case of a single lattice structure. This is possibly due to the relatively higher flexibility of the cross-arm system compared to other zones in the tower structure. Since such a tower configuration is typically used as part of a tower-insulator-conductor transmission line system, the absence of the conductors (which are typically attached to the cross-arms and provide lateral bracing at the insulator-conductor connection points) might have led to excessive vibrations and bending in the cross-arm itself. Subsequently, the increase in the resonant contribution to the total response of the cross-arms is to be expected with increasing wind speeds.

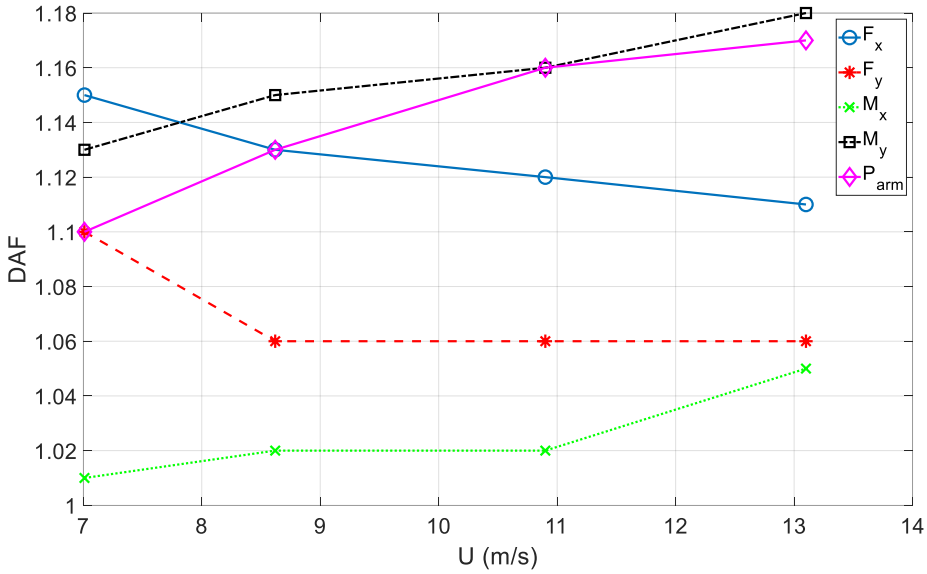

Fig. 2.18: DAF for base shears, base moments, and cross-arm force for all tested wind speeds

In comparison with previous works in the literature, Aboshosha et al. (2016) reviewed some of the current standards regarding dynamic and quasi-static buffeting response of transmission lines under synoptic and non-synoptic winds. According to the authors, ASCE 74 (2010), AS/NZS 1170.2 (2011) and BS 50341 (2001) have established a tower and conductor gust response factors G_T and G_C, respectively, in order to account for any dynamic effects on lattice towers used as transmission lines as well as electrical

conductors. For this study, the current interest rests with the tower gust response factor G_T. AS/NZS 1170.2 (2011) and BS 50341 (2001) define G_T as a constant for all wind speeds taken as 1.0 and 1.05, respectively. ASCE 74 (2010) uses Equation 2.43 to obtain G_T:

$$G_T = \frac{1 + 2.7E.\sqrt{B_T}}{K_u^2} \tag{2.43}$$

In Equation 2.43, K_u refers to the ratio of the 3-sec gust wind speed to the 10-min average wind speed (usually taken as 1.43) while parameters E and B_T are given in Equations 2.44 and 2.45:

$$E = 4.9.\sqrt{\kappa}.(\frac{33}{z_h})^{1/\alpha_{ter}} \tag{2.44}$$

$$B_T = \frac{1}{1 + \frac{0.56z_h}{L_s}} \tag{2.45}$$

The rest of the parameters of Equations 2.44 and 2.45 are given in ASCE 74 (2010) section 2.1.5.1 for different exposure categories. Using the values proposed in ASCE 74 (2010) for open terrain exposure, the value of G_T for the transmission tower tested in this project comes out to about 0.88. This value is less than the ones proposed in the rest of standards. In addition, it is also much smaller than the obtained DAF in Fig. 2.18, which might imply that dynamic effects on lattice structures used as transmission lines might still not be fully understood. More studies and testing are required in order to determine a DAF estimate to be implemented in such standards in order to reduce potential future failures of such structures.

2.4 Conclusion

An aeroelastic design and testing of a single self-supported lattice tower subjected to simulated high winds at the NHERI WOW EF was presented. The lattice tower considered is a typical structure that is used as part of a tower-insulator-conductor system for electrical transmission. The model was first designed and validated using FEM analysis, then constructed using a spine structure and non-structural cladding elements. The spine structure represented the elastic flexural and torsional properties of the tower whereas the cladding elements formed its aerodynamic shape. The model length and velocity scales selected were 1:50 and 1:7.07, respectively. The tower was instrumented with accelerometers, load cells and strain gauges at different locations. A free vibration test was conducted prior to wind load testing in order to verify the dynamic properties of the system corresponding to the first two modes. The tower was tested at various wind speeds ranging between 50 and 92 m/s (prototype speeds) for wind directions varying from 0^o to 90^o. Moreover, two techniques (ILS and RD) were utilized, modified as needed, and applied to the measured responses in order to estimate the aerodynamic damping of the structure at various wind speeds. Furthermore, a buffeting analysis was conducted in order to estimate the analytical responses of the structure and compare them with their measured counterparts. Similarly, drag and moment coefficients as well as DAF were computed from the measured responses. Drag coefficients were compared to design standards. For the DAF, a signal decomposition procedure was adopted to extract the resonance contribution from the total response of the tower. That procedure was applied to the base shear and base moment recorded time histories as well as cross-arm axial forces.

The major findings from this research are summarized below:

- The along-wind aerodynamic damping coefficients obtained from the ILS and RD techniques were in very good agreement with their analytical counterparts for both directions. In addition, the same techniques were implemented in the crosswind direction and results showed a similar trend to previously published works on tall buildings having the same length to width ratio as the spine. The along-wind aerodynamic damping is proportional to the increase in wind speeds whereas its crosswind counterpart could be related to the length to width ratio of the tower itself based on results analyzed at the WOW. However, as previously indicated, crosswind results might have been dominated by the behavior of the spine rather than that of the lattice tower. Later, the along-wind aerodynamic damping coefficients were used for the buffeting analysis.
- The buffeting theory for along-wind estimation of the responses showed good agreement with the measured RMS responses of the tower. It was found that incorporating the change in turbulence intensity along the height yields significant improvements over the traditional analytical approach developed by Loredo-Souza (1996). However, some discrepancies were observed at higher wind speeds, possibly due to the self-generated turbulence of the model which is not accounted for in the buffeting theory.
- The drag coefficients were in good agreement with values proposed by many standards adopted around the world. Similarly, moment coefficients were proposed in this study in order to account for any bending moments that might occur in members of lattice structures where the connection

could be qualified as somewhat rigid. Such aspect of the design of lattice structures is currently not incorporated in standards around the world.

- Calculated values of the DAF showed that the resonant response of the tower is in the order of 1% to 18% for all measurements. DAF of forces were somewhat reducing with increased wind speeds and such phenomenon was attributed to the increase in the aerodynamic damping with increase in wind speed, suppressing the resonant response. DAF of moments and cross-arm forces were increasing with increase in wind speed due to the extensive vibration of the spine and the absence of lateral bracing at the cross-arm level.
- Obtained DAF were typically higher than G_T values proposed by different standards around the world, signifying that the resonant contribution in the total response of lattice structures is not yet fully understood by researchers.

More testing is required on the response of lattice towers to hurricane wind speeds in order to come up with code specific values of DAF to account for the dynamic response of such structures.

2.5 Chapter II References

Aboshosha, H., Elawady, A., El Ansary, A., and El Damatty, A. (2016). "Review on dynamic and quasi-static buffeting response of transmission lines under synoptic and non-synoptic winds." Engineering Structures, 112, 23-46.

American National Standards Institute (ANSI) / Telecommunications Industry Association (TIA), ANSI/TIA-222-G (2005). "Structural Standard for Antenna Supporting Structures and Antennas." Standards and Technology Department, Arlington, VA, U.S.A.

American Society of Civil Engineers (ASCE) 7 (2016). "Minimum Design Loads and Associated Criteria for Buildings and Other Structures." ASCE/SEI 7-16, Reston, VA.

American Society of Civil Engineers (ASCE) 74 (2010). "Guidelines for electrical transmission line structural loading." ASCE manuals and reports on engineering practice, No. 74, New York, NY, USA.

Australian/New Zealand Standard (AS/NZS) 1170.2 (2011). "Structural design actions – Part 2: wind actions." SAI Global Limited, Standards Australia Limited, GPO Box 476, Sydney, NSW 2001, Standards New Zealand, PO Box 1473, Wellington 6140.

Australian Standard (AS) 3995 (1994). "Design of steel lattice towers and masts." Standards Association of Australia, The Crescent, Homebush, NSW 2140.

Axisa, R., Muscat, M., Sant, T., and Farrugia, R. N. (2017). "Structural assessment of a lattice tower for a small, multi-bladed wind turbine." International Journal of Energy and Environmental Engineering, 8, pp. 343-358.

Azzi, Z. (2016). "Behavior of Un-reinforced Concrete Masonry Infill Walls under Lateral Earthquake Loads." Lebanese American University (LAU) Repository, School of Engineering (SOE) Theses and Dissertations.

Azzi, Z., Habte, F., Elawady, A., Chowdhury, A. G., and Moravej, M. (2020a). "Aerodynamic Mitigation of Wind Uplift on Low-Rise Building Roof Using Large-Scale Testing." Frontiers in Built Environment, Wind Engineering and Science, 5:149.

Azzi, Z., Elawady, A., and Chowdhury, A. G. (2020b). "Large-Scale Aeroelastic Testing to Investigate the Resiliency of Transmission Infrastructure to Hurricane Storms." Proceedings of the 11th International Conference on Structural Dynamics (EURODYN 2020), Athens, Greece, November 23-26, pp. 1944-1957.

Azzi, Z., Matus, M., Elawady, A., Zisis, I., Irwin, P., and Chowdhury, A. G. (2020c). "Aeroelastic Testing of Span-Wire Traffic Signal Systems." Frontiers in Built Environment, Wind Engineering and Science, 6:111.

Badruddin Ahmad, M., Pande, P. K., and Krishna, P. (1984). "Self-Supporting Towers under Wind Loads". Journal of Structural Engineering, 110(2): 370-384.

Bayar, D. C. (1986). "Drag Coefficients of Latticed Towers". Journal of Structural Engineering, 112(2): 417-430.

Boudreaux, T. P. (1962). "Hurricane Carla vs. Transmission Lines." Civil Engineering and Construction Review, April, pp. 70-72.

British Standard (BS) 50341 (2001). "Overhead electrical lines exceeding AC 45 kV: Part 1 – General requirements – Common specifications." London, UK.

British Standard (BS EN) (2006). "Eurocode 3 – Design of steel structures – Part 3-1: Towers, masts and chimneys." The British Standards Institution, London, United Kingdom.

Carril Jr., C. F., Isyumov, N., and Brasil, R. M. L. R. F. (2003). "Experimental study of the wind forces on rectangular latticed communication towers with antennas". Journal of Wind Engineering and Industrial Aerodynamics, 91, 1007-1022.

Chen, Y., Pan, L., Pan, F., and Guo, Y. (2014). "Dynamical response of transmission line towers subjected to thunderstorm downbursts based on experimental study." 2014 World Congress on Advances in Civil, Environmental and Materials Research (ACEM14), Busan, Korea, August 24-28.

Choi, E. C. C., and Hidayat, F. A. (2002). "Dynamic response of structures to thunderstorm winds". Progress in Structural Engineering and Materials, Wind Response of Structures, 4:408-416.

Chopra, A. (2017). "Dynamics of Structures: Theory and Applications to Earthquake Engineering." Prentice Hall/Pearson, 5th Edition.

Chowdhury, A. G., and Sarkar, P. P. (2003). "A new technique for identification of eighteen flutter derivatives using a three-degree-of-freedom section model." Engineering Structures, 25, 1763-1772.

Chowdhury, A. G., and Sarkar, P. P. (2004). "Identification of eighteen flutter derivatives of an airfoil and a bridge deck." Wind and Structures, Vol. 7, No. 3, 187-202.

Chowdhury, A. G., Zisis, I., Irwin, P., Bitsuamlak, G., Pinelli, J.-P., Hajra, B., and Moravej, M. (2017). "Large-Scale Experimentation Using the 12-Fan Wall of Wind to Assess and Mitigate Hurricane Wind and Rain Impacts on Buildings and Infrastructure Systems." Journal of Structural Engineering, 143(7): 04017053.

da Silva, J. G. S., Vellasco, P. D. S., de Andrade, S. A., and de Oliveira, M. I. R. (2005). "Structural assessment of current steel design models of transmission and telecommunication towers." Journal of Constructional Steel Research, 61, 8, pp. 1108-1134.

Davenport, A. G. (1962a). "The response of Slender Line-Like Structures to a Gusty Wind". Proceedings of the Institution of Civil Engineers, 23, 3, 389-408.

Davenport, A. G. (1962b). "Buffeting of a Suspension Bridge by Storm Winds". Journal of the Structural Division (ASCE), 88, 3, 233-270.

Davenport, A. G. (1983). "The relationship of reliability to wind loading." Journal of Wind Engineering and Industrial Aerodynamics, 13, 3-27.

Davenport, A. G. (1988). "The response of tension structures to turbulent wind: the role of aerodynamic damping." Proceedings of the First International Oleg Kerensky Memorial Conference on Tension Structures, London, England, June 20-22.

Dempsey, D., and White B. H. (1996). “Winds Wreak Havoc on Lines”. Transmission & Distribution World, June; 48, 6; ProQuest pg. 32.

Elawady, A., and El Damatty, A. (2016). “Longitudinal Force on Transmission Towers Due to Non-Symmetric Downburst Conductor Loads”. Engineering Structures, 127, 206-226.

Elawady, A., Aboshosha, H., El Damatty, A., Bitsuamlak, G., and Hangan, H. (2017). “Aero-elastic testing of multi-spanned transmission line subjected to downbursts.” Journal of Wind Engineering and Industrial Aerodynamics, 169, 194-216.

ESDU (2001). “Characteristics of the Atmospheric Boundary Layer, Part II: Single Point Data for Strong Winds (Neutral Atmosphere).” London: Engineering Sciences Data Unit, Item 85020.

Feng, C., Chowdhury, A. G., Elawady, A., Chen, D., Azzi, Z., and Vutukuru, K. S. (2020). “Experimental Assessment of Wind Loads on Roof-to-Wall Connections for Residential Buildings.” Frontiers in Built Environment, Wind Engineering and Science, 6:10.

Haviland, R. (1976). “A study of the uncertainties in the fundamental translational periods and damping values for real buildings.” Evaluation of Seismic Safety of Buildings, Research Report 5, National Science Foundation (NSF).

Hiramatsu, K., and Akagi, H. (1988). “The Response of Latticed Steel Towers due to the Action of Wind”. Journal of Wind Engineering and Industrial Aerodynamics, 30, pp. 7-16.

Holmes, J. D. (1994). “Along-wind response of lattice towers: part I – derivation of expressions for gust response factors”. Engineering Structures, 16, 4, 287-292.

Holmes, J. D. (1996a). “Along-wind response of lattice towers: II – Aerodynamic damping and deflections.” Engineering Structures, 18:483-488.

Holmes, J. D. (1996b). “Along-wind response of lattice towers: III – Effective load distributions.” Engineering Structures, 18:489-494.

Holmes, J. D. (2015). “Wind Loading of Structures.” 3rd Edition, CRC Press, Taylor & Francis Group, Boca Raton, FL.

Huang, P., Quan, Y., and Gu, M. (2013). “Experimental Study of Aerodynamic Damping of Typical Tall Buildings.” Hindawi Publishing Corporation, Mathematical Problems in Engineering, Volume 2013, Article ID 731572.

Ibrahim, S. R., and Mikulcik, E. C. (1976). “The Experimental Determination of Vibration Parameters from Time Responses.” The Shock and Vibration Bulletin, Vol. 46, pp. 187-196.

Irwin, P. A. (1977). “Wind Tunnel and Analytical Investigations of the Response of Lions’ Gate Bridge to a Turbulent Wind.” National Research Council of Canada, NAE Report LTR-LA-210.

Irwin, P. A. (1979). “Cross-Spectra of Turbulence Velocities in Isotropic Turbulence.” Journal of Boundary Layer Meteorology, 16, pp.337-343.

Irwin, P. A. (1992). “Full aeroelastic model tests.” Aerodynamics of Large Bridges, A. Larsen (ed.), Balkema, Rotterdam.

Irwin, P. A. (1996). “Buffeting Analysis of Long-Span Bridges.” RWDI Technical Reference Document, RD1-1996.

Isyumov, N. (1972). “Wind Tunnel Methods for Evaluating Wind Effects on Buildings and Structures.” International Symposium on Experimental Mechanics, The University of Waterloo, Waterloo, June 12-16.

Jeary, A. P. (1986). “Damping in tall buildings: a mechanism and a predictor.” Earthquake Engineering and Structural Dynamics, Vol. 14, 733-750.

Jeary, A. P. (1992). “Establishing non-linear damping characteristics of structures from non-stationary response time histories.” The Structural Engineer, Vol. 70, No. 4, 61-66.

Kalaga, S., and Yenumula, P. (2017). “Design of Electrical Transmission Lines – Structures and Foundations”. CRC Press, Volume 1, Taylor & Francis Group, London, UK.

Letchford, C. W., Mans, C., and Chay, M. T. (2002). “Thunderstorms – their importance in wind engineering (a case for the next generation wind tunnel)”. Journal of Wind Engineering and Industrial Aerodynamics, 90, pp. 1415-1433.

Liang, S., Zou, L., Wang, D. and Cao, H. (2015). “Investigation on wind tunnel tests of a full aeroelastic model of electrical transmission tower-line system”. Engineering Structures, Vol. 85, pp. 63-72.

Lin, W. E., Savory, E., McIntyre, R. P., Vanderlaar, C. S., and King, J. P. C. (2011). “A single-span aeroelastic model of an overhead electrical power transmission line with guyed lattice towers”. 13th International Conference on Wind Engineering, Amsterdam.

Loredo-Souza, A. M. (1996). “The Behaviour of Transmission Lines Under High Winds.” University of Western Ontario (UWO) Digital Theses, 2650.

Loredo-Souza, A. M. (2014). “The aeroelastic wind tunnel modeling of transmission lines and their behavior under severe boundary layer winds”. Proceedings of the 9th International Conference on Structural Dynamics, EURODYN 2014, Porto, Portugal, 30 June – 2 July.

Loredo-Souza, A. M., and Davenport, A. G. (2001). “A novel approach for wind tunnel modelling of transmission line”. Journal of Wind Engineering and Industrial Aerodynamics, 89, 1017-1029.

Loredo-Souza, A. M., and Davenport, A. G. (2003). "The influence of the design methodology in the response of transmission towers to wind loading". Journal of Wind Engineering and Industrial Aerodynamics, 91, 995-1005.

Lou, W. J., Sun, B. N., and Tang, J. C. (1995). "Shape Factor Study of Tall Lattice Transmission Tower by Wind Tunnel Tests." The 7th Chinese Conference on Structural Wind Effect, Chongqing University Press, 180-186.

Lou, W. J., Sun, B. N., and Tang, J. C. (2000). "Aeroelastic Model Investigation and Spectral Analysis of a Tall Lattice Tower". Advances in Structural Engineering, 3(2):119-30.

Lou, W. J., Wang, X., and Jiang, Y. (2009). "Wind-Induced Responses of a High-Rise Transmission Tower to Thunderstorm Downbursts". The Seventh Asia-Pacific Conference on Wind Engineering, Nov. 8-12, Taipei, Taiwan.

Mara, T. G., Galsworthy J. K., and Savory, E. (2010). "Assessment of vertical wind loads on lattice frame-work with application to thunderstorm winds". Wind and Structures, Vol. 13, no.5, pp. 413-431.

Marukawa, H., Kato, N., Fujii, K., and Tamura, Y. (1996). "Experimental evaluation of aerodynamic damping of tall buildings." Journal of Wind Engineering and Industrial Aerodynamics, 59, 2-3, 177-190.

Mevada, H., and Patel, D. (2016). "Experimental determination of structural damping of different materials." Proceedings of the 12th International Conference on Vibration problems (ICOVP2015), 144, pp. 100-115.

MATLAB® and Statistics Toolbox (2020), Release 2020a, The MathWorks, Inc., Natick, Massachusetts, United States.

Newmark, N. M. (1959). "A Method of Computation for Structural Dynamics" ASCE Journal of Engineering Mechanics, pp. 67-94.

SAP2000 Version 22.0.0 (2020), Structural Analysis Program, Computers and Structures, Inc., www.csiamerica.com

Sarkar, P. P. (1992). "New-Identification Methods Applied to the Response of Flexible Bridges to Wind." PhD Thesis, The John Hopkins University, Baltimore, MD.

Sarkar, P. P., Jones, N. P., and Scanlan, R. H. (1994). "Identification of Aeroelastic Parameters of Flexible Bridges." ASCE Journal of Engineering Mechanics, 120(8), pp. 1718-1742.

Savory, E., Parke, G. A. R., Zeinoddini, M., Toy, N., and Disney, P. (2001). "Modelling of tornado and microburst-induced wind loading and failure of a lattice transmission tower". Engineering Structures, 23, 365-375.

Scanlan, R., and Tomko, J. (1971). "Airfoil and bridge deck flutter derivatives." ASCE Journal of Engineering Mechanics, 97, 1717-1737.

Shehata, A. Y., and El Damatty, A. A. (2008). “Failure analysis of a transmission tower during a microburst”. Wind and Structures, Vol. 11, No. 3, pp. 193-208.

Shichiri, Y. (1971). “Wind withstanding design for transmission line tower.” Proceedings of the Third International Conference on Wind Engineering (3ICWE), Tokyo, Japan, pp. 451-456.

Simiu, E., and Yeo, D. (2019). “Wind Effects on Structures.” John Wiley & Sons, 4th Edition.

Strelkov, S. P. (1964). “Introduction to the Theory of Vibrations.” Nauka, Moscow.

Takeuchi, M., Maeda, J., and Ishida, N. (2010). “Aerodynamic damping properties of two transmission towers estimated by combining several identification methods”. Journal of Wind Engineering and Industrial Aerodynamics, 98, 872-880.

Tamura, Y., and Suganuma, S. (1996). “Evaluation of amplitude-dependent damping and natural frequency of buildings during strong winds”. Journal of Wind Engineering and Industrial Aerodynamics, 59, 115-130.

Yang, F., and Zhang, H. (2016). “Two case studies on structural analysis of transmission towers under downburst”. Wind and Structures, Vol. 22, No. 6, 685-701.

Wang, Z., and Dragomirescu, E. (2016). “Flutter Derivatives Identification and Aerodynamic Performance of an Optimized Multibox Bridge Deck.” Hindawi, Advances in Civil Engineering, Article ID 8530154.

Zasso, A. (1996). “Flutter derivatives: Advantages of a new representation convention.” Journal of Wind Engineering and Industrial Aerodynamics, 60, 35-47.

Zhangqi, W., Zeming, S., and Wenqiang, J. (2014). “Theoretical and Experimental Research on Joint Slippage Effects of Lattice Angle Steel Tower.” Applied Mechanics and Materials, 477-478, pp. 660-665.

CHAPTER III. AEROELASTIC MODELING TO INVESTIGATE THE WIND-INDUCED RESPONSE OF A MULTI-SPAN TRANSMISSION LINES SYSTEM

3.1 Introduction

3.1.1 Vulnerability of Electrical Transmission Lines (TL)

The U.S. electric grid constitutes a vital component of the nation's critical infrastructure and serves as an essential foundation for the prosperity of the nation. The grid generates, transmits, and distributes electric power to millions of Americans in homes, schools, offices, and businesses across the country. It also delivers electricity to more than 144 million end-user customers in the U.S. and it consists of high-voltage transmission lines, local distribution systems as well as power management and control systems. High-voltage transmission lines are responsible for transportation of electric current from generation facilities to population and economic centers through substations which reduce voltage levels [(Campbell, 2012); (Executive Office of the President, 2013); (Aboshosha et al., 2016)].

Overhead transmission lines consist mainly of support towers, conductors, insulators, and ground wires. Attached to the towers using insulators, conductors are responsible for transmitting electricity from one point to another and the role of ground wires is to protect the grid from lightning strikes [(Aboshosha and El Damatty, 2014); (Aboshosha et al., 2016)]. When the site of power generation is geographically remote from population areas, optimal transmission lines design is extremely important since a failure might take a long time to repair [(Aboshosha and El Damatty, 2014); (Aboshosha et al., 2016)].

The leading cause of power outages and blackouts in the United States is severe weather. The age of the grid's components has also contributed to an increased incidence

of weather-related power outages. Over the span of 9 years between 2003 and 2012, about 679 widespread power outages were reportedly attributed to severe weather. Such events closed down schools and businesses as well as severely impacting emergency services, sometimes up to several days, leading to the disruption of the lives of millions of Americans and costing the economy billions of dollars [(Executive Office of the President, 2013); (Aboshosha and El Damatty, 2014)]. According to Campbell (2012), the inflation-adjusted cost of weather-related outages is estimated at around $25 to $70 billion annually.

Furthermore, with the improvement of the voltage level, the tower height and span in high-voltage and ultra-high-voltage transmission lines have increased. Damage accidents of transmission towers due to strong wind events happen frequently and are in a trend of increasing frequency (Liang et al., 2015). The wind design of the transmission tower-line system is a critical and yet unresolved issue in wind engineering. Due to their light weight, small structural damping and sensitivity to wind excitation, a classical approach to design transmission lines that considers the structural strength and stability under the strongest storms might not be sufficient [(Cluni et al., 2008); (Lou et al., 2009)]. In order to obtain an adequate structural performance, it is necessary to take into account the fatigue life estimation of cable structures such as transmission lines. Such analysis is also critical in retrofitting existing structures where the cables are constantly subjected to random vibrations from ambient wind [(Bartoli et al., 2006); (Cluni et al., 2008)].

In addition to the static effect caused by mean wind speed, the dynamic behavior of a transmission tower is three-dimensional. It occurs in the along-wind, the crosswind, and torsional directions under the fluctuating wind pressure [(Mara et al., 2013); (Liang

et al., 2015)]. However, current design standards still design for the along-wind response of lattice transmission towers. Moreover, cable structures are vulnerable to galloping effects, especially when they are located in cold regions where ice accretion might develop. This effect might modify the conductors' cross-sectional shape so that it becomes aerodynamically and aeroelastically unstable (Chabart and Lilien, 1998). Other vulnerabilities of cable structures could be due to vortex shedding excitation, wake interference, and buffeting due to wind gust among others [(Tokoro et al., 2000); (Bartoli et al., 2006)].

Grid resilience is becoming more important as climate change increases the intensity and frequency of severe weather. Due to anthropogenic emissions of greenhouse gasses, scientific studies predict increasing severe hurricanes and winter storms among other hazards. The U.S. energy sector in general, and the grid in particular, are vulnerable to severe weather, which is expected as the climate changes (DOE, 2013). Therefore, investment in a 21st century modernized electric grid is of utmost importance as modernization and resilience will mitigate the huge damage costs and reduce the hardship experienced by millions when extreme weather strikes (Executive Office of the President, 2013).

3.1.2 Challenges of an Aeroelastic Wind Testing of Multi-Span Systems

As previously discussed in Chapter 2, section 2.1.2, any aeroelastic scaling exercise must take into account a geometric scaling of the exterior dimensions of the structure as well as the corresponding scaling of all forces influencing its behavior. Typically, this involves the scaling of the elastic, damping, gravity, inertia, and viscous forces, respectively (Irwin, 1992). While preserving the geometry is crucial for the simulation of the aerodynamic loads, the stiffness and mass scaling are vital for the dynamic inertial loads

associated with the response of the model itself [(Loredo-Souza, 2014); (Elawady et al., 2016); (Elawady et al., 2017)].

According to Isyumov (1972), it is preferred to use prototype material to model the aeroelastic structure in order to maintain the structural damping where dynamic responses are pronounced. However, because transmission lines are classified as lightweight structures, it is impossible to satisfy the mass scaling using steel sections available in the market. As such, another lightweight metal is typically selected as an alternative such as aluminum. In Chapter 2, section 2.1.2, the different parameters required to preserve the behavior of the aeroelastic models in any scaling exercise were presented in Equations 2.1 through 2.8. These parameters include the following: the mass, the drag forces, the reduced frequency, and the aerodynamic damping along with the properties of the natural wind.

In order to accommodate long spans or even several spans of cable structures in the wind tunnel, an innovative modeling approach has to be implemented. Such an approach is based on the distortion of the length scale in order to fit multiple spans on the turntable of the wind tunnel. The basic idea is based on the concept of horizontally distorting the cable modeling but maintaining the same sag and preserving the properties of the initial model, i.e., the mass, the drag, and the frequency, which would not significantly alter its behavior. This is particularly true since the natural frequencies of the cables are primarily a function of their sags when the cable tension is not high such as the case of conductors in transmission lines. However, introducing such a technique causes few drawbacks such as the correlation of the wind forces along the cable, which must be corrected. Measured results in the wind tunnel have to be adjusted by a span distortion factor

β to take into account the effect of the distorted span on the magnitude of the wind pressure along the cable length [(Loredo-Souza, 1996); (Loredo-Souza and Davenport, 1998); (Loredo-Souza, 2014)].

The conductors' natural frequency f_1 and tension T are given in Equations 3.1 and 3.2, which were derived by Irvine (1981) for single spanned conductors:

$$f_1 = \frac{1}{2L} \cdot \sqrt{\frac{T}{M/L}} \tag{3.1}$$

$$T = \frac{w.L^2}{8s} \tag{3.2}$$

In Equation 3.1, L is the conductor length in m, M is the conductor mass in kg and T is the tension in the conductor in N. In Equation 3.2, s is the conductor sag in m and w is the cable weight per unit length in N/m. As previously mentioned, by using the horizontal distortion modeling approach, if the mass of the conductor and its sag are preserved, then the frequency and the tension should remain the same. The rest of the equations needed to implement the distortion modeling approach are summarized below. Note that subscripts p and m refer to quantities on the prototype and model, respectively (section 2.1.2). Also note that the asterisk superscript symbol * refers to a certain quantity used in the distorted model.

New Length Scale: A reduced span L_m^* obtained from the distortion of the original model span L_m by an amount β is adopted so that the following applies:

$$L_m^* = \beta.L_m \tag{3.3}$$

$$\lambda_L^* = \frac{L_m^*}{L_p} = \frac{\beta.L_m}{L_p} = \beta.\lambda_L \tag{3.4}$$

Essentially, the distorted model will have the same behavior as its original counterpart if the mass, the drag forces, the aerodynamic damping, and the reduced frequency are kept the same. Distorting the mass per unit length m and the factor ($C_D\ d$) by the same amount β guarantees that the ratio between wind and gravity forces is also preserved. Note that C_D is the drag coefficient and d is the cable diameter in m.

Aerodynamic Damping: Cable motion is dominated by its aerodynamic damping when subjected to wind loads. The structural damping ζ_s, which is typically very low (around 0.05% as documented by Bachmann et al. (2015)), does not govern the wind-induced vibration of cables, especially in strong winds. According to Davenport (1988) and Vickery (1995), the aerodynamic damping is a retarding force which is derived from the relative motion between the structure and the air. The aerodynamic damping for cables is given by Equation 3.5 [(Davenport, 1988); (Loredo-Souza, 1996); (Loredo-Souza and Davenport, 1998); (Loredo-Souza and Davenport, 2001); (Loredo-Souza and Davenport, 2002); (Loredo-Souza, 2014)]:

$$\zeta_{aj} = \left(\frac{C_D}{4\pi}\right).\left(\frac{\rho_a.d^2}{m}\right).\left(\frac{U}{f_j.d}\right) \tag{3.5}$$

In Equation 3.5, ρ_a is the density of air in kg/m^3, U is the mean wind speed at cable height in m/s, and f_j is the natural frequency of the cable in the desired mode shape j in Hz.

As such, Equations 3.6 through 3.9 show the new scaling equations required to maintain the same behavior between the original and distorted model:

$$m_m^* = \frac{m_m}{\beta} \tag{3.6}$$

$$(C_D.d)_m^* = \frac{(C_D.d)_m}{\beta} \tag{3.7}$$

$$f_m^* = f_m \tag{3.8}$$

$$(E.d^2)_m^* = \beta.(E.d^2)_m \tag{3.9}$$

If the total mass and drag forces on the distorted model have to be preserved, the original average mass per unit length and average (C_D d) per unit length needed have to increase by a factor of $1/\beta$. Furthermore, if the natural frequency of the prototype is not altered (by keeping the same axial tension), the reduced frequency and the aerodynamic damping will remain unchanged. Because the natural frequency of a cable is primarily a function of its sag (Equation 3.1), which remains unchanged, the previous conditions are satisfied. Note that E is the modulus of elasticity of the conductor in Pa.

However, due to the already mentioned limitations of aeroelastic modeling in Chapters 2 and 3, the axial tension similarity is not to be strictly followed (Loredo-Souza, 2014). The consequences of such a decision were deemed acceptable in the experimental results conducted by Loredo-Souza (1996). Another compromise that is important to mention here is the transverse wind loads transmitted by the cables to their supports. Armitt et al. (1975) reported that the conductor tension had a negligible influence on the transverse loadings. Once again, as noted by Irwin (1992), the exact matching of all the parameters is impossible. The scaling may be violated in small instances without severely affecting the response of the model and the measured results.

3.1.3 Limitations of Previous Work and Knowledge Gap

To this day, the design of transmission lines for extreme wind resistance remains an unresolved major issue in the wind engineering community [(Hawes and Dempsey, 1993); (Diana et al., 1996); (Savory et al., 2001); (Zhang, 2006); (Liang et al., 2015)]. As noted in different field measurements [(Mehta and Kadaba, 1990); (Momomura et al.,

1997)] and wind tunnel tests of aeroelastic models of transmission lines [(Loredo-Souza, 1996); (Loredo-Souza and Davenport, 2001); (Liang, 2002); (Liang et al., 2015)], analyzing wind-induced responses of the tower-line system and the coupling between components, mainly the tower and the conductors, is a complex task.

Full-scale conductor wind loading experiments as well as field measurements have been performed since the 1980's in order to acquire the conductor response and the characteristics of the forcing wind. Based on past experiments conducted by Hydro Quebec (Houle et al., 1991), Ontario Hydro (Kishnasamy, 1985) and the Bonneville Power Administration (Volpe, 1989), Shan (1994) carried out subsequent investigations to evaluate full-scale conductor behavior. Twenty-three records of wind speeds, wind directions and corresponding structural responses were recorded and analyzed by Mehta et al. (1988) and Mehta and Kadaba (1989, 1990). Such analyses were targeted to improve the analytical model developed earlier by Davenport (1979) to predict the conductor response in extreme wind scenario. The conclusions of such investigations were the following: (i) the drag coefficient of the conductor varies with the azimuthal wind direction, (ii) the resonant peaks occurred between 0.1 and 0.4 Hz in the conductor response spectra, and (iii) most of the fluctuating response of the conductors appeared to be due to the background component with slight contribution from its resonant counterpart. Such contributions were attributed to the high aerodynamic damping of the conductors, which plays a significant role at high wind speeds.

Holmes (1994, 1996a, 1996b) proposed gust response factors, along-wind aerodynamic damping, and top deflection equations for free-standing lattice towers along with static load distribution of mean, background fluctuating, and resonant components

of the wind loads. The equations considered the height effect, mean velocity profile, mode shape of the tower, along with the type of the load. However, the equations were based on assumptions that the tower was linearly tapered with uniformly decreasing cross-section along its height.

Typically, as reported by IEC 60826 (2003), Wang et al. (2009) and Lin et al. (2012), the natural frequency of lattice towers up to 60 m height is above 1 Hz. Such a value is considerably greater than the frequencies corresponding to the maximum turbulence energy. As such, this leads to a low resonant response. However, aeroelastic tests conducted by Lou et al. (2000) on a tall tower (180 m full-scale height) revealed that the specimen was sufficiently flexible in a way that might be vulnerable to dynamic excitation by wind and that the resonant component could not be assumed as negligible. On another note, Lou et al. (2000) neglected the effects from the conductors, which is worrisome since field measurements conducted by Momomura et al. (1997) have shown that the vibration characteristics of transmission towers were strongly affected by the presence of the conductors in tower-line systems. Furthermore, Lin et al. (2012) conducted aeroelastic experiments on a 1:100 scaled model of a guyed mast. However, the modeling process only utilized a half-span of lines on either end, which leads to a neglection of full- and multi-span motions.

Liang et al. (2015) investigated the wind-induced response of full aeroelastic model specimens of lattice towers with two lines of conductors using a scale of 1:30. The study concluded that including the coupling effects of the tower-insulator-conductor system in the overall response of transmission towers is important. They also suggested the

importance of including the crosswind response of transmission towers as it is neglected in design standards.

Last but not least, Loredo-Souza (1996) and Loredo-Souza and Davenport (1998, 2001) conducted aeroelastic tests on conductors with models at 1:50 scale and equivalent distorted models with a further 1:2 scale (equaling 1:100). The authors reported that the root-mean-square (RMS) response of the distorted model is slightly higher than that of the original one, but the rest of the measured responses agree well. The higher RMS was attributed to the turbulence length scale being the same for both models, but the span of the distorted model was one half that of its original counterpart. The measured responses were also compared with the statistical method employing the influence lines (Davenport, 1993). The comparison yielded a good agreement between theoretical and experimental results. The statistical method accounts for both background and resonant components of the structure. It also considers the effects of higher modes on the resonant component. In addition, the statistical method, which is general and can be used for any structure, was utilized by Loredo-Souza (1996) and Loredo-Souza and Davenport (2003) in order to obtain the theoretical response of the transmission towers. Results were compared with values given by Zar and Arena (1979) for the same tower configuration and were well in agreement. The study concluded that the dynamic response of transmission towers strongly depends on the turbulence intensity and aerodynamic damping of the towers. It was also found that using the statistical influence lines' approach was more appropriate since it allows the inclusion of a larger number of factors in the design methodology.

Most of the previously mentioned experiments on tower-line systems focused on a single-span and therefore, did not consider dynamic boundary effects from adjacent

spans when a series of transmission-line systems are subjected to turbulent winds. Consequently, potential couplings among components arising from torsional as well as out-of-phase longitudinal and transverse responses of adjacent towers have not been properly captured. This study seeks to fill this existing gap in the literature and advance the knowledge in transmission lines aeroelastic response subjected extreme winds. The latter can be achieved by conducting full aeroelastic tests on a complete transmission tower-line system comprising of three towers and four spans of conductors. The selected length scale for design is 1:50 and the distortion approach previously described will be utilized in order to accommodate as many as four spans of conductors on the WOW turntable. The horizontal distortion factor takes a value of 1:3. In the subsequent sections, the design, modeling, validation, and construction of the aeroelastic model of the transmission lines system will be thoroughly covered. In the results section, the along-wind and cross-wind damping of the tower, conductors as well as the coupled system are presented. The crosswind response, currently neglected in all design standards around the world, could prove to be crucial in the resiliency of such structures, if properly included. Furthermore, theoretical equations developed to predict the along-wind response of the conductors and comparisons of the tower responses in a single lattice structure and entire transmission lines systems are compared. Then, the wind-induced buffeting response of the model is investigated to quantify the background and resonant responses. Lastly, Dynamic Amplification Factors (DAF) are calculated using the data collected from the sensors installed on the model at various sections and are compared with similar parameters specified in different standards utilized around the world.

3.2 Experimental Setup, Design, and Validation of the Complete Model

3.2.1 Wall of Wind Experimental Facility (WOW EF)

The experiments were conducted at the National Science Foundation (NSF) Natural Hazard Engineering Research Infrastructure (NHERI) Wall of Wind (WOW) Experimental Facility (EF). The facility was previously described in Chapter 2, section 2.1. For detailed information on the facility and its capabilities, refer to publications by Chowdhury et al. (2017), Azzi et al. (2020b, 2020d) and Feng et al. (2020). Fig. 3.1 shows a schematic of the WOW in order to better visualize the different sections of the wind tunnel.

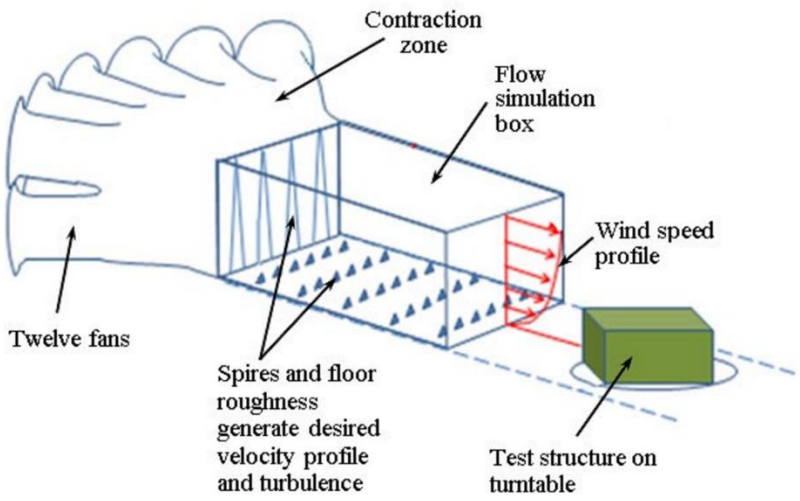

Fig. 3.1: Schematic of the different sections of the WOW

3.2.2 Aeroelastic Modeling of the System

3.2.2.1 Scaling, Design, and Construction of the Model

The transmission lines system considered in this study consists of three lattice towers, four spans of conductors, and an end-frame on each side; the towers are connected together using six conductors, spread over three different vertical levels. The towers

selected were previously described in Chapter 2, section 2.2.1, and have a geometric length scale λ_L of 1:50. Recall that the transmission towers chosen for this study are classified as self-supported steel lattice structures with fundamental frequencies ranging between 2 and 4 Hz according to ASCE 74 (2010) and ANSI/TIA-222 (2005). Also recall that the prototype lattice tower has the following full-scale dimensions: a height *h* of 27.5 m, a rectangular base with length *L* of 7.6 m, and width *B* of 2.7 m (Azzi et al., 2020a) (Fig. 2.2).

Additionally, each tower has three different levels of identical cross-arms at the top. This allows the attachment of six bundles of conductors, with two at each vertical level. The prototype conductors typically used with this tower configuration are classified as Aluminum Conductor Steel Reinforced (ACSR) cables with codename 'DRAKE'. The conductors are made of seven strands, have a diameter of 28 mm and a distributed weight of 0.15 kg/m (both values at full-scale). Typically, in the field, the conductors are attached to the tower cross-arms using insulators made of different types of materials. In this study, the insulators are made of porcelain with a length of 1.5 m and a diameter of 0.08 m (Azzi et al., 2020a). The conductors span a horizontal length of 180 m between the transmission towers and are sagged at midspan by about 3.6 m.

As previously mentioned in Chapter 2, a careful design procedure should be adopted in order to replicate the same dynamic behavior between prototype and model when undergoing a scaling process. Generally, since the structural damping is important in the dynamic response of the system, it is preferred to use prototype materials in the construction of the small-scale aeroelastic model [(Isyumov, 1972); (Irwin, 1992)]. Though, because of the lightweight nature of lattice structures and their relatively very

small structural damping, it would be challenging to satisfy the mass scaling parameter using prototype steel material. Hence, the use of another metal in the form of aluminum in such cases is usually adopted. On another note, according to Mevada and Patel (2016), the structural damping of aluminum is smaller than that of steel. However, since lattice towers and transmission lines are classified as flexible structures, the aerodynamic damping would be much more dominant than its structural counterpart, particularly at high wind speeds. Therefore, the use of aluminum instead of steel would not impact the validity of the results [(Irwin, 1992); (Azzi, 2016); (Elawady et al., 2016); (Elawady et al., 2017)].

Similar to the tests conducted in Chapter 2, Froude number *Fr* scaling is selected for the subsequent tests by linking the velocity scale λ_U to the square root of the length scale λ_L, i.e., setting the velocity scale to $1{:}50^{1/2}$ for a length scale of 1:50 (Equation 2.3). Recall that the scaling parameters for the design of the lattices towers are defined in Table 2.1. The parameters concerned with the design of the conductors are presented in Table 3.1, taken from Equations 3.5 to 3.9.

Table 3.1: Scaling parameters used in the design of the conductors (from full-scale prototype to distorted model) (β = 1:3)

Quantity Q	Scaling factor λ_Q	Quantity Q	Scaling factor λ_Q
Length L	1:150	Damping ζ	1
Velocity U	$1{:}50^{1/2}$	Time t	$1{:}50^{1/2}$
Mass m	$1{:}(1/3x50^3)$	Elastic stiffness EA	$1{:}(3x50^3)$
Acceleration a	1	Drag Force F_D	$1{:}(1/3x50^3)$

In building the model, the transmission tower shown in Fig. 2.2, Fig. 2.3, and Fig. 3.2 is used with an aluminum spine and non-structural cladding elements. For the conductors, a steel wire having a diameter of 0.56 mm is utilized. To maintain the drag, dis-

tributed weight and average diameter between prototype and model, non-structural foam cylindrical rods were installed along the span of the conductors. The rods have a diameter of 0.25 mm and a length of 3 cm. Concerning the insulators, aluminum rods of 3 cm length were utilized and their connections to the tower and conductor were both 3D printed using a resin material. The insulators were glued to the cross-arms using epoxy and the conductors were embedded inside the bottom connection of the insulators. Fig. 3.2a and 3.2b show the transmission tower previously described with and without the insulators, respectively.

a) b)

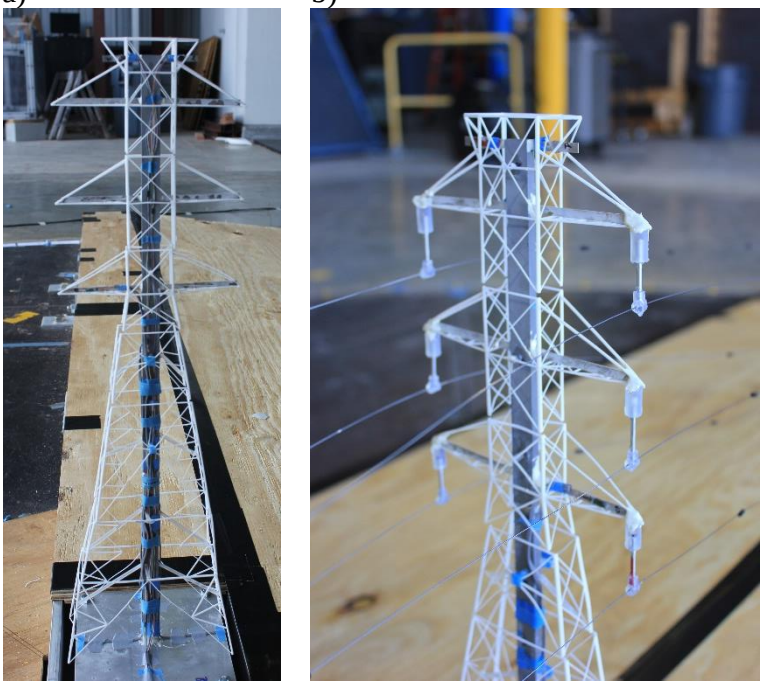

Fig. 3.2: Transmission tower tested: a) by itself, and b) as part of a tower-insulator-conductor system

To counter any unbalanced tensions in the cross-arms, a highly rigid frame was constructed at each end of the model. The frame was made of aluminum hollow square sections with the following dimensions: 25 mm x 25 mm for the column section and 25 mm x 12.5 mm for the beam section. Additionally, semi-rigid leaf springs made of stain-

less steel were installed on each frame in order to mount the conductors to them. The design of the leaf springs was based on the assumption that the actual steel sheets represent springs with stiffnesses much higher than that of the cross-arms. This ensured that the leaf springs are able to resist the axial forces in the conductors as well as not vibrate or move with the system when subjected to dynamic loading. The leaf springs were installed at the same height as the insulators on the cross-arms in order to mount the conductors on them. The conductors were attached to the leaf springs using hot glue. The ease of use of hot glue enabled the adjustment of the sag of the conductors whenever needed during the wind loading tests. Fig. 3.3 shows one of the constructed end-frames.

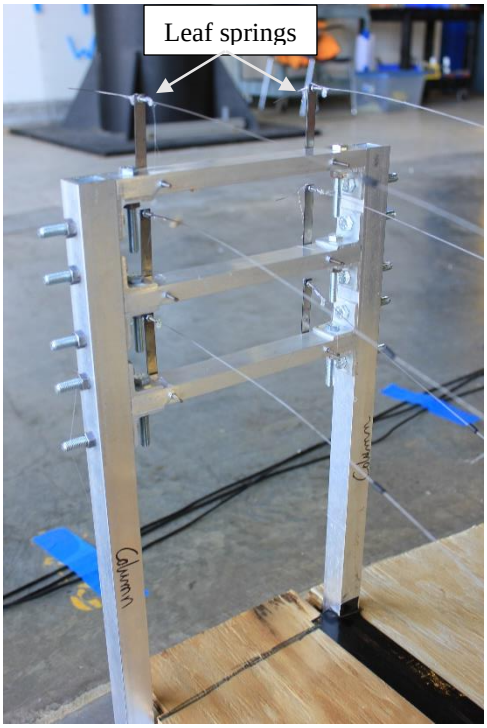

Fig. 3.3: End-frame used in the experiments

As mentioned earlier, in order to fit the entire model on the WOW turntable, the horizontal distortion described in section 3.1.2 is utilized with a distortion factor β of 1:3. Recall that β only affects the horizontal span of the conductors and reduces the distance

between supporting towers to 1.2 m (prototype span is 180 m and scaling factor is 1:50x1:3 = 1:150). Fig. 3.4a and 3.4b show from different angles the entire transmission lines system connected together before testing.

a)

b)

Fig. 3.4: Entire transmission line system: a) before testing, and b) after testing

3.2.2.2 Validation of Dynamic Parameters

Similar to Chapter 2, section 2.2.2, the FEM used to validate the design of a single tower was used in the subsequent reproduction of the complete modeling of the transmission lines system using SAP2000 (2020) software. The different sectional dimensions as well as material properties selected in the design were assigned to the FEM model. The insulators were modeled as rigid frame elements and the conductors were drawn as cable elements and assigned the required sag. Additionally, the end frames were also drawn as rigid frame elements and all material properties were allocated. Later, a modal analysis was performed and the different mode shapes with their respective frequencies were noted. The acquired frequencies were evaluated and compared to their prototype counterparts, obtained from a similar modal analysis of the full-scale complete transmission lines system. Table 3.2 illustrates the results of both modal analyses and the percent difference between the design value and the target frequencies. Fig. 3.5a, 3.5b, 3.6a and 3.6b show the first, second, third and fourth modes of vibrations generated by the FEM model, respectively. Note that, in Table 3.2, the target frequency f_t is equal to the prototype frequency times the relevant scaling factor ($\lambda_f = 50^{1/2}$ from Chapter 2, Table 2.1).

Table 3.2: Summary of modal analysis results of complete system

Mode of vibration	Prototype frequency f_p (Hz)	Target frequency f_t (Hz)	FEM-Model frequency f_m (Hz) (design)	Percent difference (%)
Conductor only	0.25	1.80	1.77	1.67
Longitudinal	2.28	16.10	16.45	2.17
Torsional	5.11	36.11	36.1	0.03
Transversal	5.12	36.24	37.1	2.37

As indicated in Table 3.2, the model frequencies obtained from the modal analysis for all four mode shapes agree well with the target frequencies. The highest percent difference is around 2.37%, observed for mode shape 4. Such results prove that the choice of materials, cross-sections and end restraints were adequate to generate the FEM model. The obtained results validated the design of the complete transmission lines system and the construction, and instrumentation of the model as well as the subsequent wind testing could proceed. Note that for the transversal mode of vibration, both the conductor and tower frequencies appear, as shown later on in Fig. 3.8.

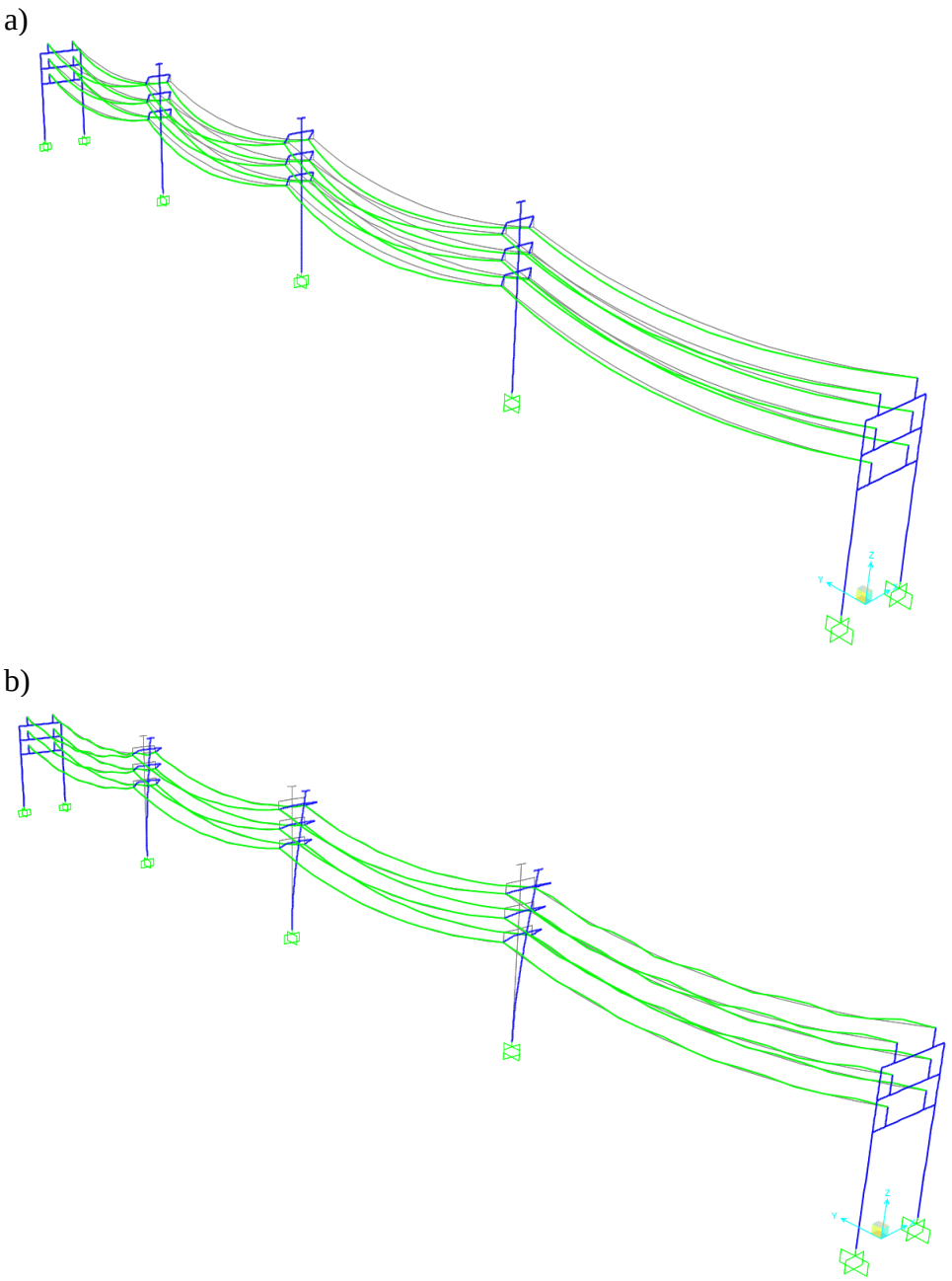

Fig. 3.5: Modal analysis of: a) conductor only (mode shape 1), and b) longitudinal (mode shape 2)

a)

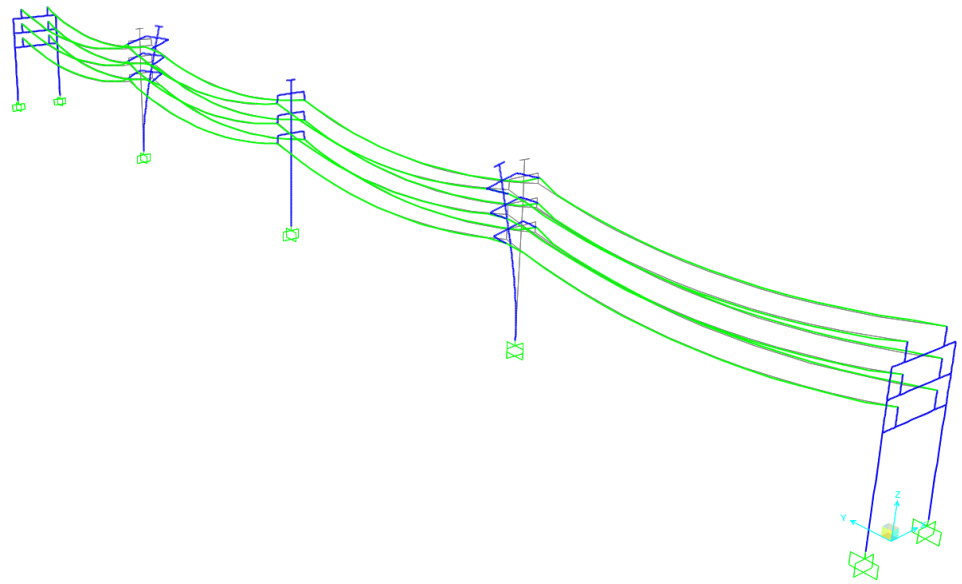

b)

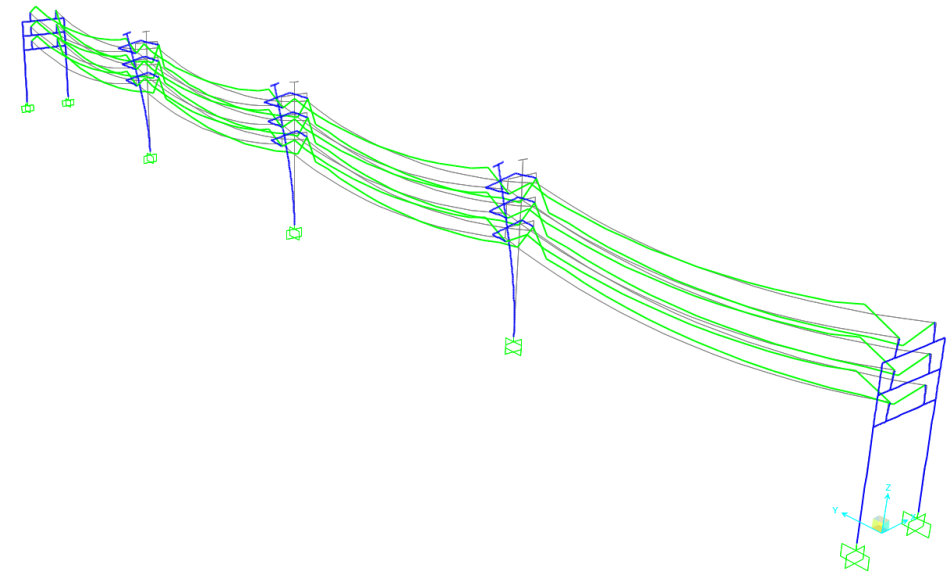

Fig. 3.6: Modal analysis of: a) torsional (mode shape 3), and b) transversal (mode shape 4)

3.2.3 Instrumentation and Testing Protocol

The complete transmission lines system was instrumented with the following sensors: (i) three 6-DOF load cells, (ii) three 3-axis accelerometers, and (iii) twenty strain gauges. One load cell was installed at the bottom of each transmission tower whereas the

three accelerometers were mounted on the middle tower with two on the top cross-arms and one at its mid-height. Eight strain gauges were glued on the cross-arms in order to measure the axial force in the aforementioned members at several conductor levels. The remaining twelve strain gauges were connected to the middle of each tower in a series of four, one on each face of the spine. Such a configuration allows for the measurements of the moments in the principal directions at the respective points of attachments. Data from the previously described instruments were sampled at 100 Hz. Fig. 3.7a, 3.7b, 3.7c, and 3.7d show the location of some of the sensors used in the experiments. To capture the wind speed time histories, three cobra probes were installed behind the model, at a distance of about 4 m from the center of the WOW turntable. The probes were fitted at the following heights: (i) one probe at 0.28 m height (mid-height of lattice towers), (ii) one probe at 0.55 m height (top height of lattice towers), and (iii) one probe at 0.94 m height. Data from the cobra probes were collected at a frequency of 2,500 Hz.

Concerning the testing protocol, it was decided to expose the model to four different wind speeds: 5, 7, 9 and 11 m/s at model tower height (0.55 m, small-scale), representing 35.4, 49.5, 63.6 and 77.8 m/s at prototype tower height (27.5 m, full-scale). The model was completely mounted on the WOW turntable and was rotated between 0^o and 90^o at 15^o increments, with each angle duration exposure lasting approximately 2 min (about 14 min, full-scale). Note that a wind direction of 0^o represents wind normal to the conductors and a wind direction of 90^o pertains to wind parallel to the conductors. The spires and roughness elements depicted in Fig. 2.1b were adjusted so that the turbulence profile matched that of an equivalent open terrain exposure.

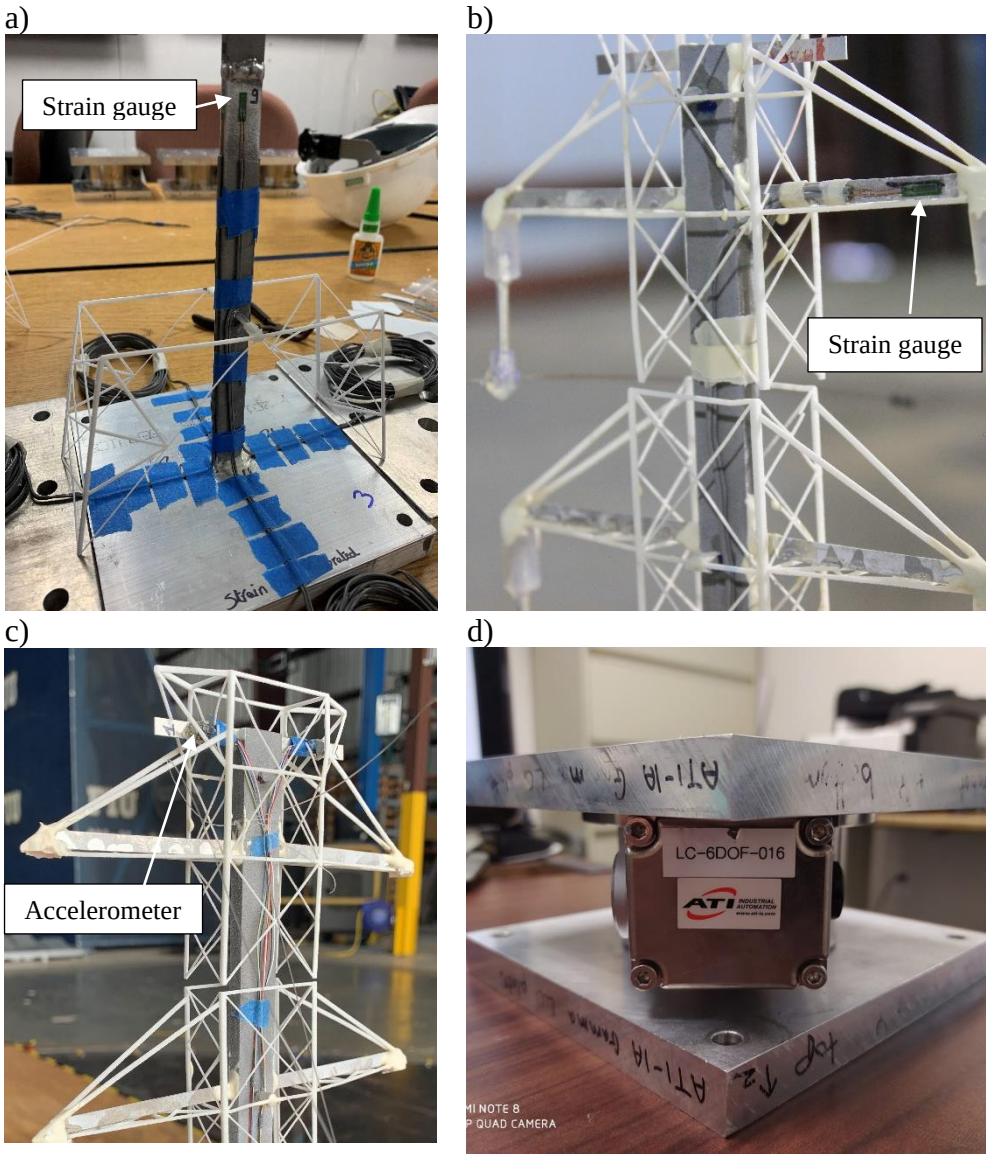

Fig. 3.7: Instrumentation used on the transmission lines model: a) strain gauge on spine, b) strain gauge on cross-arm, c) accelerometer, and d) load cell

3.3 Results and Discussion

This section investigates the analysis of the data obtained from the aeroelastic transmission lines wind testing. First, and before turning on the fans at the WOW, free vibration tests are conducted on the specimen to validate that the constructed model represents its designed counterpart in terms of mode shapes and frequencies. Second, a technique is used to decompose the acceleration data of the model in order to estimate the

aerodynamic damping ratio of the coupled tower-insulator-conductor system and compare it with that of the tower only model, presented in Chapter 2 to quantify the effect of coupling on the system identification (SID) parameters. Third, the buffeting theory, presented in Chapter 2, is used to estimate the deflection of the conductors, and drag forces acting on them. Comparisons of measured responses on the single tower model as well as the complete transmission lines system are made. Finally, dynamic amplification factors (DAF) are computed for all recorded parameters and suggestions as well as recommendations are formulated.

3.3.1 System Identification (SID) Method based on Free Vibration

Before the actual wind testing of the transmission lines specimen, a free vibrations test was conducted for the purpose of comparing the frequencies of the constructed model with those obtained in the design stage (also presented in Table 3.2). The model was excited four times in order to reproduce all four modes: (i) conductor displacement, (ii) longitudinal displacement of towers along their weak axis, (iii) rotation of middle tower and opposite transversal displacement of side towers, and (iv) transversal displacement of towers along their strong axis. This ensured the replication of the mode shapes obtained by the modal analysis of the FEM model (Table 3.2, section 3.2.2.2). In each attempt to reproduce the vibration mode required, careful displacement and/or rotation of the required structural objects was initiated. From the captured acceleration time histories, the fluctuating response as well as the corresponding frequencies can be obtained using a Fast Fourier Transform (FFT) application. Fig. 3.8, 3.9a and 3.9b show the power spectral densities (PSD) of the acceleration time histories for all four mode shapes, respectively.

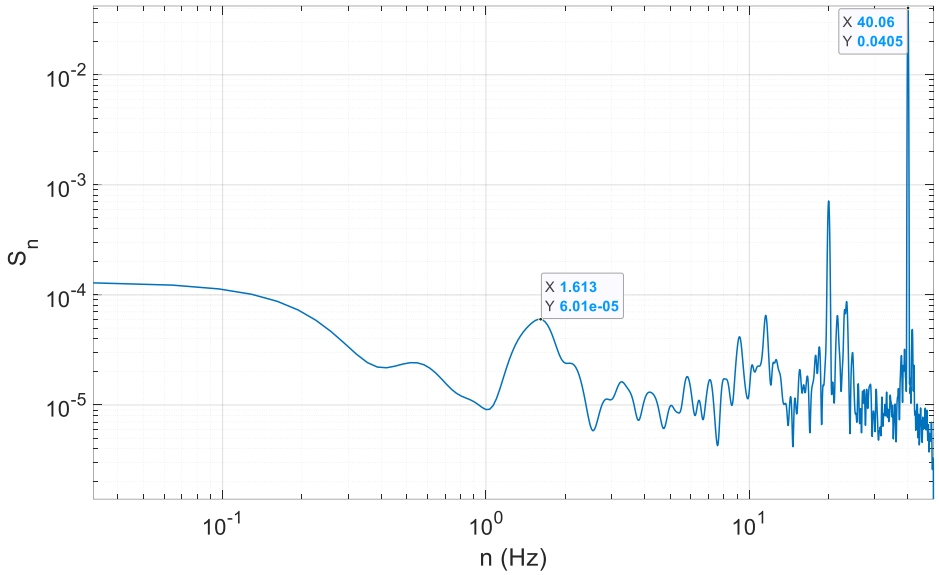

Fig. 3.8: PSD of acceleration time histories for transversal mode of vibration (conductor and tower frequencies shown) (Table 3.2)

By inspecting Fig. 3.8, it can be noted that the frequency of both modes of vibration (1 and 4) is 1.61 Hz and 40.06 Hz, respectively (seen in the data boxes). By comparison with the previously obtained target frequencies in Table 3.2, the percent difference is about 10.5% for both mode shapes. By looking at Fig. 3.9a and 3.9b, the obtained frequencies from the constructed model are 16.6 Hz and 35 Hz for mode shapes 2 and 3, respectively. In comparison with values of Table 3.2, the percent differences are 3.1% and 3%, respectively.

The small discrepancies recorded in the PSD plots of all four mode shapes could be attributed to slight mismatching of the masses and/or their distributions along the model during construction. Another reason for the small divergence could be due to unequal sags in the conductors of the transmission lines system, thereby creating different tensions in the cross-arms. Nevertheless, the obtained results and percent differences gave enough confidence for the WOW team to carry on with the wind tunnel testing and subsequent data analysis.

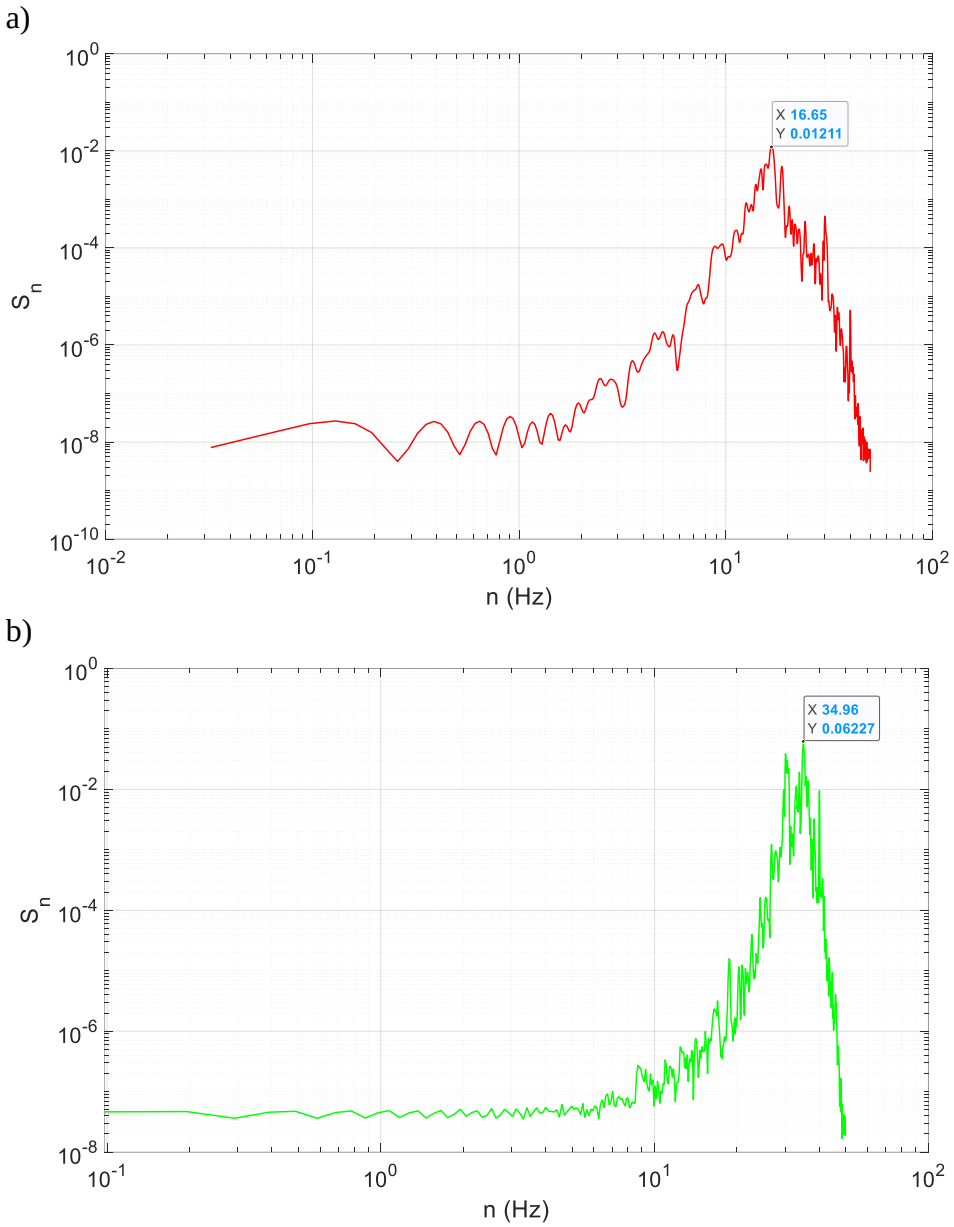

Fig. 3.9: PSD of acceleration time histories for: a) longitudinal, and b) rotational (Table 3.2)

3.3.2 Damping Estimation

Since a transmission lines system is a mix of towers and conductors having different levels of rigidity, the behavior of the conductors will greatly affect that of the towers [(Maeda et al., 1999); (Okamura et al., 2003); (Takeuchi et al., 2010)]. In addition, and because the structural damping of the tower is very small, the global response of the

system is more sensitive to aerodynamic damping of the conductors. Under the conditions of strong winds, such damping forces play an important role in the behavior of cable structures, such as conductors as well as transmission lines systems [(Davenport, 1988); (Momomura et al., 1997); (Takeuchi et al., 2010)].

On another note, it was shown in previous studies that the uncertainty inherited in the estimation of a damping ratio from the measured acceleration time histories tends to be higher than other vibration parameters. Some reports have shown that the standard deviation of the damping ratio could be as high as 70% when estimating the parameter using two different techniques based on measured data [(Haviland, 1976); (Davenport, 1983); (Takeuchi et al., 2010)].

Furthermore, the measured responses of the transmission lines system are complex as the line itself consists of many components with significant structural dynamic properties differences (i.e., tower, insulator, conductors). Thus, particular attention should be given to the decomposition of the vibration mode components in order to estimate the damping ratio of the entire system (Takeuchi et al., 2010).

Typically, damping estimation methods from measured data are divided into two categories: (i) those based on the time domain response function such as the Random Decrement (RD) technique and the Autocorrelation method (Tamura and Suganuma, 1996), and (ii) those based on the frequency domain response function such as the Hilbert Transform Method and the Half Power method (Agneni and Balis, 1988). However, the previous methods are, theoretically, applicable to single-degree-of-freedom (SDOF) systems only. In recent years, newer methods have emerged to address the response data of multi-degrees-of-freedom (MDOF) systems. Such methods include the Frequency Do-

main Decomposition (Brinker et al., 2000, 2001), the Wavelet-Logarithmic Decrement technique [(Ruzzene et al., 1997); (Lamarque et al., 2000); (Hans et al., 2000)] and the Multi-Degree-of-Freedom Random Decrement (MDOF RD) technique (Tamura et al., 2002).

In Chapter 2, the Single-Degree-of-Freedom Random Decrement (SDOF RD) technique (Tamura and Suganuma, 1996) was utilized to obtain along-wind and cross-wind aerodynamic damping values for the lattice transmission tower model tested. In this chapter, the MDOF RD (Tamura et al., 2002) technique will be adopted in order to estimate the aerodynamic damping values of the coupled tower-insulator-conductor transmission lines system. However, before proceeding to do so, the component of the tower mode needs to be extracted from the recorded time history of the accelerometers at different wind speeds. This is achieved using the Normal Decomposition Method (NDM) technique, developed by Fujimura et al. (2007). Note that the structural damping of the transmission tower was estimated in Chapter 2 using both ILS and SDOF RD methods. Recall that any technique or method selected to analyze the response data of any system will yield the total damping of that system. Therefore, to obtain the aerodynamic damping, one needs to subtract the structural damping from the total damping. Values of the structural damping for mode shapes 1 and 2 were obtained from free vibration tests conducted on the system with the WOW fans turned off. The structural damping was found to be equal to 0.56% for mode shape 1 and 1.42% for mode shape 2.

The basic theory of the NDM is described hereafter. For a MDOF system, the equation of motion can be written as follows (Equation 3.10):

$$M.\ddot{x}(t) + C.\dot{x}(t) + K.x(t) = p(t) \quad (3.10)$$

In Equation 3.10, *M*, *C*, *K* are the mass, damping, and stiffness matrices, respectively, whereas *p(t)* is the fluctuating force vector at time *t*. Similarly, *x(t)* is the displacement vector (with mean component subtracted) at time *t*. Note that the damping matrix *C* is orthonormal to the natural vibration modes vector. Also note that the displacement vector *x(t)* is written using a natural vibration mode matrix ϕ and the generalized displacement vector *q(t)* as shown in Equation 3.11:

$$x(t) = \phi.q(t) = [\varphi_1\ \varphi_2\ \varphi_3 \dots \varphi_i].[q_1\ q_2\ q_3 \dots\ q_i]^T \quad (3.11)$$

By combining Equations 3.10 and 3.11, and multiplying by ϕ^T, Equation 3.10 can be rewritten as Equation 3.12:

$$M^*.\ddot{q}(t) + C^*.\dot{q}(t) + K^*.q(t) = p^*(t) \quad (3.12)$$

In Equation 3.12, *M**, *C**, *K** are the generalized mass, damping, and stiffness matrices whereas *p*(t)* is the generalized fluctuating force vector.

The component of the restoring force in Equation 3.10 is written as follows (Equation 3.13):

$$K.x(t) = K.\phi.q(t) \quad (3.13)$$

By multiplying both sides of Equation 3.13 by ϕ^T, one obtains the expression in Equation 3.14:

$$\phi^T.K.x(t) = \phi^T.K.\phi.q(t) = K^*.q(t) \quad (3.14)$$

By double differentiation with respect to *t*, Equation 3.14 becomes Equation 3.15:

$$\phi^T.K.\ddot{x}(t) = K^*.\ddot{q}(t) \quad (3.15)$$

Consequently, the generalized acceleration of vibration mode $\ddot{q}_i(t)$ can be obtained from the measured acceleration time history $\ddot{x}(t)$ using Equation 3.16 as follows:

$$\ddot{q}(t) = K^{*-1}.\phi^{T}.K.\ddot{x}(t) \tag{3.16}$$

Using the previously described algorithm, the NDM combined with the MDOF RD techniques are utilized to characterize the measured acceleration response of the middle tower in the transmission lines system. The purpose of this analysis is to try and obtain the aerodynamic damping of the tower as part of a tower-insulator-conductor system and compare the values with those of the lattice tower by itself, given in Chapter 2. The analysis is conducted for all tested wind speeds and for two wind directions: 0° and 90°. Recall that a wind direction of 0° pertains to winds normal to the conductor spans and a wind direction of 90° involves winds along the conductor spans. Fig. 3.10 shows an example of the extraction of the different modes (conductor displacement, tower mode shape 1 and tower mode shape 2) from the recorded acceleration time histories at the top of the middle transmission tower.

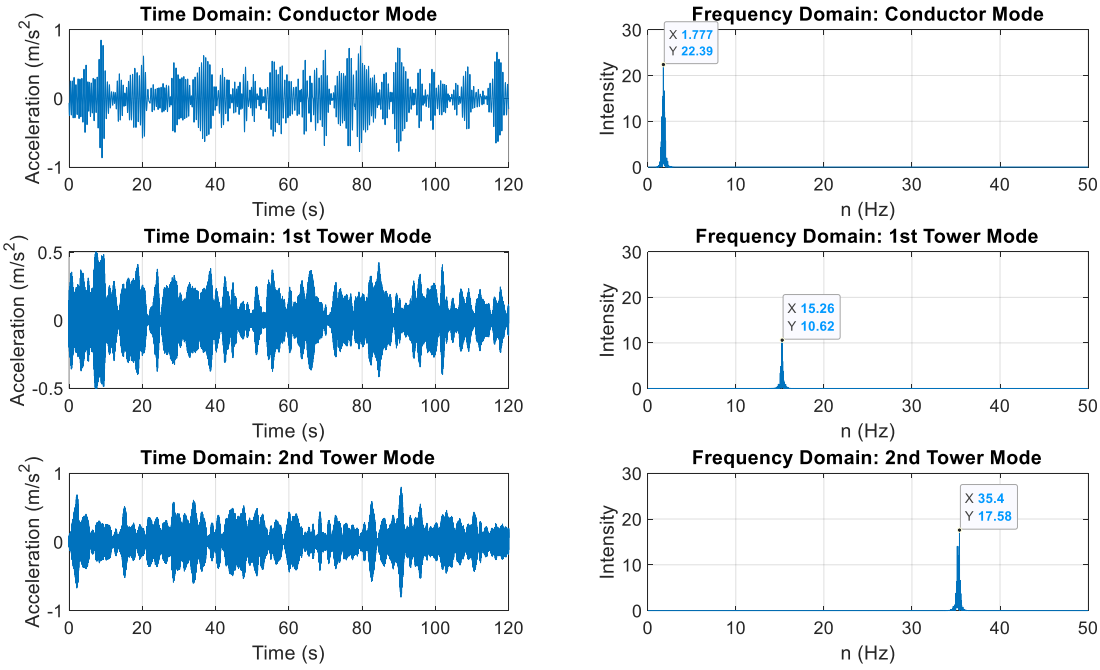

Fig. 3.10: Example of extracted component modes from the acceleration time histories of the middle transmission tower at 0° wind direction at U = 5 m/s (wind normal to conductors)

As can be seen in Fig. 3.10, all three dominant modes of vibration of the system appear when the signal is decomposed and processed using the NDM technique. The conductor mode surfaces around 1.78 Hz (1.8 Hz from Table 3.2) whereas the tower's first and second modes appear at 15.3 Hz and 35.4 Hz, respectively (16.1 Hz and 36.1 Hz from Table 3.2). This process is repeated for all wind speeds and the resulting time histories from the decomposition of the signals are used for the subsequent analysis with the MDOF RD technique. Specifically, the resulting time histories of the first and second tower modes are of interest as they showcase the effect of the coupling of the tower-insulator-conductor system with respect to the tower by itself (analysis conducted in Chapter 2). Note that, by comparing the obtained frequencies for modes 1 and 2 from above with previous values for the single tower case (Chapter 2), the percent difference is about 4.7% for tower mode 1 and 1% for tower mode 2. Fig. 3.11 shows the along-wind aerodynamic damping values (analytical and experimental) for the single tower case and the entire transmission lines system case, estimated analytically as well as experimentally. Note the following: (i) the analytical damping values for the transmission tower acting as a self-supported lattice tower are based on Equation 2.13, (ii) the SDOF RD (Tamura and Suganuma, 1996) aerodynamic damping values are estimated from the wind tests done on the self-supported lattice tower specimen, and (iii) the MDOF RD (Tamura et al., 2002) aerodynamic damping values are extracted from the wind tests conducted on the entire transmission lines system described above. Also note that the aerodynamic damping equation for cable structures (Equation 3.5) only applies to winds normal to the conductors, i.e., 0^o wind direction in the case of the experiments at the WOW. It is also worthwhile mentioning that the aerodynamic damping values of the conductors are the

following: 7.1%, 9.1%, 11.8%, and 14.8% at full-scale wind speeds of 35.4, 49.5, 63.6 and 77.8 m/s, respectively (calculated using Equation 3.5).

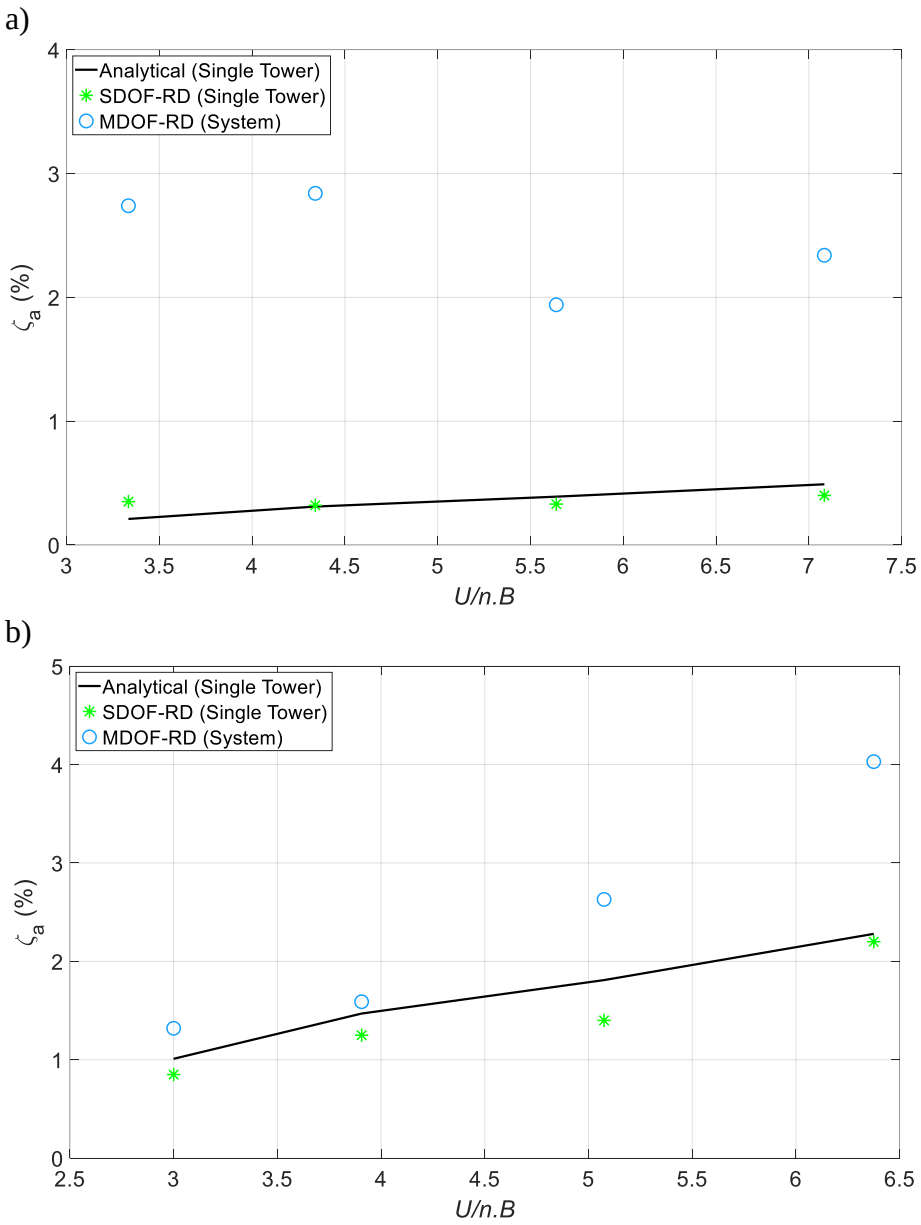

Fig. 3.11: Along-wind aerodynamic damping values for tower and transmission lines system for: a) 0^o wind direction, and b) 90^o wind direction

As seen in Fig. 3.11, the along-wind aerodynamic damping of the tower is highly affected by its coupling with the conductors and insulators. Values estimated using the MDOF RD show that the along-wind aerodynamic damping of the tower significantly

increases. At 0^o wind direction, the aerodynamic damping of the system fluctuates at around 2.9% for all tested wind speeds, compared to only about 0.5% for the single tower case. Similarly, at 90^o wind direction, ζ_a of the system in the along-wind direction is linearly increasing with increasing wind speeds. Values reach a maximum of 4.2% at a normalized velocity of $U/(n.B)$ of 6.4, compared to only 2.25% for the single tower case. This increase in the aerodynamic damping of the system could be attributed to the presence of the conductors. As noted earlier, at high wind speeds, ζ_a of the conductors reaches a value of about 14.8%. The presence of the conductors provides lateral bracing to the tower cross-arms at the different points of attachments, thereby reducing the acceleration and vibration of the towers and subsequently, providing higher damping.

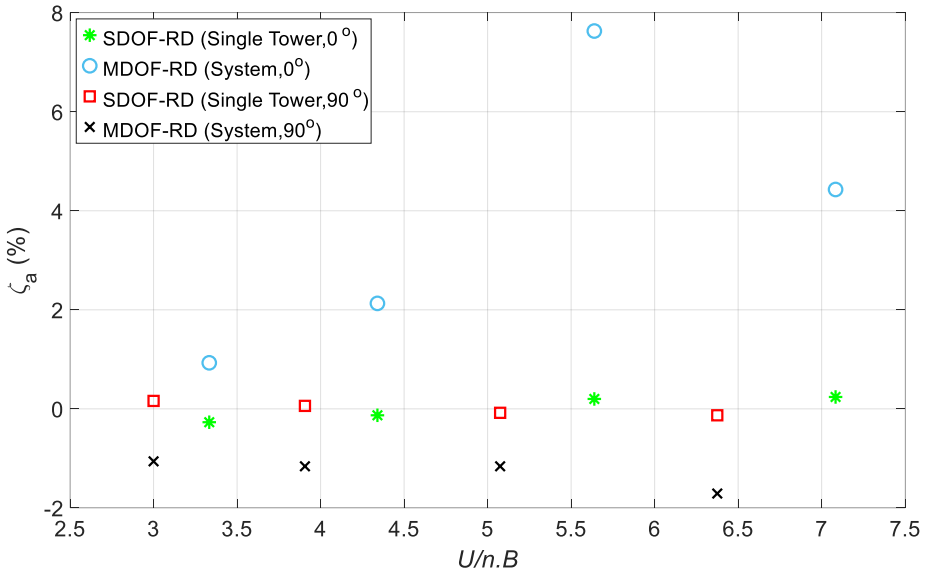

Fig. 3.12: Crosswind aerodynamic damping estimation for tower and transmission lines system (0^o and 90^o wind directions)

As shown in Fig. 3.12, the crosswind aerodynamic damping is also affected by the configuration. At 0^o wind direction, values of the crosswind ζ_a are largely increasing with increasing wind speeds for the transmission lines system, compared to the tower only configuration. The increase between both configurations, although not perfectly linear,

reaches a maximum of about 7.5% at a $U/(n.B)$ of about 5.6. However, for a wind direction of 90^o, the crosswind aerodynamic damping is reducing linearly with increasing wind speeds for the transmission lines system, as observed by the black X marks. The maximum difference is -1.7% at a $U/(n.B)$ of about 6.4.

Although the aerodynamic damping of the transmission tower as part of a tower-insulator-conductor system has largely increased, it has also reduced in the case of crosswind aerodynamic damping of the entire system for 90^o where the aerodynamic damping is showing negative values. This indicates that the coupling effects between transmission tower and conductor lines are rather strong, and current national and international standards do not adequately incorporate such effects into the design of transmission lines. As shown in Fig. 3.11 and 3.12, the incorporation of such effects seems favorable for the along-wind aerodynamic damping at 0^o and 90^o as well as the crosswind one at 0^o. This is seen by a large increase in the aerodynamic damping which could enable reducing the resonance effects. However, for its crosswind counterpart at 90^o, the coupling effects look rather unfavorable as there is a significant decrease in its values for all tested wind speeds, which could lead to higher resonance effects. However, as previously mentioned in Chapter 2, the crosswind damping results might have been more representative of the behavior of the spine rather than the lattice tower or transmission lines system. More testing is required in order to quantify the coupling effects of transmission towers and conductors in order to come up with standard specific values for design purposes.

3.3.3 Buffeting Theory and Comparison between Analytical and Experimental Results

Similar to Chapter 2, section 3.3, this section addresses the theoretical buffeting response of flexible structures for the case of the conductors. Using previously established equations in Chapter 2, the theoretical response of the deflection and drag on the conductors are estimated. Furthermore, the responses of the single lattice tower by itself and as part of the complete transmission lines system are compared. Recall that, in order to perform the buffeting analysis on the conductors, the following assumptions are made:

- The aerodynamic force coefficients measured in a steady flow can be used to estimate the fluctuating wind loads, using a quasi-steady approach.
- The analysis is only conducted in the along-wind direction (0^o wind direction).
- The conductors are also assumed to behave as simply supported line-like structures.

Estimation of Conductor Drag: This subsection makes use of previously established equations by Loredo-Souza (1996) and Loredo-Souza and Davenport (2001) to calculate the theoretical drag forces acting on the conductors and compare the obtained values to measured ones from the strain gauges mounted on the cross-arms of the transmission towers. According to Davenport (1993) and Loredo-Souza (1996), the mean drag force acting on the conductors is given in Equation 3.17:

$$\bar{F} = \int_0^l \frac{1}{2}\rho.U^2.C_D.d.i(x).dx = \frac{1}{2}\rho.U^2.C_D.d.\int_0^l i(x).dx \tag{3.17}$$

In Equation 3.17, ρ_a is the density of air (in kg/m^3), U is the mean wind speed at conductor height (in m/s), C_D is the drag coefficient of the cable, d is the diameter of the cable

(in m), *l* is the length of the cable (in m), and *i(x)* is the influence line per each length *x* of the cable.

As was the case for the RMS of base shears on transmission towers (Equation 2.24), the RMS of forces acting on the conductors is given in Equation 3.18, and the background and resonant responses are defined in Equation 3.19 and 3.20:

$$\sigma_{drag} = \sqrt{\sigma_{B,drag}^2 + \sigma_{R,drag}^2} \tag{3.18}$$

$$\sigma_{B,drag}^2 = (\rho . U^2 . d . I_u)^2 . \int_0^l \int_0^l e^{-\left(\Delta x / {}^x L_u\right)} . i(x) . i(x') . dx . dx' \tag{3.19}$$

$$\sigma_{R,drag} = \sqrt{\frac{\pi}{4} . \frac{n . S_F(n)}{\zeta_{tot}}} . \frac{\int_0^l m(x) . \mu_j(x) . i(x) . dx}{\int_0^l m(x) . \mu_j^2(x) . dx} \tag{3.20}$$

In Equation 3.19, I_u is the turbulence intensity at the height of the conductors, Δx is the difference in lengths between two cable spans *x* and *x'* along the entire length of the conductors (in m), and ${}^xL_u$ is the integral length scale of longitudinal turbulence (in m). Additionally, in Equation 3.20, $n.S_F(n)$ is the spectra of the generalized force acting on the conductors, given in Equation 3.21, whereas $m(x)$, $\mu_j(x)$, and $i(x)$ are the respective mass (in kg/m), mode shape and influence line per cable length *x* along the conductor span *l*.

$$n . S_F(n) = (\rho . U^2 . d . I_u)^2 . \frac{n_0 . S_u(n_0)}{\sigma_u^2} . \int_0^l \int_0^l e^{\frac{-c . |\Delta x| . n}{U}} . \mu_j(x) . \mu_j(x') . dx . dx' \tag{3.21}$$

In Equation 3.21, the Von Karman approximation of the expression $n_o.S_u(n_o)/\sigma_u^2$ is given in Equation 2.20 and repeated below in Equation 3.22. Recall that *c* is the exponential decay factor for "narrow band" correlation (usually taken as 7). The value of *c* was pro-

posed by Davenport (1962b, 1963) in his empirical simplification expression for the variation of the normalized cross-spectrum $\overline{S}_{uu}$ for long structures.

$$\frac{n_0.S_u(n_0)}{\sigma_u^2} = \frac{4.\frac{n_0.\,^xL_u}{U}}{(1+70.78(\frac{n_0.\,^xL_u}{U})^2)^{5/6}} \tag{3.22}$$

As such, Equation 3.18 is used to estimate the RMS of drag forces on the conductors at the top level. The analytical values are compared to the measured response from the strain gauges installed on the tower cross-arms, and the comparison is illustrated in Fig. 3.13 for a wind direction of 0°. The measured drag is presented for the front conductor as well as the back one. Recall that there are two conductors on each level (three levels, six conductors in total). Note that all the analytical and measured responses of the conductors and towers in the subsequent figures have been converted to full-scale using the appropriate factors from Tables 2.1 and 3.1.

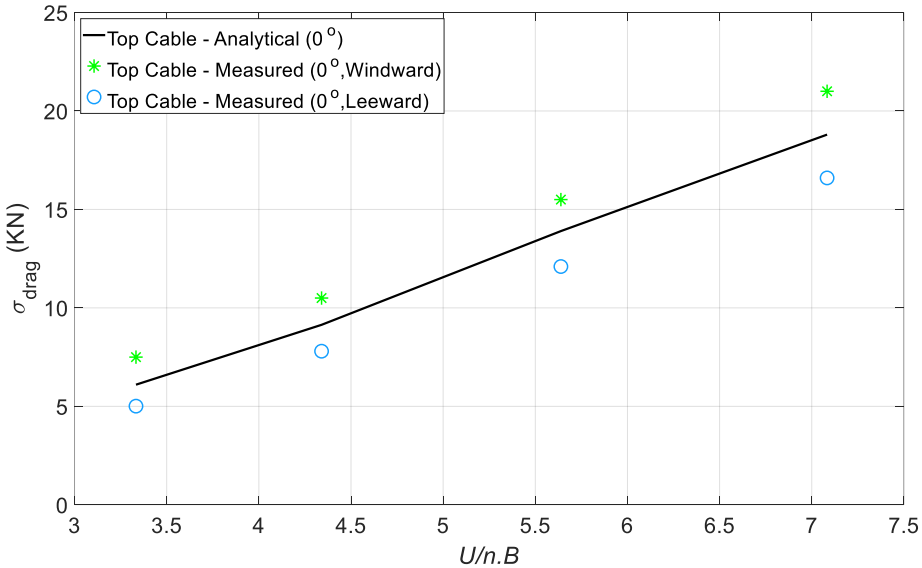

Fig. 3.13: Comparison of analytical and measured RMS of drag forces on conductors for 0° wind direction (top cable)

As shown in Fig. 3.13, values of the RMS of drag forces estimated on the windward cable are slightly smaller than their measured counterparts. The percent difference varies between 10% and 20%. Note that the analytical approach was applied to the full-scale properties of the conductors using the entire span length (180 m). The reason for the discrepancy could be due to the fact that, although the wind characteristics are the same for both analytical and experimental approaches, the turbulence is causing a larger correlation in the case of the distorted model (i.e., measured values from the model constructed at the WOW), and therefore, the RMS is larger. This phenomenon was also observed in Loredo-Souza (1996) when testing the distortion theory on cable structures. For transverse winds, i.e., 0^o wind direction, Loredo-Souza (1996) found out that the RMS values were overestimated by roughly 40% in some cases due to the higher turbulence correlation for the distorted span case in comparison to undistorted cables. Such findings are very important since they showcase the effect of turbulence in the dynamic response of structures. As observed and stated by Loredo-Souza (1996), the variance of a certain response is directly proportional to the ratio between the turbulence length scale and the span of a certain structure. This is exactly what is demonstrated in Fig. 3.13.

On another note, Fig. 3.13 also provides an insight into the shielding effects created by the windward conductor over its leeward counterpart. The leeward conductor experienced a reduction of the drag forces of about 20% to 30% compared to its windward equivalent in some instances. Typically, ASCE 74 (2010) considers shielding factors for lattice members of transmission towers but does not provide any guidelines for conductors. ANSI/TIA-222 (2005) does not consider any shielding reduction for members spaced at a distance of four times the diameter of the member or larger (which is the case

in the experiments conducted above). It is also worthwhile noting that, although cables moved independently from each other at higher wind speeds, no clashing between conductors was observed during the tests conducted at the WOW. More testing is required in order to quantify the effects of shielding of parallel cables at different wind speeds and with varying spacings and cable diameters.

Estimation of Conductor Deflection: Recall, from Chapter 2, section 3.3, that the power spectrum of deflection S_q at the top level of the conductors, at mid-span, as well as the top of the middle tower (in a single tower configuration) is given by Equation 2.14, re-written here as Equation 3.23 [(Davenport, 1962a); (Davenport, 1962b); (Irwin, 1977); (Irwin, 1979); (Irwin, 1996)].

$$S_q(n) = \frac{(\rho . U . C_{x0} . A)^2}{M_G^2 \omega_0^4} . \left| H\left(\frac{n}{n_0}, \zeta_{tot}\right)\right|^2 . \left|\chi_y(n)\right|^2 . |\chi_{2D}(n)|^2 . S_u(n) \tag{3.23}$$

If Equation 3.23 is integrated over all frequencies, one can obtain the variance of the deflection fluctuations σ_q^2 from the power spectrum and the RMS of the deflection σ_q can then be expressed in terms of background and resonant terms using Equation 3.24 (previously described in Chapter 2, section 3.3).

$$\sigma_q = \frac{\rho . U^2 . C_{x0} . A . I_u}{M_G . \omega_0^2} . \sqrt{B + R} \tag{3.24}$$

The background B and resonant R terms were also defined in Chapter 2 in Equations 2.17 and 2.18, repeated below in Equations 3.25 and 3.26. The rest of the terms in Equations 3.23, 3.24, 3.25 and 3.26 can be found earlier in Chapter 2.

$$B = \int_0^{+\infty} \left|\chi_y(n)\right|^2 . |\chi_{2D}(n)|^2 . \frac{S_u(n)}{\sigma_u^2} . dn \tag{3.25}$$

$$R = \left|\chi_y(n_o)\right|^2 . |\chi_{2D}(n_o)|^2 . \frac{n_0 . S_u(n_0)}{\sigma_u^2} . \frac{\pi}{4 . \zeta_{tot}} \tag{3.26}$$

To estimate the mean and peak deflection values of the conductors, Equations 3.27 and 3.28, which are based on influence lines [(Loredo-Souza, 1996); (Loredo-Souza and Davenport, 2003)], can be used.

$$\bar{q} = \frac{\bar{F}}{K} \tag{3.27}$$

$$\hat{q} = \bar{q} + g_s . \sigma_q \tag{3.28}$$

In Equation 3.27, $\bar{q}$, $\bar{F}$, and K are the mean deflection at mid-span (in m), the mean drag force (in N) (calculated using Equation 3.17), and the stiffness of the conductors (in N/m), respectively. The stiffness of the conductors K can be calculated by multiplying the square of the angular frequency ω of one conductor by its total mass M. In Equation 3.28, $\hat{q}$ is the peak deflection of the conductors at mid-span (in m) and g_s is the statistical peak factor, defined in Equation 3.29.

$$g_s = \sqrt{2 \times \ln(\nu . T)} + \frac{0.577}{\sqrt{2 \times \ln(\nu . T)}} \tag{3.29}$$

In Equation 3.29, T is the time (in sec) taken between 1,200 sec and 3,600 sec and ν is the crossing rate, given in Equation 3.30.

$$\nu^2 = \frac{\sum n_j^2 . R_j^2}{B^2 + R_j^2} \tag{3.30}$$

The terms B and R were previously defined in Equations 3.25 and 3.26, n is the natural frequency (in Hz), and j is the mode of vibration under investigation. Using Equations 3.24, 3.25 and 3.26, the RMS, mean and peak deflections of the top level of front conductors at mid-span are given in Fig. 3.14 for all tested wind speeds for 0^o wind direction.

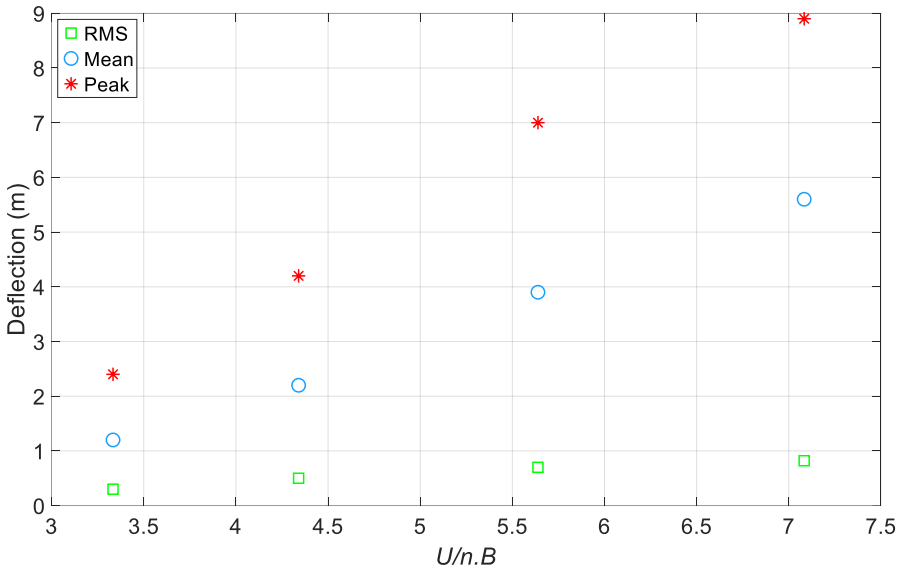

Fig. 3.14: RMS, mean, and peak deflection values of top-level front conductors at 0° wind direction

As observed in Fig. 3.14, the increase in all three variables is almost linear with increasing wind speeds. Using Equation 3.28, the maximum estimated deflection $\hat{q}$ is about 8.7 m (full-scale). Unfortunately, no instrument was installed on the conductors in order to verify whether the estimated values are close to the measured ones. It is worthwhile mentioning that, typically, it is extremely challenging to instrument conductors and cables in aeroelastic testing. This is due to the high vibration of the conductors under high wind speeds as well as the installation and wiring of instrumentation (accelerometers or deflectometers) on such thin structures.

Comparison of Measured Responses in both Aeroelastic Models: The acceleration response of the lattice tower when used as a self-supported lattice structure and tested in Chapter 2 is shown in Fig. 3.15 along with measured values from the complete transmission lines system. Note that, in the legend of the following figures, 'Single Tower' and 'System' stand for the single tower (Chapter 2) and complete transmission lines response results, respectively.

As observed in Fig. 3.15, the presence of the conductors has drastically lowered the acceleration values of the system, thereby limiting the significant vibrations previously observed in the wind testing of the single tower. The conductors, spread over three levels, created a lateral bracing for the transmission towers, which reduced their accelerations for both wind directions: 0° and 90°. Another reason for the difference is attributed to the increase in the aerodynamic damping of the system once the conductors have been attached to the insulators and subsequently to the tower cross-arms. As previously observed in Fig. 3.11, the along-wind aerodynamic damping of the system for both wind directions is much higher than that of the single tower by itself. Such a phenomenon leads to a big dampening in the response of the system, thereby reducing its acceleration.

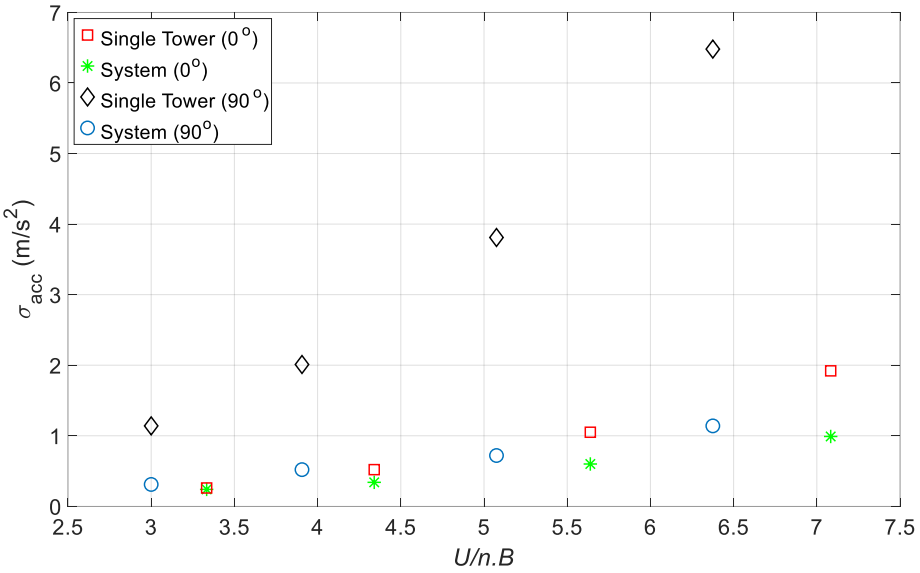

Fig. 3.15: Comparison of measured σ_{acc} values for 0° and 90° wind direction (single tower and complete transmission lines models)

Similar to the acceleration comparison in the previous paragraph, Fig. 3.16a and 3.16b show the measured results for the along-wind base shears of both aeroelastic models for 0° and 90° wind directions. Fig. 3.16b also shows the crosswind base shears for 90° wind direction.

As can be seen in Fig. 3.16a, the single tower response values are roughly between 1.5 to 2 times higher than their system counterparts at 0^o wind direction. At 90^o wind direction, the single tower response values are about 4 to 5 times greater than the system response. Similar to the reasons proposed for the differences in the acceleration results, the same could be said for the case of the base shears. Such divergences in the results are attributed to the increase in the along-wind aerodynamic damping of the system (which is inversely proportional to the RMS values of the responses) as well as the presence of the conductors, creating lateral bracing points at several heights on the transmission towers. In addition, for the 0^o wind direction, the difference in the base shears for all three transmission towers tends to get larger at higher wind speeds. At a $U/(n.B)$ of 7.2, the middle tower experienced greater loads than the side towers. This indicates that some conductors experienced more drag forces than others, particularly the ones contributing to the tributary area allocated to the middle tower.

Concerning the comparison of the base moments between both models, Fig. 3.17a and 3.17b show the measured RMS results for the along-wind base moments of all three transmission towers for 0^o and 90^o wind directions. Additionally, Fig. 3.17b illustrates the crosswind base moments for 90^o wind direction.

As previously observed in Fig. 3.15, 3.16, and 3.17, there is considerable difference in the measured response of both models. The single tower values are between 1.5 to 2 times and 4 to 6 times greater than their system counterparts at 0^o and 90^o wind directions, respectively. Again, such differences in the results could be due to the increase in the along-wind aerodynamic damping of the system, created by the presence of the conductors. At 90^o wind direction, the crosswind base moments are also higher than their

along-wind counterparts for all tested wind speeds. This justifies the need for considering the crosswind response of transmission lines systems in design standards worldwide.

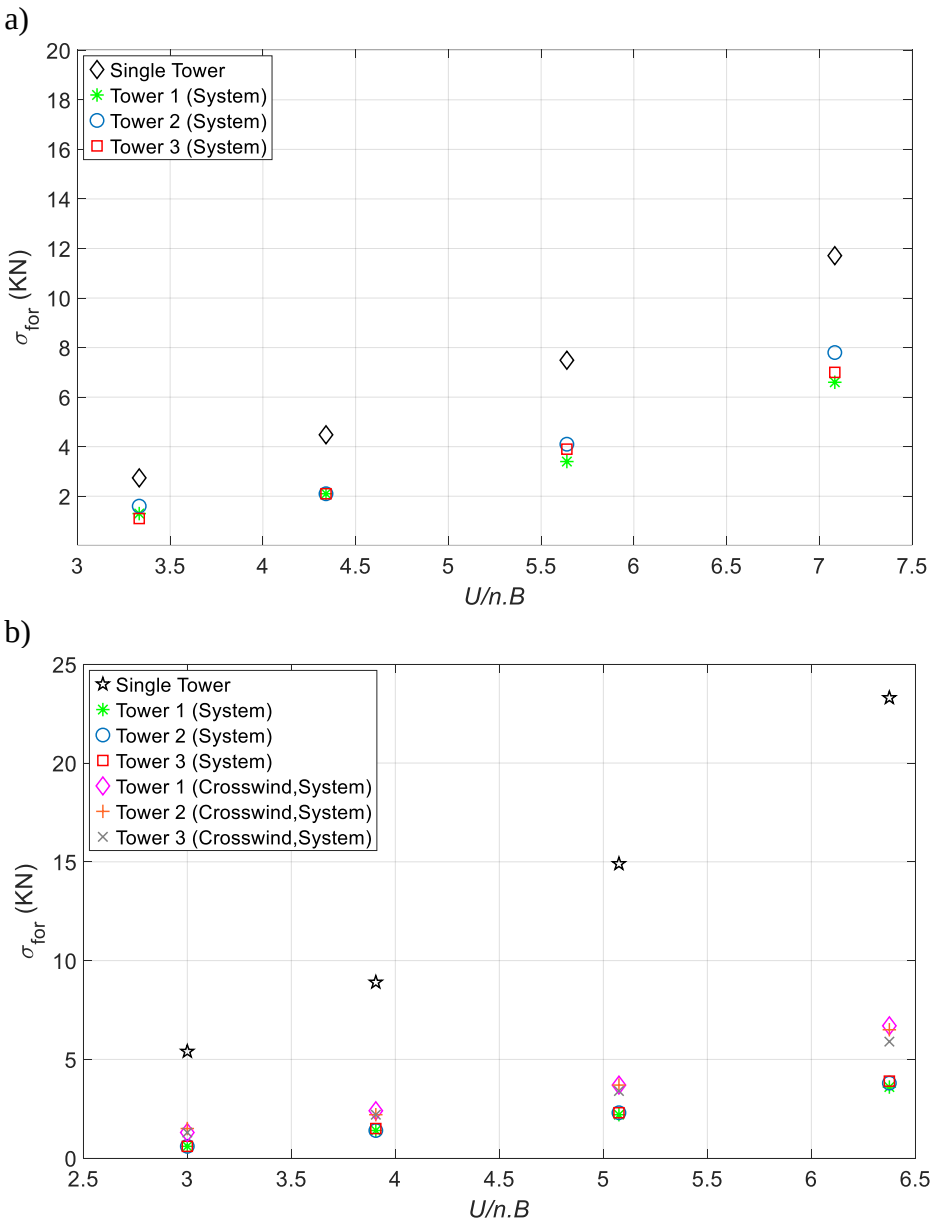

Fig. 3.16: Comparison of measured σ_{for} (both models) at: a) 0° wind direction, b) 90° wind direction (cross-wind measured responses are also included)

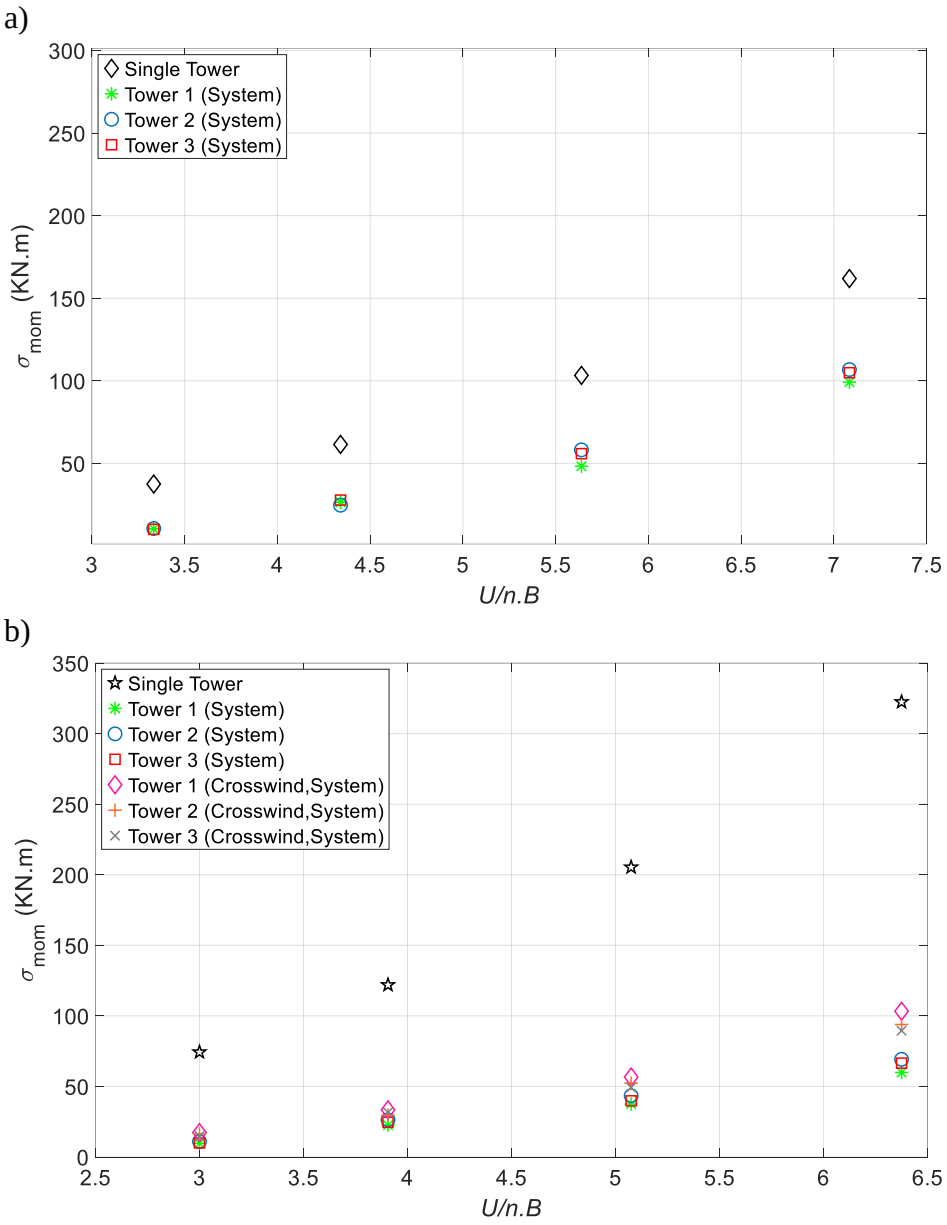

Fig. 3.17: Comparison of measured σ_{mom} (both models) at: a) 0° wind direction, b) 90° wind direction (cross-wind measured responses are also included)

At 90° wind direction and as shown in Fig. 3.16b and 3.17b, the crosswind base shears and base moments are largely greater than their along-wind counterparts for all tested wind speeds in the case of the system response. This is particularly important since, as stated in Chapter 2, standards typically target the along-wind response and neglect the contribution of its crosswind counterpart. This issue becomes even more im-

portant since the crosswind aerodynamic damping of the coupled transmission-tower-insulator system is less than that of the lattice tower by itself (as seen in Fig. 3.12). Therefore, it is crucial to investigate the crosswind response in order to check whether that assumption is adequate or not.

However, in the tests conducted at 90^o wind direction, both RMS of base shears and base moments did not exceed their 0^o wind direction along-wind counterparts. Nevertheless, more testing is required in order to quantify the crosswind aerodynamic damping and response of transmission systems and possibly account for them in future design standards.

3.3.4 Dynamic Amplification Factors

For the next subsection of this chapter, the dynamic amplification factors (DAF) for each measured response are computed. Equation 2.42, previously defined in Chapter 2, is utilized for the computation of the DAF at several wind speeds [(Elawady et al., 2017); (Azzi et al., 2020c)]. Subsequently, several observations are conducted related to how the DAFs change with the increase in wind speeds as well as a comparison between the single lattice tower case and the complete transmission lines system.

Recall that the quasi-static response signifies the summation of the mean and the background responses. Furthermore, the resonant response is connected to resonance amplification of components (i.e., forces, moments, displacements, accelerations, …) with frequencies near or equivalent to the natural frequency of the structure in a given mode shape. Also note that the background response contains no resonant amplification of any sorts [(Elawady et al., 2017); (Simiu and Yeo, 2019); (Azzi et al., 2020c)].

It is worthwhile recalling that the entire concept of computing values of DAF is based on the assumption that the fluctuating wind field is responsible for the fluctuating

response of the structure. As such, the assumptions made in Chapter 2, section 3.5, still hold. Similarly, the procedure of computing the DAF is utilized once again for the complete transmission lines system.

The described procedure in Chapter 2 along with the assumptions for the computation of the DAF are used for all tested angles and wind speeds on all the recorded responses by the different sensors installed on the model. Fig. 3.18 illustrates a plot of a decomposition sample of the base moment M_x at 0^o wind direction. Fig. 3.18a shows the initial plot obtained from the decomposition process, revealing the peak and background spectra as well as the resonance detection and normalized cumulative spectra (CPSD). Fig. 3.18b is a zoomed in plot of Fig. 3.18a, revealing the resonance detection at several natural frequencies of the system. More information and detailed description of the DAF method can be found in Elawady et al. (2017) and Azzi et al. (2020c). Fig. 3.19 shows the DAF values for all the responses measured during the wind testing at several wind speeds. Table 3.3 depicts a comparison between DAF values for a single lattice tower (taken from Fig. 2.18 in Chapter 2) and those of the complete transmission lines system (Fig. 3.19).

Some response measurements have shown a high contribution of the resonant component while others did not. As shown in Fig. 3.18a, the CPSD curve (drawn in green) is steadily going up until reaching its maximum value of 1. The largest contribution to the resonant response manifests itself between frequencies of 0.1 Hz and 5 Hz. Such frequencies are typically attributed to the vibration of the conductors and this is clearly shown in Fig. 3.19b where values of the DAF of the axial forces in the cross-arms (attributed to the drag forces on the conductors) are very high at small wind speeds (35

m/s, full-scale). Although the natural frequencies related to the transmission towers' vibrations did appear on Fig. 3.18a and 3.18b (at around 16 Hz, 32 Hz, and 40 Hz); i.e., their contribution to the resonant response was minor. This is clearly observed in Fig. 3.19a where the DAF for the base shears and moments are very small at low wind speeds.

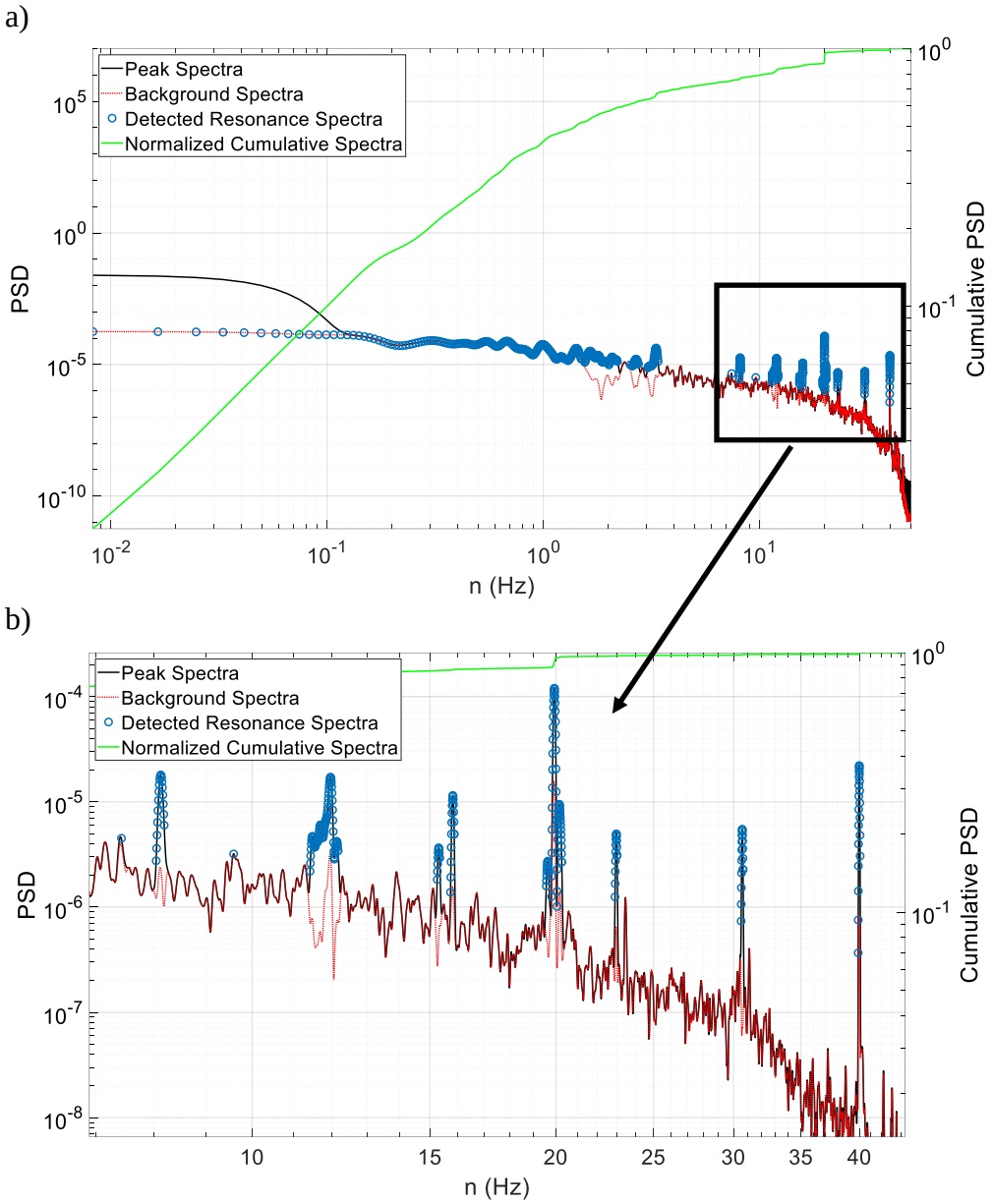

Fig. 3.18: Decomposition sample of one signal M_x at 35.4 m/s (full-scale) (0° wind direction, i.e., winds are normal to the conductors): a) initial plot, and b) resonance detection (zoomed in plot of Fig. 3.18a)

Looking at Fig. 3.19, values of DAF for all measured responses vary between 1 and 1.3. It can be observed that values of base shears and base moments (Fig. 3.19a) are increasing with the increase in the wind speed. However, this was not the case for the single lattice tower case (Table 3.3). For the single tower case, the DAF for the base shears were observed to decrease and this phenomenon was attributed to the increase in the aerodynamic damping of the tower as the wind speed increases. The DAF of the base moments increased and that was due to the excessive vibration of the single tower, especially at higher wind speeds, which might have overshadowed the effects of the increase in the aerodynamic damping.

Concerning the DAF for the cross-arms axial forces, although the values start at relatively high numbers, they also decrease with increasing wind speeds. This is due to the increase in aerodynamic damping of the conductors, which reaches a maximum of about 15% at the highest wind speed (reported earlier). This decrease in DAF is observed for all three levels of cross-arms in the complete transmission lines system. Yet, the same could not be said about the DAF of the cross-arm axial forces in the single lattice tower case. And this was attributed to the high local flexibility of the cross-arms. It is presumed that the presence of the conductors reduced the flexibility of the cross-arms by providing lateral bracing to the tower at several locations.

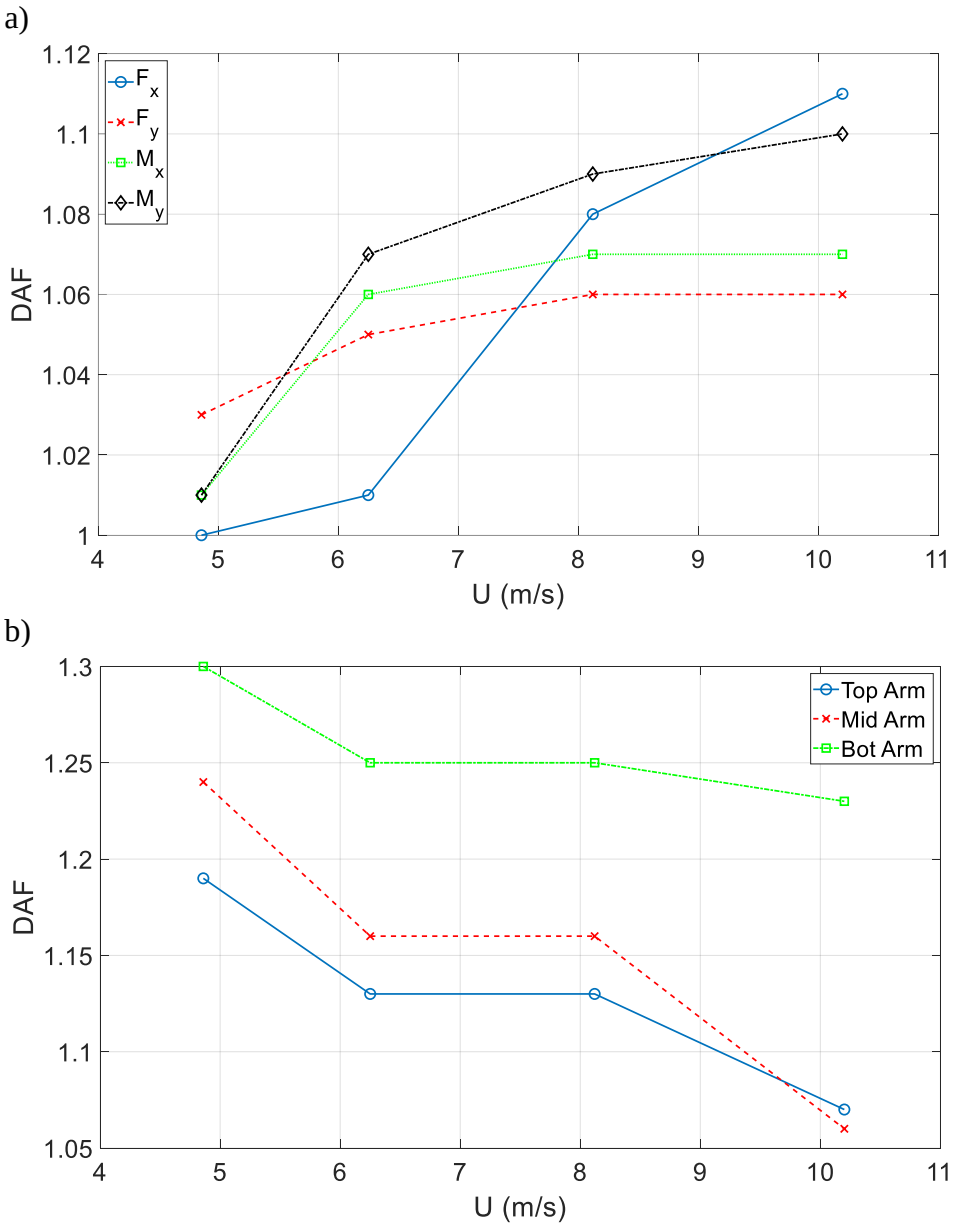

Fig. 3.19: Obtained values of DAF for: a) base shears and base moments, and b) cross-arms axial forces

Table 3.3: Summary of DAF results for both aeroelastic models tested

Model	Response	DAF		Observation
		At 35 m/s	At 78 m/s	
Single lattice tower	Base shear F_x	1.15	1.11	Decreasing
	Base shear F_y	1.1	1.06	Decreasing
	Base moment M_x	1.01	1.05	Increasing
	Base moment M_y	1.13	1.18	Increasing
	Bottom arm axial force P	1.1	1.17	Increasing
	Middle arm axial force P	N/A	N/A	N/A
	Top arm axial force P	N/A	N/A	N/A
Complete transmission lines system	Base shear F_x	1	1.11	Increasing
	Base shear F_y	1.03	1.06	Increasing
	Base moment M_x	1.01	1.07	Increasing
	Base moment M_y	1.01	1.1	Increasing
	Bottom arm axial force P	1.3	1.23	Decreasing
	Middle arm axial force P	1.24	1.06	Decreasing
	Top arm axial force P	1.19	1.07	Decreasing

Previously published studies on the dynamic response of transmission lines systems [(Davenport, 1962b); (Momomura et al., 1997); (Loredo-Souza and Davenport, 1998); (Holmes, 2008); (Lin et al., 2012); (Aboshosha et al., 2016)] showed that the tower conductors and the turbulent winds might have close frequencies. However, the resonant effect is almost also negligible due to the effect of high aerodynamic damping resulting from the conductors' behavior. This holds true under high-speed winds as observed in Fig. 3.19b where the DAF is largely decreasing with increasing wind speeds. However, at low wind speeds, the aerodynamic damping decreases thus resonant effects can possibly occur. This was also shown in Fig. 3.19b where the resonant contribution is almost equal to 30% of the total contribution (DAF is about 1.3 for bottom cross-arm).

In comparison with previously published literature and similarly to Chapter 2, Aboshosha et al. (2016) reviewed some of the current standards regarding dynamic and quasi-static buffeting response of transmission lines under synoptic and non-synoptic winds. According to the authors, ASCE 74 (2010), AS/NZS 1170.2 (2011) and BS 50341 (2001) have established a tower and conductor gust response factors G_T and G_C, respectively, in order to account for any dynamic effects on lattice towers used as transmission lines as well as electrical conductors. AS/NZS 1170.2 (2011) and BS 50341 (2001) define G_T as a constant for all wind speeds taken as 1.0 and 1.05, respectively. On the other hand, ASCE 74 (2010) establishes Equations 2.43, 2.44 and 2.45 (given and defined in Chapter 2 and redefined below as Equations 3.31, 3.32 and 3.33) in order to obtain G_T:

$$G_T = \frac{1 + 2.7E.\sqrt{B_T}}{K_u^2} \tag{3.31}$$

$$E = 4.9.\sqrt{\kappa}.\left(\frac{33}{z_h}\right)^{1/\alpha_{ter}} \tag{3.32}$$

$$B_T = \frac{1}{1 + \frac{0.56z_h}{L_s}} \tag{3.33}$$

The rest of the parameters of Equations 3.32 and 3.33 are given in ASCE 74 (2010) section 2.1.5.1 for different exposure categories. Note that the gust response factors G_T and G_C proposed by the standards are equal to the ratio of the peak load effect on the structure divided by the mean load effect corresponding to the wind speed.

For open terrain exposure, the value of G_T for the transmission tower tested in this project comes out to about 0.88. This value is less than the ones proposed in the rest of standards. In addition, it is also much smaller than the obtained DAF values in Table 3.3

for the lattice tower by itself as well as its use as part of a tower-insulator-conductor system.

Concerning the conductor gust response factor G_C, ASCE 74 (2010) proposes Equation 3.34, coupled with Equation 3.35:

$$G_C = \frac{1 + 2.7E.\sqrt{B_C}}{K_u^2} \tag{3.34}$$

$$B_C = \frac{1}{1 + \frac{0.8S}{L_s}} \tag{3.35}$$

In Equation 3.34, K_u refers to the ratio of the 3-sec gust wind speed to the 10-min average wind speed (usually taken as 1.43), S refers to the span length of the conductors (in ft for Equation 3.35 but in m everywhere else) while parameters E, B_T and B_C are given in Equations 3.32, 3.33 and 3.35. Once again, the rest of the parameters of Equations 3.34 and 3.35 are given in ASCE 74 (2010) section 2.1.5.1. Using the previous equations for an open terrain exposure, the values of G_T and G_C for the complete transmission lines system tested are equal to 0.88 and 0.74, respectively.

On the other hand, AS/NZS 1170.2 (2011) and BS 50341 (2001) define G_C as follows, using Equations 3.36 and 3.37, respectively:

$$G_C = 0.59 + 0.41e^{(-S/210)} \tag{3.36}$$

$$G_C = 1.3 - a.\ln(S) \tag{3.37}$$

In Equations 3.36 and 3.37, S is expressed in m whereas a is a terrain exposure coefficient, taken as 0.082 for open terrain. Using the previous equations, the values of G_C amount to 0.76 and 0.87, respectively. All the previously calculated factors are much less than the values of the DAF given in Table 3.3.

Such findings imply that the dynamic effects on lattice structures as well as transmission lines are still not fully understood. For this particular reason, and since design engineers use the 3-sec gust in their wind load calculations on transmission towers and conductors, it was decided to propose a table in order to account for any dynamic effects on transmission lines. Table 3.4 presents suggested factors to be used with the 3-sec gust for the design of transmission lines components. The choice of the range of factors is based on the results obtained in Chapters 2 and 3 as well as values presented in Table 3.3. Note that the range of design factors provided in Table 3.4 is based on the current tests conducted at the WOW and that the use of such factors should account for the entire dynamic response of transmission lines systems. By using Table 3.4, design engineers would not need to use the gust response factors in their calculations. This topic requires further investigation and testing in order to assess the validity of such factors for other lattice tower shapes as well as transmission lines configurations.

Table 3.4: Suggested range of design factors to account for possible dynamic effects

Response	Design 3-sec gust depending on location of transmission lines			
	U_{3sec} = 35 m/s	U_{3sec} = 50 m/s	U_{3sec} = 65 m/s	U_{3sec} = 78 m/s
Base shear	1.1 - 1.2	1.1 - 1.2	1.1 - 1.2	1.1 - 1.2
Base moment	1.1 - 1.2	1.1 - 1.2	1.1 - 1.2	1.1 - 1.2
Cross-arm axial force	1.1 - 1.4	1.1 - 1.3	1.1 - 1.3	1.1 - 1.3

3.3.5 Reynolds Number *Re* Effects

As noted earlier in the dissertation manuscript, it is challenging to satisfy the Reynolds number *Re* similitude and thus, it is possible that the drag on the lattice structures could be affected by the distortion in the *Re* similitude [(Lou et al., 1995); (Lou et al., 2000); (Loredo-Souza, 2014)]. Moreover, possible *Re* effects might also arise due to the fact that the scaled model was designed using two complementing components, un-

like the prototype lattice angles: (i) a structural element also known as a “spine”, and (ii) non-structural elements referred to as ”cladding”. To check for possible *Re* effects, it is worthwhile to plot the mean drag and moment coefficients at the base of the transmission towers with respect to the wind speeds tested. Fig. 3.21a, 3.21b, 3.22a, and 3.22b show the mean drag and moment coefficients (calculated using Equations 2.33 and 2.34) at the base of the tower for both longitudinal and lateral directions, for all tested wind directions and wind speeds. Recall that 0^o wind direction means the wind is along the strong axis of the tower (y-axis) and 90^o wind direction implies the wind is along the weak axis of the tower (x-axis) (shown in Fig. 3.20).

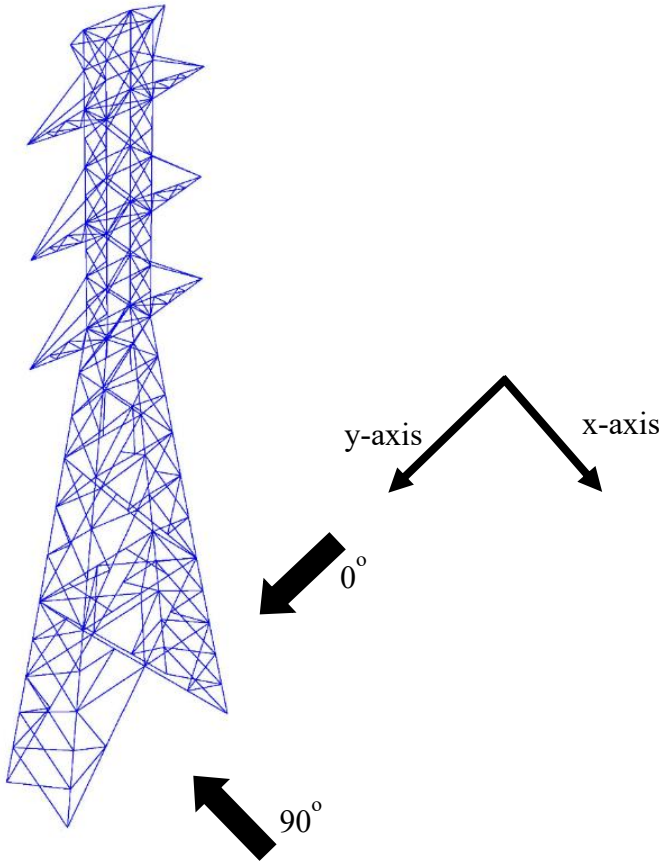

Fig. 3.20: Tower principal axes and wind directions

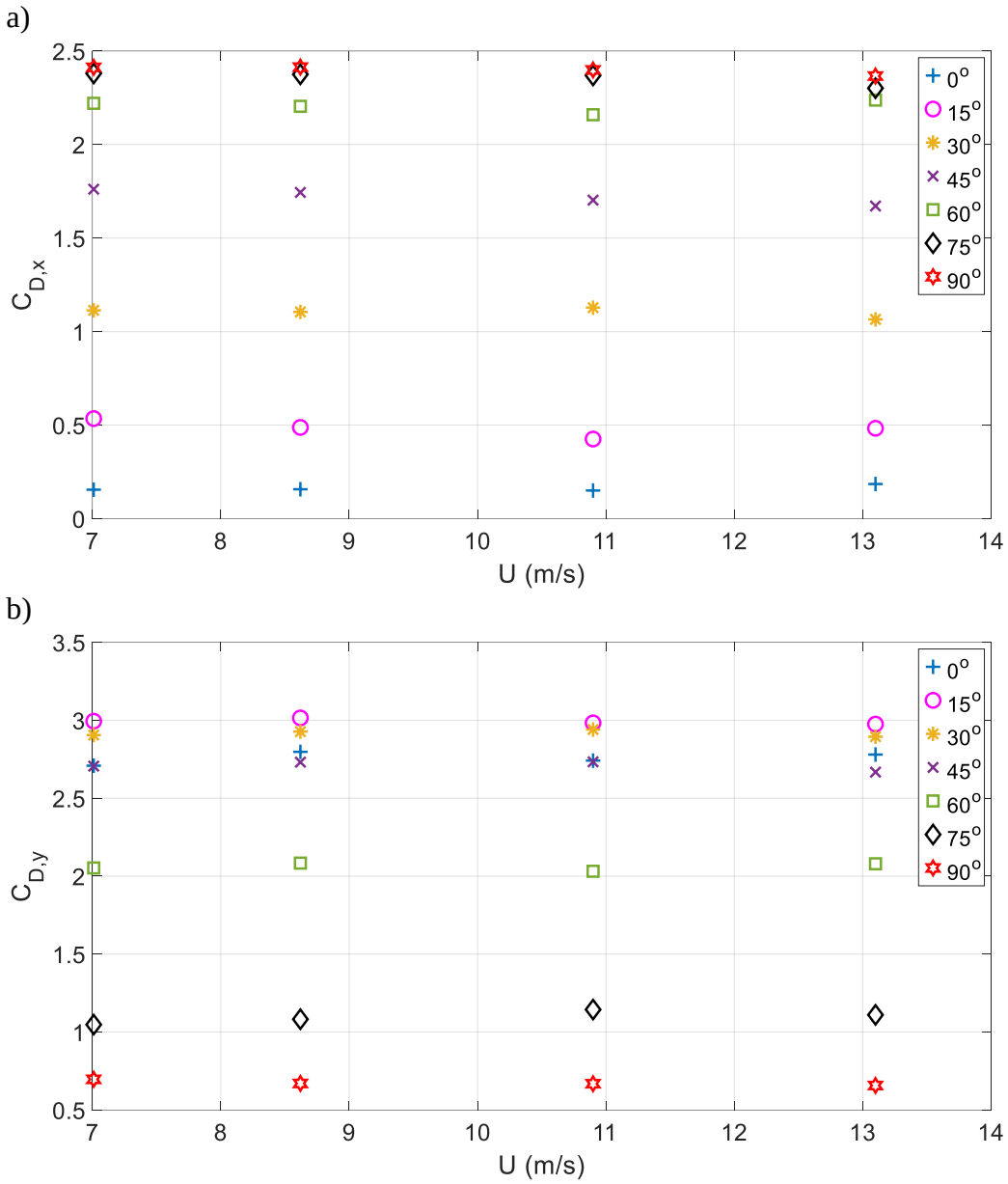

Fig. 3.21: Mean drag coefficient values at all tested wind speeds and wind directions for: a) x-axis, and b) y-axis

As can be seen in Fig. 3.21a, 3.21b, 3.22a, and 3.22b, the mean drag and moment coefficient values for all wind directions are approximately constant as the wind speed increases. There is no noticeable change in the values at any particular wind speed and at any given wind direction. Therefore, it is clear that no Reynolds number (*Re*) effects appeared during the wind testing at the WOW.

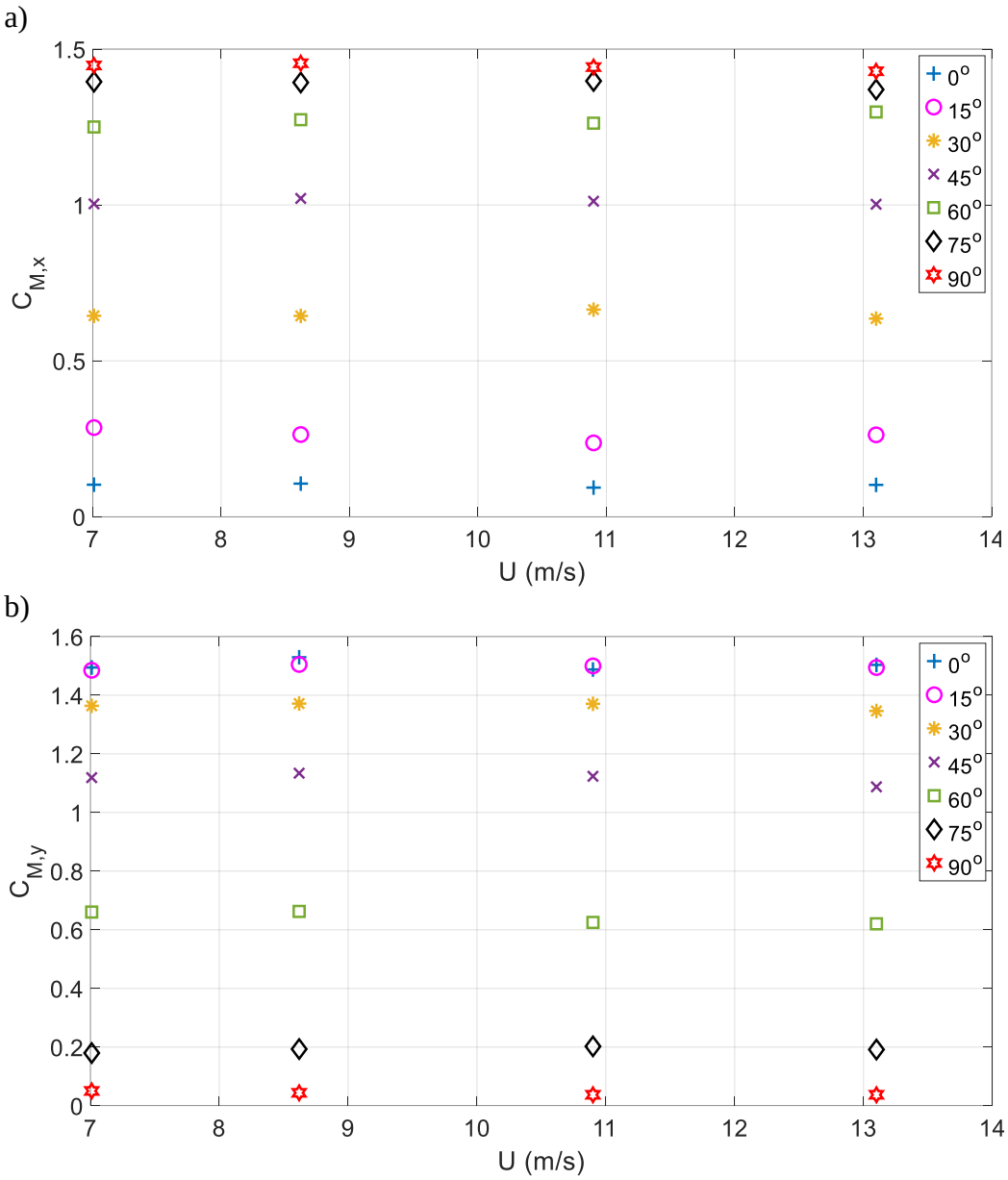

Fig. 3.22: Mean moment coefficient values at all tested wind speeds and wind directions for: a) x-axis, and b) y-axis

3.3.6 Effects of Wind Direction

Generally, design standards of lattice structures and transmission lines systems only consider the along-wind direction. As such, the structures are designed for loads acting along their principal axes, i.e., 0^o (normal to the span of the conductors) and 90^o (along the span of the conductors).

However, past research has stressed on the importance of including off-design conditions (such as loads coming from certain wind directions among others) in the analysis and design of transmission towers. In particular, Mara el al. (2010) noted that wind direction plays an important role in lattice sections design due to the change in aerodynamic properties of the latter with the change in solidity ratio. Such parameters can greatly vary over small angles of wind direction. Furthermore, Mara and Hong (2013) found that the tower's capacity (i.e., strength) greatly depends on the wind direction.

Fig. 3.23 shows the peak base shears and peak base moments obtained for all wind directions at 78 m/s (full-scale). Note that the values were extracted from the recordings of the load cells at the base of the transmission towers. As can be seen in Fig. 3.23, for the single tower case, the maximum base shears and base moments occur at 0^o and 90^o. However, for the system case, the maximum base shears and base moments occur at 60^o and 15^o wind directions for the reaction along the x-axis and y-axis, respectively. Although the design along the major axes of the structure seems appropriate for the single lattice tower case, the same cannot be said for the complete transmission lines system. The base shear is greater by around 25% in the x-direction and around 8% in the y-direction. Similarly, the base moment is larger by around 16% in the x-direction and around 11% in the y-direction. Such phenomena could be explained by the presence of the conductors, altering the total projected frontal area of the system, and thereby increasing the total drag as well as the overturning moment at certain wind directions. More studies are needed to assess these observations for other lattice tower types and transmission lines systems.

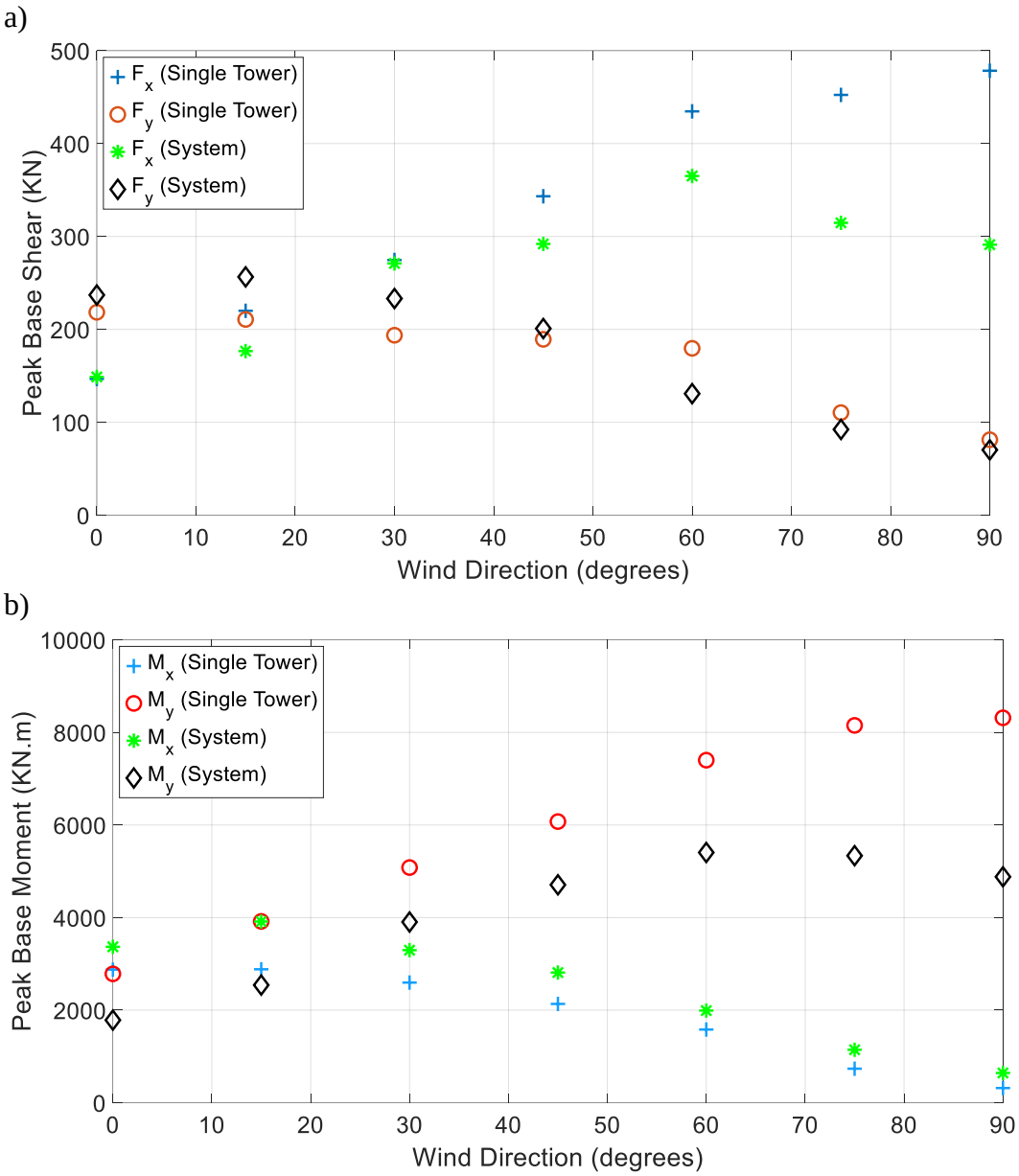

Fig. 3.23: Tower base reactions at the highest tested wind speed (78 m/s full-scale) for: a) shear, and b) moment

3.4 Conclusion

An aeroelastic modeling and testing of a transmission lines system consisting of three lattice towers, four spans of conductors and two end-frames was presented. A technique of horizontally distorting the span of the conductors was utilized in the design of the model. The model was subjected to different simulated wind intensities at the NHERI

WOW EF. The aeroelastic model was first designed and validated using a FEM analysis. The major findings of this research are summarized below:

- The coupling of the tower-insulator-conductor increased the along-wind aerodynamic damping of the system, as compared to the lattice tower only case, for winds normal and parallel to the span of the conductors. Extracted values from the MDOF RD technique were higher than that for the case of the lattice tower only. This was attributed to the presence of the conductors, especially at high wind speeds. However, the coupling also reduced the crosswind aerodynamic damping of the system for one particular wind speed. This raised doubts about the exclusion of the crosswind aerodynamic damping from design standards around the world.
- The estimation of the drag forces on the conductors using previously established equations is well in agreement with measured values at the WOW. It was also shown that the shielding effect was noticeable in the tests conducted and the drag on the leeward conductors was less than their windward counterparts.
- The tower response estimated using equations from Loredo-Souza (1996) and modified by this study (by incorporating the change in turbulence intensity along the height) appear to effectively estimate the measured values in the single lattice tower case only. However, the presence of the conductors significantly reduces the measured response of the transmission lines system, especially at high wind speeds where the aerodynamic damping of the conductors reaches about 15%.
- Calculated DAF values showed that the resonant response of the tower is in the order of 1% to 30% of the total response for all measurements. DAF of forces and

moments increased with the increase in wind speeds. However, DAF of the conductors largely decreased with increasing wind speeds, and this was attributed to the increase in the aerodynamic damping. DAF of conductors at low wind speeds were relatively high, which enforces previous findings that transmission lines systems might be vulnerable at low wind speeds.

- Design factors suggested in Table 3.4 are strongly recommended for use by design engineers of overhead transmission lines systems, coupled with the 3-sec gust. This would ensure that dynamic effects are accounted for and no vulnerability could arise, even at low wind speeds where the aerodynamic damping is not large enough to suppress the resonance effects. Such factors should be accounted for in design standards.

More research is suggested in the field of transmission lines in order to verify the previously mentioned design factors and quantify the effects of coupling on the behavior of the entire system. If such factors are deemed to be adequate and subsequently included in design standards, it would potentially ensure a safer design and a reduction of losses to overhead transmission lines system.

3.5 Chapter III References

Aboshosha, H., Elawady, A., El Ansary, A. and El Damatty, A. (2016). "Review on dynamic and quasi-static buffeting response of transmission lines under synoptic and non-synoptic winds." Engineering Structures, 112, 23-46.

Aboshosha, H. and El Damatty, A. (2014). "Effective Technique to Analyze Transmission Line Conductors under High Intensity Winds." Wind and Structures, Vol. 18, No. 3.

Agneni, A., and Balis, C. L. (1988). "Analytical signal in the damping coefficient estimation." Proceedings of the International Conference on Spacecraft and Mechanical Testing, pp. 133-139.

American National Standards Institute (ANSI) / Telecommunications Industry Association (TIA), ANSI/TIA-222-G (2005). "Structural Standard for Antenna Supporting Structures and Antennas.". Standards and Technology Department, Arlington, VA, U.S.A.

American Society of Civil Engineers (ASCE) 7 (2016). "Minimum Design Loads and Associated Criteria for Buildings and Other Structures." ASCE/SEI 7-16, Reston, VA.

American Society of Civil Engineers (ASCE) 74 (2010). "Guidelines for electrical transmission line structural loading." ASCE manuals and reports on engineering practice, No. 74, New York, NY, USA.

Armitt, J., Cojan, M., Manuzio, C., and Nicolini, P. (1975) "Calculation of wind loadings on components of overhead lines." Proceedings of the IEEE, 1222(11).

Australian/New Zealand Standard (AS/NZS) 1170.2 (2011). "Structural design actions – Part 2: wind actions." SAI Global Limited, Standards Australia Limited, GPO Box 476, Sydney, NSW 2001, Standards New Zealand, PO Box 1473, Wellington 6140.

Axisa, R., Muscat, M., Sant, T., and Farrugia, R. N. (2017). "Structural assessment of a lattice tower for a small, multi-bladed wind turbine." International Journal of Energy and Environmental Engineering, 8, pp. 343-358.

Azzi, Z. (2016). "Behavior of Un-reinforced Concrete Masonry Infill Walls under Lateral Earthquake Loads." Lebanese American University (LAU) Repository, School of Engineering (SOE) Theses and Dissertations.

Azzi, Z., Elawady, A., and Chowdhury, A. G. (2020a). "Large-Scale Aeroelastic Testing to Investigate the Resiliency of Transmission Infrastructure to Hurricane Storms." Proceedings of the 11th International Conference on Structural Dynamics (EURODYN 2020), Athens, Greece, November 23-26, pp. 1944-1957.

Azzi, Z., Habte, F., Elawady, A., Chowdhury, A. G., and Moravej, M. (2020b). "Aerodynamic Mitigation of Wind Uplift on Low-Rise Building Roof Using Large-Scale Testing." Frontiers in Built Environment, Wind Engineering and Science, 5:149.

Azzi, Z., Matus, M., Elawady, A., Zisis, I., Irwin, P., and Chowdhury, A. G. (2020c). "Aeroelastic Testing of Span-Wire Traffic Signal Systems." Frontiers in Built Environment, Wind Engineering and Science, 6:111.

Azzi, Z., Habte, F., Vutukuru, K. S., Chowdhury, A. G., and Moravej, M. (2020d). "Effects of roof geometric details on aerodynamic performance of standing seam metal roofs." Engineering Structures, 225, 111303.

Bachmann et al. (1995). "Vibration problems in structures." Basel: Birkhauser.

Bartoli, G., Cluni, F., Gusella, V. and Procino, L. (2006). "Dynamics of cable under wind action: Wind tunnel experimental analysis." Journal of Wind Engineering and Industrial Aerodynamics, 94, 259-273.

Brincker, R., Zhang, L., and Andersen, P. (2000). "Modal identification from ambient response using Frequency Domain Decomposition." Proceedings of the 18th IMAC, pp. 625-630.

Brincker, R., Ventura, C. E., and Andersen, P. (2001). "Damping estimation by frequency domain decomposition." Proceedings of the 19th IMAC, pp. 698-703.

British Standard (BS) 50341 (2001). "Overhead electrical lines exceeding AC 45 kV: Part 1 – General requirements – Common specifications." London, UK.

British Standard (BS EN) (2006). "Eurocode 3 – Design of steel structures – Part 3-1: Towers, masts and chimneys." The British Standards Institution, London, United Kingdom.

Campbell R. J. (2012). "Weather-Related Power Outages and Electric System Resiliency." Congressional Research Service, Library of Congress, R42696.

Chabart, O. and Lilien, J. L. (1998). "Galloping of electrical lines in wind tunnel facilities." Journal of Wind Engineering and Industrial Aerodynamics, 74-76, 967-976.

Cheng, S., Larose, G. L., Savage, M. G. and Tanaka, H. (2003). "Aerodynamic forces on an inclined circular cylinder." Wind and Structures, Vol. 6, No.3, 197-208.

Chowdhury, A. G., Zisis, I., Irwin, P., Bitsuamlak, G., Pinelli, J.-P., Hajra, B., and Moravej, M. (2017). "Large-Scale Experimentation Using the 12-Fan Wall of Wind to Assess and Mitigate Hurricane Wind and Rain Impacts on Buildings and Infrastructure Systems." Journal of Structural Engineering, 143(7): 04017053.

Cluni, F., Gusella, V. and Bartoli, G. (2008). "Wind tunnel scale model testing of suspended cables and numerical comparison." Journal of Wind Engineering and Industrial Aerodynamics, Vol. 96, no. 6, pp. 1134-1140.

da Silva, J. G. S., Vellasco, P. D. S., de Andrade, S. A., and de Oliveira, M. I. R. (2005). "Structural assessment of current steel design models of transmission and telecommunication towers." Journal of Constructional Steel Research, 61, 8, pp. 1108-1134.

Davenport, A. G. (1962a). "The response of Slender Line-Like Structures to a Gusty Wind." Proceedings of the Institution of Civil Engineers, 23, 3, 389-408.

Davenport, A. G. (1962b). "Buffeting of a Suspension Bridge by Storm Winds." Journal of the Structural Division (ASCE), 88, 3, 233-270.

Davenport, A. G. (1963). "The Relationship of Wind Structure to Wind Loading." Proceedings of the First International Conference on Wind Effects on Buildings and Structures, Teddington, UK, Vol. 1, pp. 53-102.

Davenport, A. G. (1979). “Gust response factors for transmission line loading.” Proceedings of the Fifth International Conference on Wind Engineering (5ICWE), Fort Collins, CO, USA.

Davenport, A. G. (1983). “The relationship of reliability to wind loading.” Journal of Wind Engineering and Industrial Aerodynamics, 13, 3-27.

Davenport, A. G. (1988). “The response of tension structures to turbulent wind: the role of aerodynamic damping.” Proceedings of the First International Oleg Kerensky Memorial Conference on Tension Structures, London, England, June 20-22.

Davenport, A. G. (1993). “How can we simplify and generalize wind loads?” Keynote lecture at the third Asia-Pacific symposium on wind engineering, Hong-Kong, China.

Diana, G., Bruni, S., Cheli, F., Fossati, F., and Manenti, A. (1996). “Dynamic analysis of the transmission line crossing.” Journal of Wind Engineering and Industrial Aerodynamics, 74-76, 977-986.

Elawady, A., Aboshosha, H., El Damatty, A. and Bitsuamlak, G. (2016). “Wind Tunnel Testing of a Multiple Span Aeroelastic Transmission Line Subjected to Downburst Wind.” Resilient Infrastructure, June 1-4.

Elawady, A., Aboshosha, H., El Damatty, A., Bitsuamlak, G., and Hangan, H. (2017). “Aero-elastic testing of multi-spanned transmission line subjected to downbursts.” Journal of Wind Engineering and Industrial Aerodynamics, 169, 194-216.

Executive Office of the President (2013). “Economic Benefits of Increasing Electric Resilience to Weather Outages-August 2013”. IEEE USA Books & eBooks, p. 29.

Feng, C., Chowdhury, A. G., Elawady, A., Chen, D., Azzi, Z., and Vutukuru, K. S. (2020). “Experimental Assessment of Wind Loads on Roof-to-Wall Connections for Residential Buildings.” Frontiers in Built Environment, Wind Engineering and Science, 6:10.

Fujimura, M., Maeda, J., Morimoto, Y., and Ishida, N. (2007). “Aerodynamic damping properties of a transmission tower estimated using a new identification method.” Proceedings of the 12th International Conference on Wind Engineering (12ICWE), pp. 1047-1054.

Hans, S., Ibraim, E., Pernot, S., Boutin, C., and Lamarque, C. H. (2000). “Damping identification in multi-degree-of-freedom system via Wavelet-Logarithmic Decrement – part 2: study of a civil engineering building.” Journal of Sound and Vibration, 235 (3), 375-403.

Haviland, R. (1976). “A study of the uncertainties in the fundamental translational periods and damping values for real buildings.” Evaluation of Seismic Safety of Buildings, Research Report 5, National Science Foundation (NSF).

Hawes, H., and Dempsey, D. (1993). “Review of recent Australian transmission line failure due to high intensity winds.” Proceedings of the task force of high intensive wind on transmission lines, Buenos Aires, Argentina.

Holmes, J. D. (1994). “Along-wind response of lattice towers: Part 1 – derivation of expressions for gust response factors.” Engineering Structures, 16, 287-292.

Holmes, J. D. (1996a). “Along-wind response of lattice towers: Part 2 – aerodynamic damping and deflections.” Engineering Structures, 18, 483-488.

Holmes, J. D. (1996b). “Along-wind response of lattice towers: Part 3 – effective load distribution.” Engineering Structures, 18, 489-494.

Holmes, J. D. (2008). “Recent developments in the specification of wind loads on transmission lines.” Journal of Wind Engineering and Industrial Aerodynamics, 5(1), 8-18.

Holmes, J. D. (2015). “Wind Loading of Structures.” 3rd Edition, CRC Press, Taylor & Francis Group, Boca Raton, FL.

Houle, S., Ghannoum, E., and Hardy, C. (1991). “Static and dynamic testing of transmission lines subjected to real wind conditions.” CIGRE symposium, Leningrad, USSR.

International Electrotechnical Commission (IEC) 60826. (2003). “Design criteria of overhead transmission lines.” Geneva, Switzerland.

Irvine, H. M. (1981). “Cable Structures.” MIT Press, Cambridge, MA, USA.

Irwin, P. A. (1977). “Wind Tunnel and Analytical Investigations of the Response of Lions’ Gate Bridge to a Turbulent Wind.” National Research Council of Canada, NAE Report LTR-LA-210.

Irwin, P. A. (1979). “Cross-Spectra of Turbulence Velocities in Isotropic Turbulence.” Journal of Boundary Layer Meteorology, 16, pp.337-343.

Irwin, P. A. (1992). “Full aeroelastic model tests.” Aerodynamics of Large Bridges, A. Larsen (ed.), Balkema, Rotterdam.

Irwin, P. A. (1996). “Buffeting Analysis of Long-Span Bridges.” RWDI Technical Reference Document, RD1-1996.

Isyumov, N. (1972). “Wind Tunnel Methods for Evaluating Wind Effects on Buildings and Structures.” International Symposium on Experimental Mechanics, The University of Waterloo, Waterloo, June 12-16.

Kishnasamy, S. (1985). “Wind and ice loading research in Ontario Hydro.” Proceedings of the fifth US national conference on wind engineering, Lubbock, Texas, USA.

Lamarque, C. H., Pernot, S., and Cuer, A. (2000). "Damping identification in multi-degree-of-freedom system via Wavelet-Logarithmic Decrement – part 1: theory." Journal of Sound and Vibration, 235 (3), 361-374.

Liang, S. (2002). "Research report on wind vibration response calculation and aeroelastic model wind tunnel test of transmission tower-line system." State key laboratory of civil engineering disaster prevention, Tongji University, Shanghai, China.

Liang, S., Zou, L., Wang, D. and Cao, H. (2015). "Investigation on wind tunnel tests of a full aeroelastic model of electrical transmission tower-line system." Engineering Structures, Vol. 85, pp. 63-72.

Lin, W. E., Savory, E., McIntyre, R. P., Vandelaar, C. S. and King, J. P. C. (2012). "The response of an overhead electrical power transmission line to two types of wind forcing". Journal of Wind Engineering and Industrial Aerodynamics, 102, 48-60.

Loredo-Souza, A. M. (1996). "The Behaviour of Transmission Lines Under High Winds." University of Western Ontario (UWO) Digital Theses, 2650.

Loredo-Souza, A. M. and Davenport, A. G. (1998). "The effects of high winds on transmission lines." Journal of Wind Engineering and Industrial Aerodynamics, 74-76, 987-994.

Loredo-Souza, A. M., and Davenport, A. G. (2001). "A novel approach for wind tunnel modelling of transmission line". Journal of Wind Engineering and Industrial Aerodynamics, 89, 1017-1029.

Loredo-Souza, A. M. and Davenport, A.G. (2002). "Wind tunnel aeroelastic studies on the behavior of two parallel cables". Journal of Wind Engineering and Industrial Aerodynamics, 90, 407-414.

Loredo-Souza, A. M., and Davenport, A. G. (2003). "The influence of the design methodology in the response of transmission towers to wind loading". Journal of Wind Engineering and Industrial Aerodynamics, 91, 995-1005.

Loredo-Souza, A. M. (2014). "The aeroelastic wind tunnel modeling of transmission lines and their behavior under severe boundary layer winds." Proceedings of the 9th International Conference on Structural Dynamics (EURODYN 2014), Porto, Portugal, 30 June – 2 July.

Lou, W. J., Sun, B. N., and Tang, J. C. (2000). "Aeroelastic Model Investigation and Spectral Analysis of a Tall Lattice Tower". Advances in Structural Engineering, 3(2):119-30.

Lou, W. J., Wang, X. and Jiang, Y. (2009). "Wind-Induced Responses of a High-Rise Transmission Tower to Thunderstorm Downbursts." The Seventh Asia-Pacific Conference on Wind Engineering, Nov. 8-12, Taipei, Taiwan.

Maeda, J., Imamura, Y., and Morimoto, Y. (1999). “Wind response behavior of a power transmission tower using new displacement measurement.” Proceedings of the 10th International Conference on Wind Engineering (10ICWE), pp. 481-486.

Mara, T. G., Galsworthy J. K., and Savory, E. (2010). “Assessment of vertical wind loads on lattice frame-work with application to thunderstorm winds”. Wind and Structures, Vol. 13, no.5, pp. 413-431.

Mara, T. G. and Hong, H. P. (2013). “Effect of wind direction on the response and capacity surface of a transmission tower.” Engineering Structures, 57, 493-501.

Mehta, K. C., Kadaba, R., and Kempner, L. (1988). “Conductor response to extreme winds.” Proceedings of the Second International Symposium on Probability Methods to Electric Power Systems, Oakland, CA, USA.

Mehta, K. C., and Kadaba, R. (1989). “Wind induced response of transmission line conductors.” Recent advances in wind engineering, Proceedings of the second Asia-Pacific symposium on wind engineering, Beijing, China, vol. 2, p.748-755.

Mehta, K. C., and Kadaba, R. (1990). “Field data analysis of electrical conductor response to winds.” Journal of Wind Engineering and Industrial Aerodynamics, 36, 329-338.

Momomura, Y., Marukawa, H., Okamura, T., Hongo, E. and Ohkuma, T. (1997). “Full-scale measurements of wind-induced vibration of a transmission line system in a mountainous area.” Journal of Wind Engineering and Industrial Aerodynamics, 72, 241-252.

Okamura, T., Ohkuma, T., Hongo, E., and Okada, H. (2003). “Wind response analysis of transmission tower in mountainous area.” Journal of Wind Engineering and Industrial Aerodynamics, 91, 53-63.

Ruzzene, M., Fasana, A., Garibaldi, L., and Piombo, B. (1997). “Natural frequency and damping identification using Wavelet Transform.” Mechanical System & Signal Processing, 11 (2), 207-218.

SAP2000 Version 22.0.0 (2020), Structural Analysis Program, Computers and Structures, Inc., www.csiamerica.com.

Savory, E. , Parke, G. A. R., Zeinoddini, M., Toy, N., and Disney, P. (2001). “Modelling of tornado and microburst-induced wind loading and failure of a lattice transmission tower.” Engineering Structures, 23, 365-375.

Shan, L. (1994). “Evaluation of the results of several full-scale conductor wind loading experiments.” EPRI TR-100479.

Simiu, E., and Yeo, D. (2019). “Wind Effects on Structures.” John Wiley & Sons, 4th Edition.

Takeuchi, M., Maeda, J., and Ishida, N. (2010). "Aerodynamic damping properties of two transmission towers estimated by combining several identification methods." Journal of Wind Engineering and Industrial Aerodynamics, 98, 872-880.

Tamura, Y., and Suganuma, S. (1996). "Evaluation of amplitude-dependent damping and natural frequency of buildings during strong winds." Journal of Wind Engineering and Industrial Aerodynamics, 59, 115-130.

Tamura, Y., Zhang, L., Yoshida, A., Nakata, S., and Itoh, T. (2002). "Ambient vibration tests and modal identification of structures by FDD and 2DOF-RD technique." Proceedings of the structural engineers world congress, T1-1-a-1.

Tokoro, S., Komatsu, H., Nakasu, M., Mizuguchi, K. and Kazuga, A. (2000). "A study on wake-galloping employing full aeroelastic twin cable model." Journal of Wind Engineering and Industrial Aerodynamics, 88, 247-261.

U.S. Department of Energy (DOE) (2013). "U.S. Energy Sector Vulnerabilities to Climate Change and Extreme Weather." DOE/PI-0013, https://www.energy.gov/sites/prod/files/2013/07/f2/20130716-Energy%20Sector%20Vulnerabilities%20Report.pdf

Vickery, B. J. (1995). "The response of chimneys and tower-like structures to wind loading." A State of the Art in Wind Engineering, Ninth International Conference on Wind Engineering (9ICWE), New Delhi, India, Davenport Sixtieth Birth Anniversary Volume, pp. 205-233.

Volpe, H. (1989). "Wind effects on conductors for span factors." Final project report, line design section, division of facilities engineering, Portland, OR, USA: Bonneville Power Administration.

Wang, X., Lou, W., Li, H., and Chen, Y. (2009). "Wind-induced dynamic response of high-rise transmission tower under downburst wind load." Journal of Zhejiang University, 43, 8, 1520-1525.

Zar, M., and Arena, J. R. (1979). "Towers and Transmission Pole Structures." Structural Engineering Handbook, Section 24, McGraw-Hill Book Co.

Zhang, Y. (2016). "Situation and countermeasures on hurricane defense of electric transmission line." East China Electric Power, 3:28-31.

Zhangqi, W., Zeming, S., and Wenqiang, J. (2014). "Theoretical and Experimental Research on Joint Slippage Effects of Lattice Angle Steel Tower." Applied Mechanics and Materials, 477-478, pp. 660-665.

CHAPTER IV. SUMMARY AND CONCLUSIONS

4.1 Summary

The research conducted in this dissertation consists of two main parts that provided significant knowledge advancements regarding the response of self-supported lattice towers and transmissions lines systems to hurricane wind speeds. The research activities carried out herein comprised of two activities: (1) aeroelastic large-scale wind testing; and (2) theoretical analysis. The experiments conducted at the NSF NHERI WOW EF on 1:50 scaled models of a single self-supported steel lattice transmission tower and a four-span transmission lines system provided deeper insights into the highly complex dynamic behavior at system levels. The experimental program was designed with four main objectives in mind. The first objective is to design and conduct tests on a single self-supported lattice tower, providing an investigation into the dynamic response of lattice structures to hurricane winds. Part of the first objective is also to assess the adequacy of drag coefficients of lattice sections suggested by various design standards, especially after the recent hurricane-induced damage incidents. The second objective is to design and conduct aeroelastic wind tests on a multi-span transmission-insulator-conductor system to investigate possible coupling effects among system components as well as boundary effects and consequences of adjacent spans. The third objective is to develop analytical techniques validated by the experimentally measured responses.

Both main chapters of the dissertation extensively describe the challenges faced when designing the aeroelastic models as well as several equations that needed to be satisfied in order to obtain valid results. More specifically, Chapter 3 introduced the concept of horizontal distortion technique that sheds light on an approach into the design of multi-

span systems such as transmission lines. The design, validation, and construction of both aeroelastic models at the scale of 1:50 were described. Subsequently, experimental techniques were modified and then applied to measured acceleration data in order to obtain a realistic estimate of the along-wind and crosswind aerodynamic damping coefficients of lattice structures as well as transmission lines systems. Similarly, analytical equations were derived, and others adopted from previous studies on lattice structures to estimate the response and compare with measured data at the WOW. Drag and moment coefficients were obtained from strain gauges data. Subsequently, comparisons were made with various design standards for the drag coefficients of lattice sections according to their solidity ratios. Finally, dynamic amplification factors (DAF) were defined, calculated, and estimations of resonant and background responses of different reactions on the models were obtained.

The assumptions, results and conclusions made in this dissertation are of importance to the design and analysis of lattice structures as well as transmission lines systems. Findings are believed to be useful to the improvement of design standards in the U.S. and around the world, and thus enhance the resiliency of lifeline infrastructure against windstorms.

4.2 Conclusions of Dissertation

The main conclusions of the aeroelastic experimental and analytical studies on scaled models of lattice structures and transmission lines systems are presented below:

- The along-wind aerodynamic damping coefficients obtained from the Iterative Least Squares (ILS) and Random Decrement (RD) techniques were in good agreement with their analytical counterparts for both directions for the case of

single lattice tower. In addition, the same techniques were implemented in the crosswind direction and results showed a similar trend to previously published works on tall buildings having the same length to width ratio as the spine which implies an accuracy of the applied methods. The along-wind aerodynamic damping is proportional to the increase in wind speeds whereas its crosswind counterpart is related to the length to width ratio of the tower itself as well as wind speed.

- The coupling of the tower-insulator-conductor has increased the along-wind aerodynamic damping of the transmission lines system for winds normal and parallel to the span of the conductors. Extracted values from the Multi-Degrees-of-Freedom (MDOF) (tower-insulator-conductor) RD technique were higher than for the case of the single lattice tower. This was attributed to the presence of the conductors, especially at high wind speeds. However, the coupling reduced the crosswind aerodynamic damping of the system for one particular wind direction. This raised questions about the exclusion of the crosswind aerodynamic damping from design standards around the world.
- The buffeting analysis results in the along-wind direction showed good agreement with the measured RMS responses of the single lattice tower. It was found that incorporating the change in turbulence intensity along the height yields significant improvements over the traditional analytical approach developed by Loredo-Souza (1996) for single lattice transmission towers. However, some discrepancies were observed at higher wind speeds, possibly due to the self-generated turbulence of the model induced by the excessive tower vibrations, a phenomenon not accounted for in the buffeting theory.

- The estimates of the drag forces on the conductors using previously established equations are well in agreement with measured values at the WOW. It was also shown that the shielding effect plays a role in reducing the drag on the leeward conductors.
- The tower response estimated using equations from Loredo-Souza (1996) and modified by the author (by including the change in the turbulence intensity along the height of the model) appear to correctly estimate the measured values in the single lattice tower case only. However, when the lattice towers are used in a tower-insulator-conductor transmission lines system, the analytically developed response equations overestimate their measured counterparts. This is particularly observed at high wind speeds where the aerodynamic damping of the conductors reaches about 15%.
- The mean drag coefficients of the single lattice tower case based on its solidity ratio were in good agreement with values proposed by many standards adopted around the world. However, the latter fail to suggest moment coefficients in order to account for any bending that might occur in members of lattice structures where the connection could be qualified as somewhat rigid. Such an aspect of the design of lattice structures is not discussed in standards around the world. This dissertation suggested some moment coefficient values which could be of use in the design of lattice structures having the same range of solidity ratios.
- Calculated DAF showed that the resonant response of the single tower is in the order of 1% to 18% for all measurements. DAF of forces somewhat reduced with increased wind speeds and such phenomenon was attributed to the increase in the

aerodynamic damping with increasing wind speeds, suppressing the resonant response. DAF values of moments and cross-arm forces increased with increase in wind speed due to the vibration of the spine and the absence of lateral bracing at the cross-arm level.

- Obtained DAF results in the case of the single tower model were typically higher than tower gust response G_T values proposed by different standards around the world, signifying that the resonant contribution in the total response of lattice structures is not yet fully understood.
- Calculated DAF values showed that the resonant response of the tower in a complete transmission system is in the order of 1% to 30% for all measurements. Typically, DAF for the cross-arms were in the order of 20% to 30% whereas those of the base shears and base moments ranged between 1% and 15%. DAF of forces and moments increased with the increase in wind speeds. However, DAF of the conductors were largely reducing, and this was attributed to the increase in the aerodynamic damping. DAF of conductors at low wind speeds were relatively high, which emphasize previous findings that transmission lines systems might be vulnerable at low wind speeds.
- The suggested factors given in Table 3.4 are recommended for use in the design of transmission lines systems. Such factors are based on the design 3-sec gust according to the location of the structure and their inclusion would account for any dynamic response of the system that might occur at low wind speeds as well as high ones.

4.3 Possible Design Recommendations and Code Changes

Based on the current work presented in this dissertation and the observations noted, the following points are recommended in order to potentially enhance the current codes regarding the design of lattice structures as well as transmission systems:

- The aeroelastic test results showed that certain wind directions (typically 15^o and 60^o) produce higher loads on transmission lines systems than for directions (0^o and 90^o) proposed in the standards by as much as 25% in some instances. Therefore, it is important to allow for the effects of winds coming from different directions on such structures.
- The incorporation of the change in the turbulence intensity along the height of the transmission tower in the buffeting equations (based on the influence lines) has shown improvements over traditional equations developed by Loredo-Souza (1996), particularly at higher wind speeds.
- Currently, the crosswind response is not taken into account in the design of both lattice structures and transmission lines systems. However, the measurements obtained for the crosswind response have indicated the need to account for it in the design.
- The coupling of the tower-insulator-conductor in the transmission lines model changes the structural and aerodynamic damping of the system in a favorable way. This could be considered in formulating standards.
- Table 3.4 is suggested to account for the dynamic amplification of forces on conductors and transmission towers based on the design 3-sec gust.

CHAPTER V. FUTURE RESEARCH RECOMMENDATIONS

Possible future research and additional work are suggested below.

- This study focused on one type of lattice structures used as transmission towers. Other lattice structure configurations with varying solidity ratios should also be investigated for dynamic behavior under high winds.
- The tests conducted in this research only focused on transmission lines and lattice structures located in flat lands. It would be worthwhile looking at the effects of topography (such as regions will hills and escarpments) change on the behavior of the tested structures.
- The coupling of the tower-insulator-conductor has led to a change in the aerodynamic damping of the system. In most cases, the system damping has increased due to the presence of the conductors. However, it also reduced in its crosswind aspect. Additionally, comparisons between measured responses on the single lattice tower and the complete transmission lines models have shown that the latter model experienced much smaller values. This is due to the presence of the conductors which lead to an increase in the aerodynamic damping of the system, thereby reducing the response. More testing is recommended in order to quantify the effects of the coupling on the system.
- The estimation of crosswind aerodynamic damping coefficients using experimental techniques has proven the need to implement such a factor in design standards. Hence, a quantification of such a coefficient is important for design purposes and future research aimed at developing appropriate design values at different wind speeds is critical.

- The DAF obtained for both tested models have shown that the resonant contribution is important. Values of DAF were largely higher than their standards counterparts. It is important to conduct more research on this aspect, taking into account different terrain exposures and tower configurations.

VITA

ZIAD AZZI

Born, Ajaltoun, Lebanon

2008 - 2013	B.E., Civil Engineering Lebanese American University Beirut, Lebanon
2013 - 2016	M.S., Civil Engineering (Engineering Mechanics) Lebanese American University Beirut, Lebanon
2016 - 2020	Teaching and Research Assistant Florida International University Miami, Florida, USA
2016 - 2020	M.S., Civil Engineering (Structural Engineering) Florida International University Miami, Florida, USA
2016 - 2020	Doctoral Candidate, Civil Engineering (Structural Engineering) Florida International University Miami, Florida, USA
2020	UGS Dissertation Year Fellow Florida International University Miami, Florida, USA

PUBLICATIONS

Azzi, Z., and Abi Shdid, C. (2021). "Seismic Behavior of Unreinforced Concrete Masonry Infill Walls." Proceedings of the 11th International Structural Engineering and Construction Conference (11ISEC), Cairo, Egypt, July 26-31.

Azzi, Z., Elawady, A., and Chowdhury, A. G. (2020). "Large-Scale Aeroelastic Testing to Investigate the Resiliency of Transmission Infrastructure to Hurricane Storms." Proceedings of the 11th International Conference on Structural Dynamics (EURODYN 2020), Athens, Greece, November 23-26, pp. 1944-1957.

Azzi, Z., Habte, F., Vutukuru, K. S., Chowdhury, A. G., and Moravej, M. (2020). "Effects of roof geometric details on aerodynamic performance of standing seam metal roofs." Engineering Structures, 225, 111303. DOI: 10.1016/j.engstruct.2020.111303.

Azzi, Z., Matus, M., Elawady, A., Zisis, I., Irwin, P., and Chowdhury, A. G. (2020). "Aeroelastic Testing of Span-Wire Traffic Signals." Frontiers in Built Environment, Wing Engineering and Science, 6:111. DOI: 10.3389/fbuil.2020.00111.

Feng, C., Chowdhury, A. G., Elawady, A., Chen, D., Azzi, Z., and Vutukuru, K. S. (2020). "Experimental Assessment of Wind Loads on Roof-to-Wall Connections for Residential Buildings." Frontiers in Built Environment, Wind Engineering and Science, 6:10. DOI: 10.3389/fbuil.2020.00010.

Azzi, Z., Habte, F., Elawady, A., Chowdhury, A. G., and Moravej, M. (2020). "Aerodynamic Mitigation of Wind Uplift on Low-Rise Building Roof Using Large-Scale Testing." Frontiers in Built Environment, Wind Engineering and Science, 5:149. DOI: 10.3389/fbuil.2019.00149.

Azzi, Z., Elawady, A., and Chowdhury, A. G. (2020). "Determining the Efficacy of a Retrofit Technique for Residential Buildings using Holistic Testing." Proceedings of the ASCE/SEI 2020 Structures Congress, pp. 360-369, St. Louis, Missouri, USA, April 5-8.

Azzi, Z., Elawady, A., Matus, M., Zisis, I., and Irwin, P. (2019). "Buffeting Response of Span-Wire Traffic Signals using Large-Scale Aeroelastic Wind Testing." Proceedings of the 15th International Conference on Wind Engineering (15ICWE), Beijing, China, September 1-6.

Azzi, Z., Matus, M., Elawady, A., Zisis, I., and Irwin, P. (2018). "Large-scale aeroelastic testing to investigate the performance of span wire traffic signals." Proceedings of the 5th American Association for Wind Engineering Workshop (5AAWE), Miami, Florida, USA, August 12-14.

Azzi, Z., Moravej, M., Habte, F., Elawady, A., and Chowdhury, A. G. (2018). "Roof Uplift under Cornering Winds and Wind Uplift Mitigation." Proceedings of the 5th American Association for Wind Engineering Workshop (5AAWE), Miami, Florida, USA, August 12-14.